



**Politecnico  
di Torino**

**Politecnico di Torino**

Master degree in Energy and Nuclear Engineering – Renewable Energy  
Systems

Academic year 2022/2023

Graduation Session of October 2023

**Assessment of a Mediterranean Hydrogen  
Generation Hub powered by Offshore Floating  
Wind for the Decarbonization of the Maritime  
Shipping Sector**

Supervisor:

Massimo Santarelli

Candidate:

Federico Puleo

Co-Supervisors:

Domenico Ferrero

Alberto Ghigo

Giovanni Bracco



# Abstract

Nowadays around 80-90% of global trade is performed via maritime shipping and as indicated by the International Maritime Organization, by 2050 this number could increase up to 115% with respect to 2020 levels. The shipping sector is responsible for around 3% of the annual global greenhouse gas emissions on a carbon dioxide equivalent basis and approximately 13% and 12% of the annual global nitrogen oxides and sulfur oxides emissions, respectively. Considering that about 99% of the energy demanded by the international shipping industry is met by fossil fuels, the utilization of alternative fuels is needed to mitigate the CO<sub>2</sub> and GHG emissions.

Among the alternative fuels, hydrogen can be used in fuel cells, as a fuel mixture with traditional fuels and as a substitute in combustion processes. In maritime application, it can be stored on board as compressed gas, liquid, or chemically bounded. The storage of compressed gaseous hydrogen require enormous volumes for long-range routes, due to its low volumetric density. The volumetric density of liquid hydrogen is instead 71 times higher than that of the gaseous form. Therefore, in maritime shipping one alternative could be to store this fuel in the cryogenic liquid phase.

In this master thesis, the assessment of a hydrogen generation hub for ship refueling powered by a offshore floating wind farm in the Mediterranean Sea was performed. The Mediterranean Sea has been selected in this work because it is one of the most crowded shipping areas of the World, accounting for around 15% of the global shipping activity. First of all, the most suitable plant location in the Mediterranean Sea was evaluated considering different constraints as vessel route density, bathymetry, wind resource, distance from coast, geological context, habitats preservation and maritime boundaries. A techno-economic analysis was performed considering two different scenarios, calculating the levelized cost of hydrogen (LCOH) and the net present cost (NPC) for each scenario. In the first scenario, the proposed plant is composed of two main sections, namely the wind farm and the liquid hydrogen production and distribution facility. In this case the refuelling is performed offshore. In the second scenario, the plant was modified considering a subsea pipeline connection with the port of Porto Empedocle transporting the gaseous hydrogen produced by the electrolyzer. In this case, the refuelling is performed onshore. The annual hydrogen production for the specific plant location has been then calculated, considering a floating offshore wind farm of 300 MW of rated capacity located in the Strait of Sicily.

# Index

1 Introduction.....	6
1.1 Decarbonizing the maritime sector .....	6
1.2 Liquid hydrogen in the maritime sector .....	9
1.3 Aim of the work .....	11
2 Plant Components .....	12
2.1 Plant layout .....	12
2.2 Wind farm .....	14
2.2.1 Floating substructure.....	15
2.2.2 Mooring system .....	16
2.2.3 Anchoring system.....	17
2.2.4 Selected wind turbine.....	18
2.3 Electrolysis.....	22
2.4 Water treatment .....	25
2.5 Liquefaction .....	26
2.6 Storage .....	28
2.7 Refueling Station .....	30
3 Methodology.....	31
3.1 Plant location methodology .....	31
3.1.1 Vessels route density .....	31
3.1.2 Bathymetry.....	34
3.1.3 Wind resource .....	36
3.1.5 Geological considerations .....	37
3.1.6 Habitat preservation .....	39
3.1.7 Additional considerations.....	39
3.2 Wind power model.....	41
3.2.1 WAsP model.....	41
3.2.2 Wind Profile Model.....	46
3.3 Liquid hydrogen production model .....	50
3.4 Technoeconomic analysis .....	54

3.4.1 Scenario 1.....	56
3.4.2 Scenario 2.....	58
4 Results.....	62
4.1 Plant location .....	62
4.2 Wind Farm Production.....	66
4.2.1 WAsP results .....	66
4.2.2 Wind Profile Model results .....	70
4.3 Liquid hydrogen production .....	73
4.4 Technoeconomic analysis .....	75
4.4.1 Scenario 1.....	75
4.4.2 Scenario 2.....	77
5 Discussion and conclusion.....	80
References.....	84

# 1 Introduction

## 1.1 Decarbonizing the maritime sector

Urgent action is required to speed up the energy transformation and decarbonization of the global economy, including the shipping sector, which is a strategic component of the global economy being essential for the production and distribution of goods and energy.[1]

According to the International Maritime Organization's (IMO) Fourth GHG study of 2020, the energy demand in global shipping in 2018 accounted for nearly 11 exajoules (EJ), which represents approximately 1 billion tons of carbon dioxide (CO<sub>2</sub>) emissions, including both international shipping and domestic navigation. This represents about 3% of the total annual global greenhouse gas (GHG) emissions. Considering only the international shipping, it contributes to around 9% of the transportation sector global emissions [1].

Additionally, IMO reported that the international shipping contributes annually to approximately 12% and 13%, respectively, of the global emissions of sulphur oxides (SO<sub>x</sub>) and nitrogen oxides (NO<sub>x</sub>). Nevertheless, it must be emphasized that the maritime industry in recent years made some significant efforts to reduce air pollution, especially to reduce the SO<sub>x</sub> emissions limiting the sulphur content of fuels [2].

To put these numbers in perspective, if the international shipping sector is considered as a state, its CO<sub>2</sub> emissions would rank it as the sixth to seventh-largest emitter, similar in scale to Germany's emissions [2].

The maritime shipping is a strategic sector in the global economy because enables approximately 80 to 90% of global trade [1]. To accelerate the decarbonization of this sector is fundamental, especially because it is predicted an increase of maritime trade in near future. More specifically, the IMO predicts that by 2050, the maritime trade could increase by 40% to 115% compared to 2020 levels [2]. Additionally, currently fossil fuels provide up to 99% of the energy demand in the international shipping. Therefore, IMO predicted that without significant actions the GHG emissions from the shipping sector could increase between 50% and 250% with respect to 2008 emission levels [1].

The shift from fossil fuels to zero-carbon fuels is particularly crucial to meet the European Green Deal targets, which aim to reduce emissions by 55% in 2030 compared to 1990 and achieve a climate-neutral economy by 2050 [2].

A crucial step to accelerate the decarbonization of this sector is to identify specific targets of high priority. While only accounting for about the 20% of the global fleets, certain types of vessels, such as the bulk and container carriers, as well as oil and chemical tankers, are responsible for 85% of the net GHG emissions of the shipping sector [1].

A schematic representation of the voyage-based distribution of the energy consumption for the international shipping is given in the following figure:

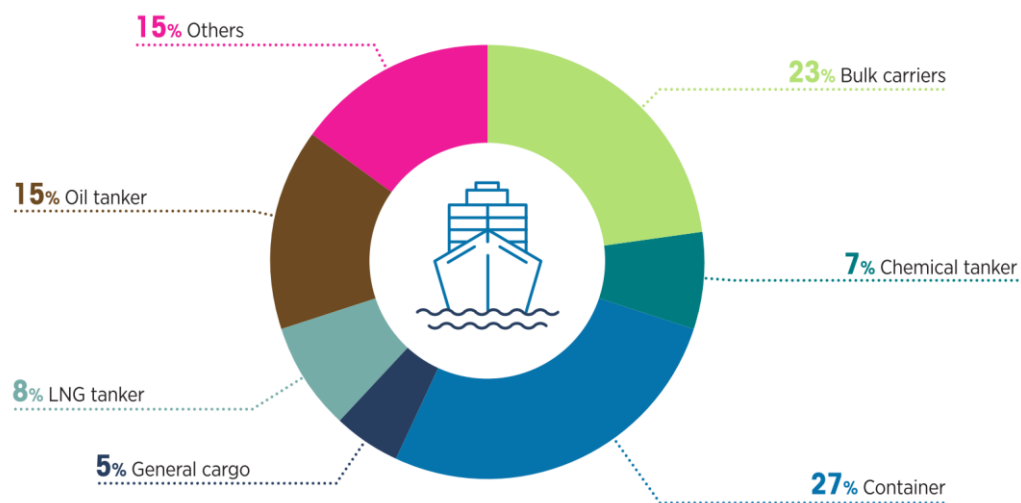


Figure 1 distribution of the energy consumption for the international shipping [1]

Geographical boundaries significantly impact trade routes, consequently, can be identified certain key international maritime routes which connect the world's industrial regions. Some specific points of international relevance and the main shipping traffic routes can be identified in Figure 2. Four strategic points are: the Panama Canal, which offers direct access between Atlantic and Pacific; the Suez Canal, which connects the Gulf of Suez and the Mediterranean Sea providing a direct route between Indian and Atlantic Oceans (allowing shorter commercial routes between Asia and Europe); the Strait of Malacca, which connects the Pacific and Indian Oceans [1].

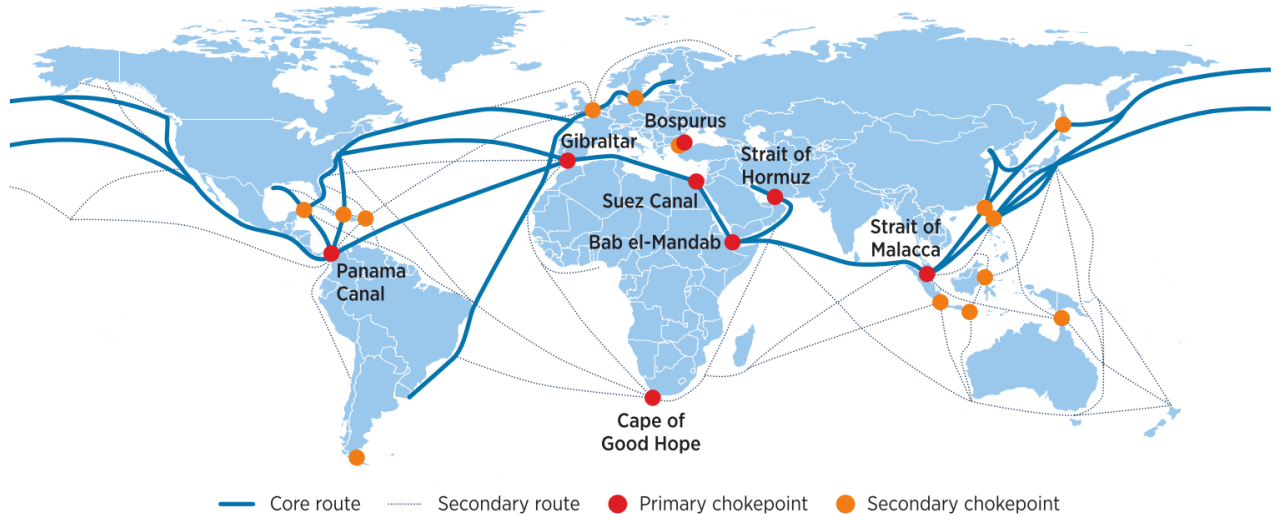


Figure 2 Main international shipping traffic routes [1]

To obtain a significant acceleration of the reduction of GHG associated to the maritime shipping sector, it is of fundamental importance to identify the locations that could push rapidly the energy transition. The key trading ports, the ports of strategical relevance for fuel supply and the infrastructures built along the main navigation routes highlighted in Figure 2 will play a crucial role [1].

According to [2], the transitioning to alternative fuels must begin now due to the long lifetime of vessels, which is around 30 years or even longer for smaller ships. Considering that around half of the currently operational ships are more than 15 years old, and one-third are more than 25 years old, to replace fossil-fueled ships with zero-carbon alternatives represents an urgent action to avoid that the ships commissioned in the next years will continue to utilize fossil fuels for the next decades.

Alternative fuels, from the technical perspective, must be characterized by different characteristics. First of all a high energy density is required. However, unfortunately, the volumetric energy density of alternative fuels cannot compete with that of currently used fuels. The second aspect to take in consideration is the availability and security of supply, therefore it will be necessary to build a worldwide dedicated infrastructure to satisfy the future demand for these alternative fuels. The third characteristic is related to sustainability. More specifically, alternative fuels must have a neutral GHG emission from well to propeller. To this extent, the IMO is trying to consider not only the tank to propeller GHG intensity of alternative fuels, as it is currently done, but also the well-to-tank contribution. In this context, pure hydrogen and hydrogen-based fuels and hydrogen-based technologies possess substantial potential within the maritime sector. Moreover, if effectively exploited, they have the capacity to substantially contribute to the process of decarbonizing the global fleet while simultaneously mitigating air pollution. [2]

In this work, among the possible alternative fuels, pure hydrogen was selected analyzing both the liquefied hydrogen and the compressed hydrogen solutions in two separate case studies.

## 1.2 Liquid hydrogen in the maritime sector

The volumetric energy density of liquid hydrogen is considerably higher than that of gaseous hydrogen, more specifically, approximately 71 times greater. However, it still only accounts for about the 16% of the density of marine gas oil currently used. Consequently, considering this energy density, a volume of around five times higher the volume required to store the same amount of energy as conventional marine gas oil is required. [2]

This represents a disadvantage for its use, but it is worth to mention that alternative fuels' energy density is in general not comparable to that of conventional carbon based fuels.

One of the primary challenges associated with on-board storage and handling of liquid hydrogen is its extremely low temperature, ( $-253^{\circ}\text{C}$  at atmospheric pressure), making it one of the coldest cryogenic fluids. Therefore, specific equipment is needed for its storage and handling, and this results in still limited availability and high costs. Nevertheless, liquid hydrogen emerges as one of the few viable solutions for transporting substantial quantities of hydrogen over long distances and powering large and long-range vehicles such as airplanes and ships [17].

The utilization of hydrogen as a fuel in the maritime sector presents distinct challenges, due to the absence of infrastructures for hydrogen storage and distribution worldwide. The retrofitting of existing ships with hydrogen tanks, fuel cells, electric motors or hydrogen-powered internal combustion engines is a fundamental prerequisite for its implementation in the sector [17].

Various methods can be employed to generate the power required for propulsion and onboard energy supply using LH<sub>2</sub>, including internal combustion engines, fuel cells, hybrid systems combining batteries and fuel cells, as well as gas or steam turbines. Most of the literature studies are based on the utilization of fuel cells systems or hybrid setups to maximize the ship efficiency. Kawasaki Heavy Industries stands out as the only company to design ship utilizing liquid hydrogen in gas engines. [17]

In particular, fuel cells demonstrate the highest efficiency, with a range of 50% to 60% and potentially greater efficiency when heat recovery system is integrated. Conversely, adapted combustion engines achieve lower efficiencies, between 40% and 50%. The conversion of hydrogen into energy in fuel cells results in zero emissions, producing only water as product. Therefore, the overall emissions from Well-To-Wake depend entirely on the method of hydrogen production. It is also possible to utilize dual-fuel internal combustion engines, blending hydrogen with conventional fuels, enhancing both combustion properties of the engine while reducing the greenhouse gas emissions. More specifically, even a 50/50 mixture of heavy fuel oil and hydrogen could reduce CO<sub>2</sub> emissions by up to 43% per ton-kilometer. Nowadays, efforts to design single-fuel hydrogen combustion engines are also performed.

Currently, the Suiso Frontier is the only operational liquid hydrogen ship. It is a liquid hydrogen carrier, which transport 1250 m<sup>3</sup> of liquid hydrogen, obtained through brown

coal gasification coal in Australia, from the Hastings port towards the port of Kobe in Japan covering a distance of 9000 km [17]. The Suiso Frontier, represented in Figure 3 is propelled by a diesel engine developed by Kawasaki Heavy Industries, and was designed and constructed in 2019 during the HySTRA project.



*Figure 3 Suiso Frontier liquid hydrogen tanker [35]*

Other liquid hydrogen vessels are currently under construction or in design phase. An extensive review of the liquid hydrogen vessels currently in design and of the conceptual designs developed in literature is presented in [17].

## 1.3 Aim of the work

In this thesis, the assessment of a Mediterranean hydrogen generation hub powered by an offshore floating wind farm for the decarbonization of the maritime shipping sector was carried out. The Mediterranean sea currently hosts one-third of the global container shipping services and in recent years, it has ranked first in terms of trade growth. The proposed hydrogen generation hub was situated in the Strait of Sicily, specifically within the Southern Sicily Continental Shelf maritime region. This region holds strategic significance for the international shipping sector, as it encompasses the core route connecting the Suez Canal to the Gibraltar Strait, which are two primary chokepoints as identified in Figure 2.

A technoeconomic analysis was performed considering two different scenarios, calculating the levelized cost of hydrogen (LCOH) and the net present cost (NPC) for each scenario.

In the first scenario, the proposed plant is composed of two main sections, namely the wind farm and the liquid hydrogen production and distribution facility. The plant was considered to be disconnected from the electrical grid and the liquid hydrogen produced is entirely employed to perform the vessel refuelling directly on sea.

In the second scenario, the plant was modified considering a subsea pipeline connection with the port of Porto Empedocle transporting the gaseous hydrogen produced by the electrolyzer. In this case, the refuelling is performed onshore.

A variation of the selected target ship categories in the two scenarios was considered. More specifically, in the first scenario the offshore refuelling is intended to be performed for medium-size cargo ships, whereas in the second scenario is performed the onshore ship refuelling for the other vessel categories excluded in the first scenario.

Therefore, the aim of the work is to assess the techno-economic feasibility of the proposed plant for the two scenarios evaluating the LCOH, evaluating which of the two alternatives is more convenient at the current technological state of the art.

# 2 Plant Components

## 2.1 Plant layout

The plant proposed in this work is composed by a high number of components. Therefore, to have a clear understanding of the system operation, these components can be schematized as listed below:

- Wind farm
- Water treatment system
- Electrolyzer
- Hydrogen liquefaction system
- Liquid hydrogen storage
- Refuelling station
- Platform

The offshore platform hosts the water treatment system, the electrolyzer, the hydrogen liquefaction system, the liquid hydrogen storage tank, the refuelling station and all the auxiliary components necessary for the plant functioning. The general plant layout can be visualized in the following figure:

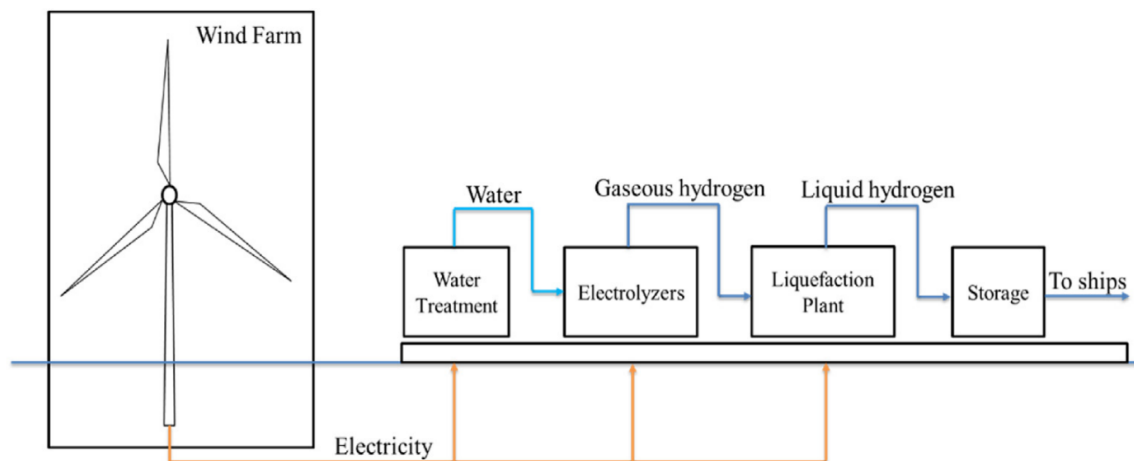


Figure 4 Plant layout [14]

Two offshore electrolysis configurations were analyzed: centralized and individual (in turbine) electrolyzers. In the centralized electrolysis configuration, the power produced by the wind farm is transmitted through underwater cables to the platform. A fraction of the wind farm power output is used to run the water treatment system, the liquefaction plant, the refuelling station and the associated auxiliaries, while the remaining part is used to run the electrolyzer.

This configuration presents two main problems: firstly, in case of failure of the water treatment system or of the electrolyzer system there is a disturbance in the whole system because the centralized configuration has no redundancy; secondly, the brine discharge in a concentrated area could have a great impact on the marine ecosystem [3].

Contrarily, the individual electrolyzer configuration is not affected by these two abovementioned problems.

First of all, in this configuration each turbine is equipped by one electrolyzer, a sea water treatment system and respective auxiliaries. These components are hosted onto the wind turbine platform, which should be modified to accommodate the additional weight, to create a floor on which components are placed and a structure to shield from waves and water splashing [4]. The semi-submersible platform, among the different floating platform, is the most promising option mainly because of the ample deck area. The footprint and weight of the components in this configuration has a higher importance with respect to the centralized configuration. The gaseous hydrogen produced by the electrolyzer should be transmitted to the central platform through unbonded flexible pipes to be then liquefied by the liquefaction system. The main advantage of this configuration is that in case of electrolyzer fail, hydrogen production does not stop because it continues in other turbines [3].

Secondly, another advantage of this decentralized configuration with respect to the centralized is that the brine discharge is decentralized, and this reduces the risk of a negative impact on the marine ecosystem [3].

Considering that the decentralized electrolysis configuration increases further the degree of complexity of the system, the centralized electrolysis configuration was selected in this work.

## 2.2 Wind farm

The Mediterranean Sea is characterized by the presence of significant water depths relatively close to the coastline. This precludes the large scale deployment of the bottom fixed wind turbines, whose installation is not feasible in water deeper than 60 m. On the other hand, there are extensive regions suitable for the deployment of floating offshore wind turbines. More specifically, these areas include much of the Aegean and Adriatic Seas, the areas surrounding the Balearic Islands, Malta, Cyprus and Sicily [5].

A critical factor in the exploitation of the potential wind resource in deepwater is the cost competitiveness of floating wind technology compared to the more established fixed-bottom offshore technology [6]. However, it is expected in the coming years a rapid reduction of the floating wind prices which will give economically competitive access to the abovementioned resources [4]. Differently from bottom fixed wind turbines, floating turbines could also be completely assembled on land and be subsequently towed to the project location using a standard tugboat; this simplified installation process can contribute to cost reduction particularly as economies of scale will have their effect with the production of multiple floating substructures. Moreover, the technology readiness level (TRL) of floating wind turbines was already demonstrated to be advanced by several prototypes and small pilot farms which are currently under construction in Europe. However, despite this technical readiness, the cost remains high [4]. The cost reduction needed to make these technologies more economically viable could be reached through commercialization, increasing investments [3].

As far as concern the foundation structure, nowadays more than 30 floating wind concepts are under development and there is not a definitive winner among them, because each concept is characterized by its own strengths and weaknesses. These attributes are frequently influenced by the unique conditions of the specific site in question. In the following figure is presented a schematization of some categories of floating and bottom fixed foundation structures.

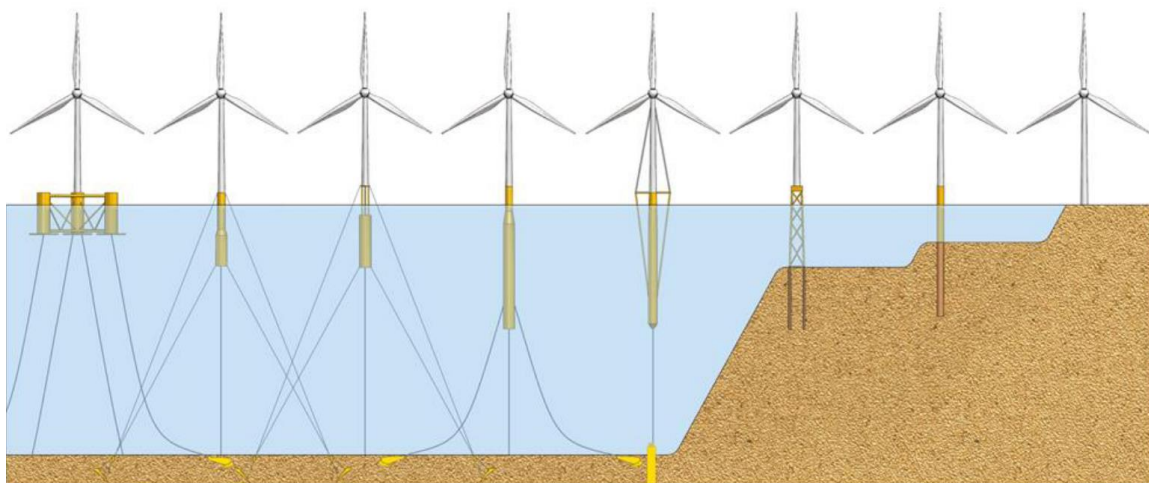


*Figure 5 Floating and bottom fixed foundation structures [22]*

A floating wind turbine is a complex system composed by the wind turbine, floating the substructure, the mooring and anchoring systems.

## 2.2.1 Floating substructure

The floating substructures can be classified in three dominant categories: the semi-submersible, the spar-buoy and the tension leg platform. A schematic representation of these main substructures is presented in the following figure:

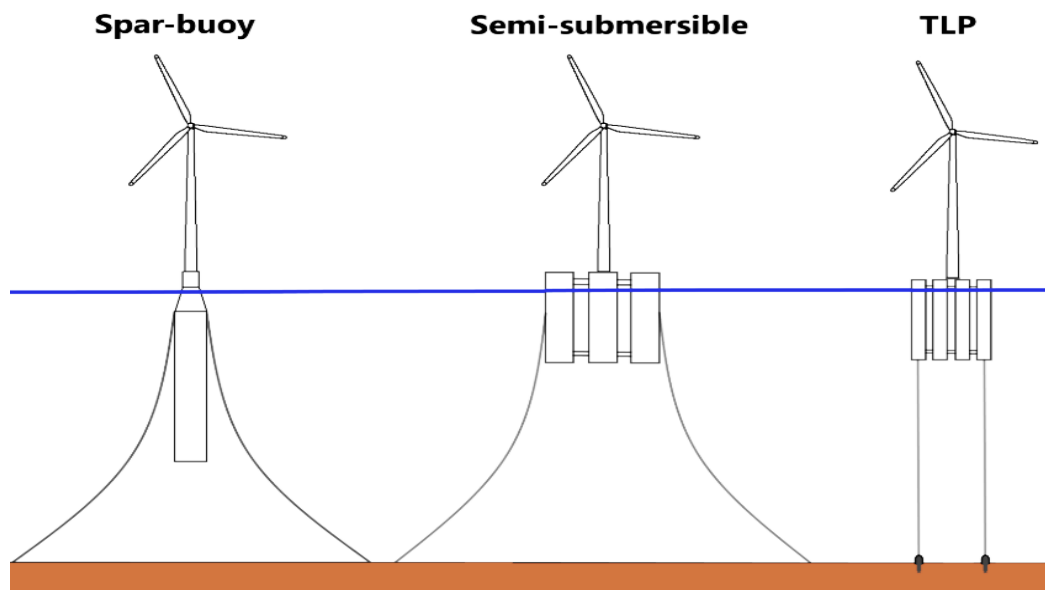


Figure 6 Main floating wind substructures [20]

The semi-submersible is a buoyancy stabilized platform that remains semi-submersed on the ocean's surface. This design typically necessitates a heavy and large structure to maintain the stability, and it anchored to the seabed using catenary mooring lines. Moreover, it is characterized by a shallow draft, which represents an advantage because it enables more versatile applications and simpler installation. More specifically, it can operate in shallow water depths, allows the turbine assembly onshore and the utilization of basic tug boats for its installation in the project site [6].

The spar-buoy instead consists in a cylindrical ballast-stabilized structure, which achieves the stability by having its center of gravity lower in the water than its center of buoyancy. This means that the upper part of the structure is light, while the lower section is typically heavier, raising therefore the center of buoyancy. The design is simple and easy to manufacture and it provides excellent stability. A disadvantage with respect to the other two categories consists in the fact that it requires significant draft. This can pose logistical challenges and at the same time limits its deployment in water deeper than 100 m. In the considered plant location this category of substructure cannot be employed, since the water depth of the selected location is not exceeding 100 m, as will be better explained in the following chapters. A disadvantage of this design with respect to the other two consist

in the fact that the turbine assembly has to be performed offshore and requires dynamic positioning vessels and heavy lift cranes, which increase the complexity and the cost of the installation process [6].

The tension leg platform (TLP) is a semi-submerged buoyant structure which is anchored to the seabed using tensioned mooring lines to provide the required stability of the system. This design is characterized by a shallow draft, relies on tension for stability, resulting therefore in a smaller and lighter structure. This permits, as the semi-submersible type, to perform the turbine assembly onshore. A disadvantage of this design with respect to other two is that high loads are placed on the mooring and anchoring systems due to the tension requirements. [6]

## 2.2.2 Mooring system

Floating wind turbines are kept in position through mooring and anchoring systems, whose dimensioning is defined in function of the soil characteristics, which are site dependent and must be determined by geophysical and geotechnical investigations. Nowadays, the most common mooring systems can be divided into three classes: catenary (a), semi-taut (b) and taut-leg (c). A schematic representation of these is presented in the following figure:

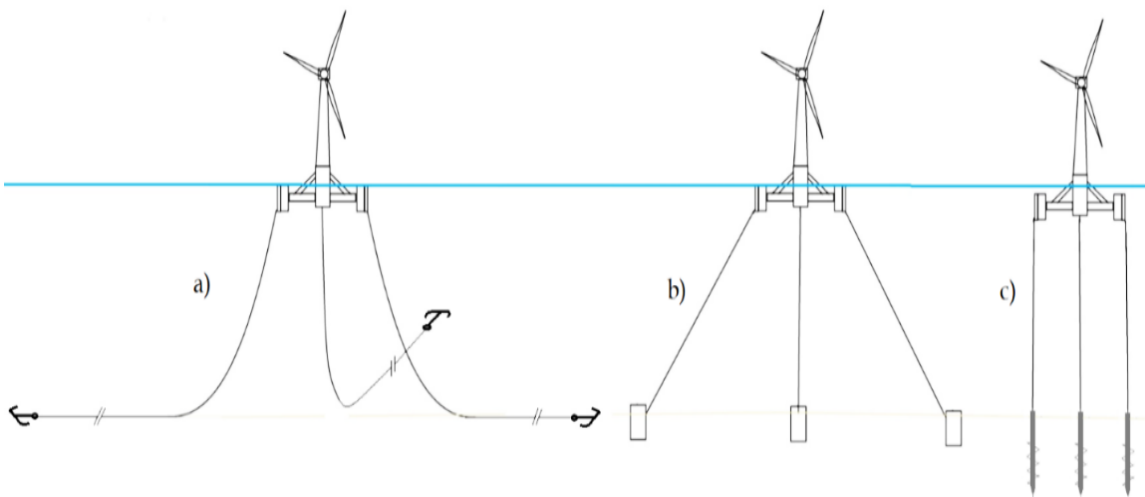


Figure 7 Main mooring system classes [7]

The catenary mooring configuration (a) employs long steel chains and wires, majorly suspended in water, which connect the floating platform to the anchoring system. The catenary mooring takes this name because the mooring lines suspended in water take the characteristic shape of a catenary curve, which is geometrically equal to the graph of a hyperbolic cosine function [7]. This curved shape plays a crucial role in holding the floating platform in place. More specifically, as the floating wind turbine moves from its equilibrium condition, the variation of the catenary geometry from its equilibrium condition creates the restoring force, due to the weight of lines, necessary to bring back

the floating wind turbine to the equilibrium position. The long mooring lines partially rest on the seabed and this reduces the loads on the anchors, which are mostly subjected to horizontal forces.[6,7] Compared to taut-leg and semi-taut, this mooring configuration presents greater freedom of movement. This results in a larger footprint associated to the lower section of the chain that rests on the seabed, which moves in stormy conditions [6]

The taut-leg mooring configuration presents taut synthetic fibers or wires which connect the floating platform to the anchoring system. The taut wires use the buoyancy of the floater and firm anchor to the seabed to maintain the high tension needed to maintain the floater stability [6]. Such system require pre-tensioning to guarantee a mooring line tension sufficiently high to keep them taut and able to provide the restoring force when floater tends to move from its equilibrium condition due to environmental loads [7]. In this configuration the restoring force is related to the elastic modulus of the mooring line material. Differently from catenary mooring, a very limited horizontal movement is present, since at the anchoring point the load is vertical. This very limited horizontal movement implies a minimal disruption of the seabed [6].

The semi-taut mooring configuration consists in taut synthetic fibers or wires which connect the floating platform to the anchoring system. The mooring lines are inclined with respect to the seabed, usually around 45 degrees with respect to the anchoring point. Therefore, both horizontal and vertical load components are transferred to the anchors [6,7].

### **2.2.3 Anchoring system**

It exists a large variety of anchoring systems available, differing in shape and installation method. Numerous factors, such as the seabed conditions, the adopted mooring configuration, the required holding capacity [6] and the seabed depth have to be taken into account in the selection of the most suited anchoring solution for the specific plant location. Two degrees of freedom in the dimensioning of the anchoring system are the anchor weight and size. Heavier and larger anchors typically generate greater holding capacity [6].

An anchoring system has to fulfill two primary performance requirements: capacity and installability. In particular, an anchoring system must exceed the design value of the mooring load applied via the attached mooring line, throughout its entire design lifetime. Moreover, the anchor must be reliably installable in the local seabed condition, to a specific embedment depth at which the required holding capacity is available [8]. In this context, the design optimization has to meet the capacity and installability requirements minimizing the costs and risks [8].

The angle and magnitude of the load transferred to an anchoring system depends on the type of mooring employe [8]. Therefore, certain anchoring configurations are better suited for specific mooring configurations. More specifically, catenary mooring configurations

frequently employ drag-embedded anchors to manage the horizontal loading which is prevalent, although piled and gravity anchors can also be used. On the other hand, taut-leg moorings typically rely on suction piles, drive piles or gravity anchors to handle the significant vertical loads which are applied to both the anchoring and mooring systems [6].

The seabed conditions are a key parameter in the choice of the anchoring system. In general, higher holding capacities are typically achieved in sands and hard clays compared to soft clays. Instead, where the seabed penetration is challenging, configurations as the gravity based or piled anchors may be necessary to ensure the required holding capacity [6].

In Figure 7 is presented a schematic representation of the main anchor configurations, which have been already extensively used in the oil and gas industry and maritime sector.

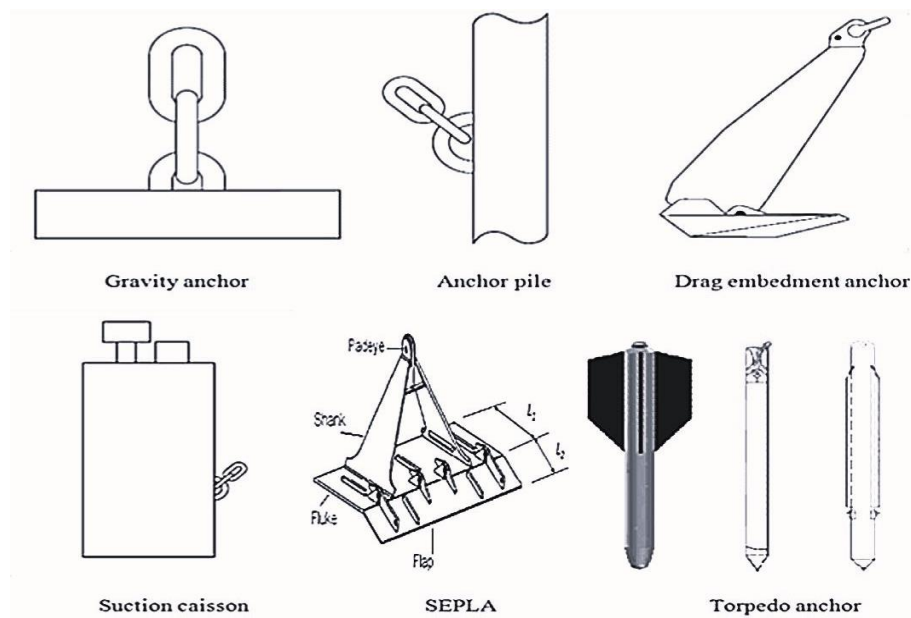


Figure 8 Main anchor configurations [20]

## 2.2.4 Selected wind turbine

In this work, a floating offshore wind farm located in the Mediterranean Sea was considered. The wind farm is composed by 20 turbines, each having a power rating of 15 MW, for a total power rating corresponding to 300 MW. More specifically, it was selected the IEA 15-Megawatt Offshore Reference Wind Turbine [9], designed by the National Renewable Energy Laboratory (NREL) and the Technical University of Denmark (DTU).

The turbine is classified as a Class IB direct-drive machine, with a hub height of 150 m and a rotor diameter of 240 m. The tower height was selected in order to have a hub height of 150 m, while length of each blade is equal to 117m and it is designed to reach a

power coefficient  $C_p$  equal to 0,489. Moreover, it adopts a direct-drive configuration, utilizing a permanent magnet, synchronous radial flux generator that results in simple and compact nacelle. The direct drive generator presents several advantages with respect to geared drivetrains such as a reduced number of components, increased reliability, decreased complexity and higher flexibility in designing. However, the direct coupling of the generator at very low speeds necessitates higher mass and larger physical dimensions, which can pose challenges in terms of assembly, transportation and maintenance. [9]

The cut-in wind speed of the turbine is equal to 3 m/s, the rated wind speed to 10,59 m/s and the cut-out wind speed to 25 m/s. The key parameters for the IEA wind 15-MW turbine are listed in the following table:

*Table 1 IEA 15-MW reference turbine key parameters [9]*

<b>Parameter</b>	<b>Units</b>	<b>Value</b>
Power rating	MW	15
Turbine class	-	IEC Class 1B
Specific rating	W/m <sup>2</sup>	332
Rotor orientation	-	Upwind
Number of blades	-	3
Control	-	Variable speed Collective pitch
Cut-in wind speed	m/s	3
Rated wind speed	m/s	10,59
Cut-out wind speed	m/s	25
Design tip-speed ratio	-	90
Minimum rotor speed	rpm	5,0
Maximum rotor speed	rpm	7,56
Maximum tip speed	m/s	95
Rotor diameter	m	240
Hub height	m	150
Hub diameter	m	7,94
Blade mass	t	65
Drivetrain	-	Direct drive
Shaft tilt angle	deg	6
Rotor nacelle assembly mass	t	1017
Tower mass	t	860

In the following Figure 8 are represented the generator power curve (in blue) and the rotor thrust curve (in red) of the reference turbine:

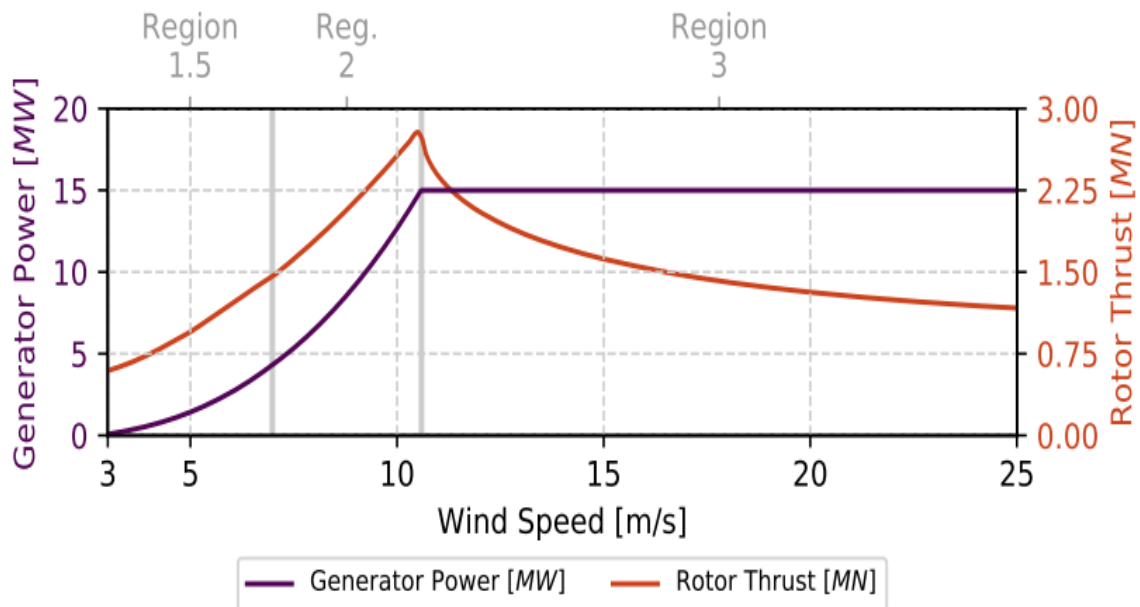


Figure 9 Power and thrust curves of the reference turbine [9]

The UMaine VoltturnUS-S Reference Platform [10] was specifically designed by the University of Maine to support the IEA-15-240-RWT 15-megawatt reference wind turbine. The reference platform falls into the category of semisubmersible substructures and is composed of four steel columns. The hull includes three radially spaced buoyant columns with a diameter of 12,5 m, whose centers are located 51,57 m from the vertical axis of the tower. The connection between tower and platform is situated on the top of a fourth buoyant column positioned at the center of the platform. The central column that sustain the turbine is linked to the outer buoyant columns through pontoons at the bottom and radial struts at the top [10]. A schematic representation of the described UMaine VoltturnUS-S Reference Platform is given in Figure 9.

The designed mooring system consists of three chain catenary lines, each connected to one of the platform's three outer buoyant columns. The catenary lines radially extend to anchors which are equally spaced at 120 degrees in the surge-sway plane. [10]

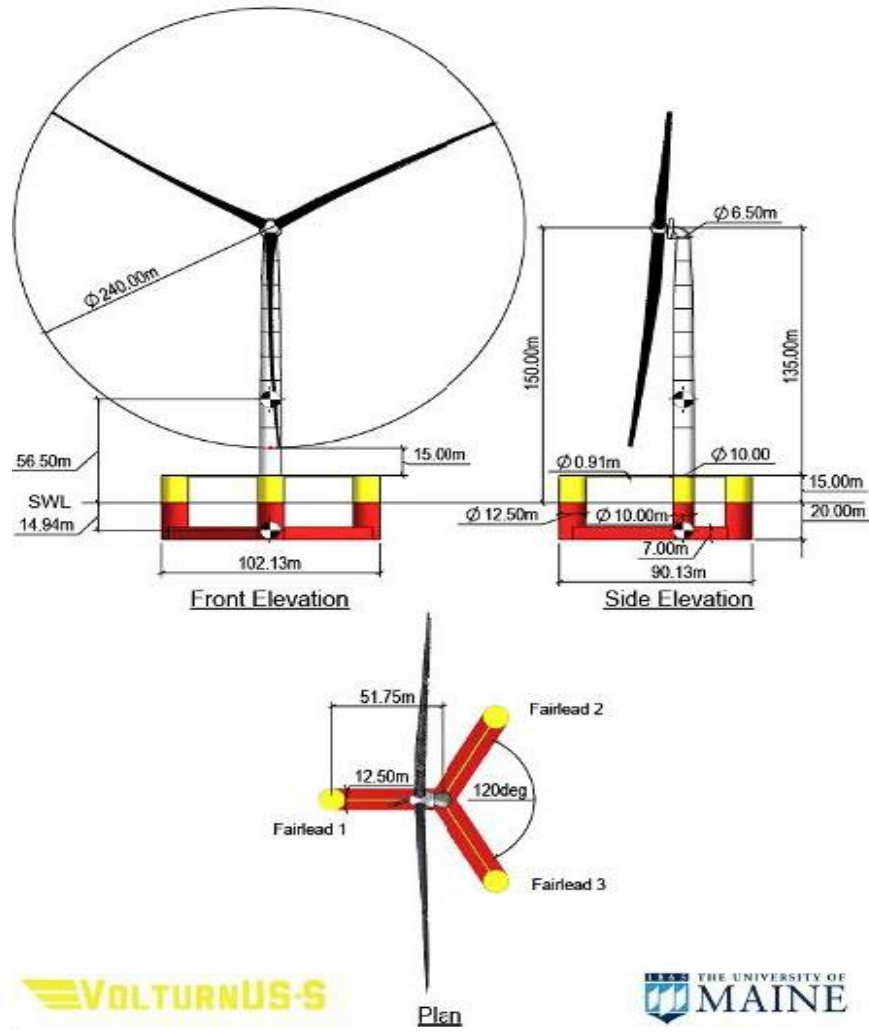
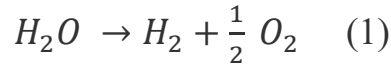


Figure 10 UMaine VoltturnUS-S Reference Platform [10]

## 2.3 Electrolysis

A water electrolyzer is a device that allows the splitting of the water molecule in hydrogen and oxygen atoms through a chemical reaction, when direct current electricity and water are supplied to the cell. The overall water electrolysis reaction is described in equation (1):



Although the various water electrolysis technologies are characterized by the use of different materials and may have slight operational variations, they all share a common structure consisting in an anode and a cathode separated by an electrolyte. Nowadays, the Proton Exchange Membrane Electrolyzer (PEMEL) and the Alkaline Electrolyzer (AEL) are employed in commercial applications for the production of hydrogen [4].

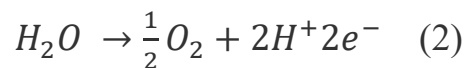
The PEMEL and AEL technologies are low temperature electrolysis technologies, and are identified as the most promising technologies for the production of hydrogen in near and mid term, when coupled with wind turbines. More specifically, when coupled with a variable renewable power source as offshore wind, the electrolyzer must be able to follow the variation in electrical supply. Therefore, fast response and high range of operability conditions are key aspects to take into account [3].

PEMELs, with respect to AELs are characterized by faster start-up times, higher hydrogen purity, higher output pressure, possibility to operate beyond the nominal power and higher current densities [4]. Moreover, they are characterized by fast response, allowing the quick adjustments in hydrogen production to meet the fluctuation of the electrical input [3], by high conversion efficiency, also at partial load operation, by compact and modular design, which is a characteristic of undoubtedly importance in the proposed plant due to the limited space available.

In the proposed system the electrolyzer is placed offshore and not grid connected. In this context, another advantage of the PEMEL is that during standby periods it requires low amount of energy to maintain system operation [4].

For the abovementioned characteristics, the proton exchange membrane electrolyzer was selected in this study.

For an electrolyzer with a protonic conductor as electrolyte, the overall water electrolysis reaction of equation (1) is the combination of the anodic half reaction of equation (2) and the cathodic half reaction of equation (3).



A schematics of the proton exchange membrane cell is showed in the following figure:

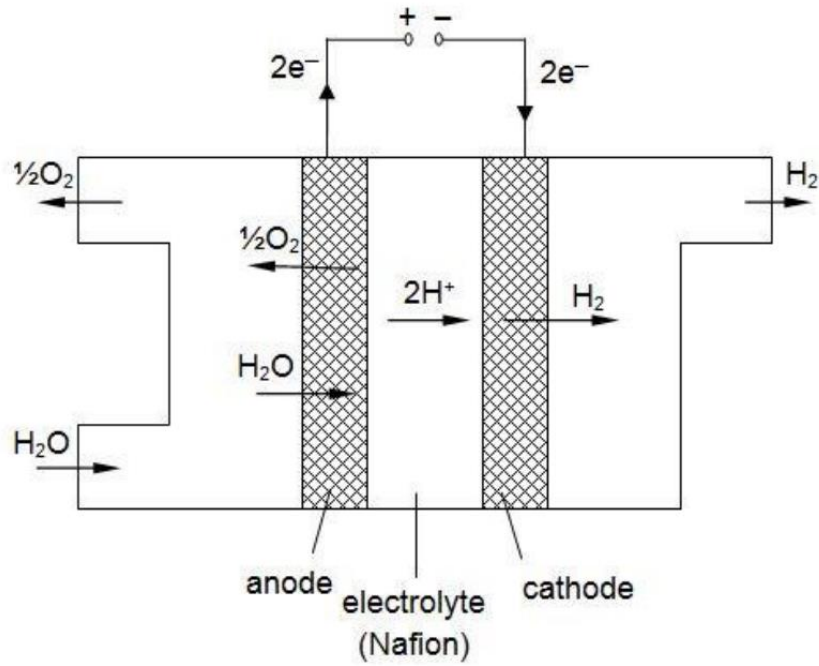


Figure 11 Proton exchange membrane cell schematic representation [11]

The cell and system efficiency curves of the PEM electrolyzer at 60°C and 30 bar is showed in the following figure:

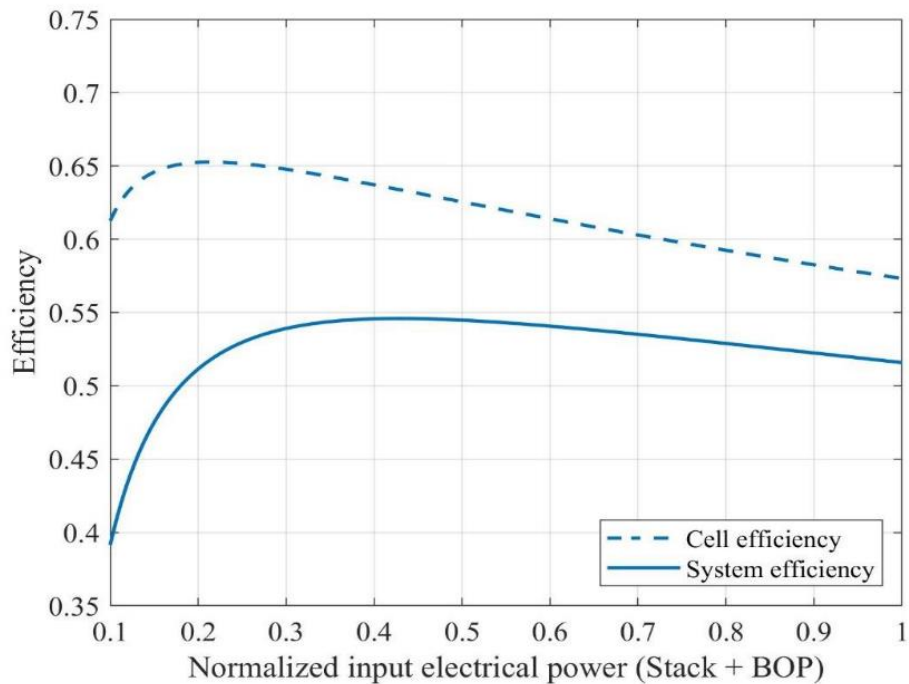


Figure 12 Cell and system efficiency curves of the PEM electrolyzer [11]

The primary drawback of the PEMELs until now is represented by the high cost, primarily connected to the utilization of noble materials inside the electrolyzer [4]. The high price is connected to the use of expensive catalyst materials used in the cell. More specifically, the central component of the proton exchange membrane cell is the proton-

conducting membrane, whose surface is coated by two catalytic layers. Typically, at the cathode Pt nanoparticles are employed to facilitate the Hydrogen Evolution Reaction (HER). On the other hand, at the anode catalysts as iridium dioxide or alternative catalysts-based particles are used to promote the Oxygen Evolution Reaction (OER) [11].

Despite the significant progress of recent years, PEMELs are still considerably more expensive and shows a reduced lifetime with respect AELs. However, a continuous decrease of capital cost, operation and maintenance costs and of the degradation is expected in the near future.

As reported by [12], a cost reduction and an increase of the performance of the PEMEL technology are predicted in the near future, as it is shown in the following table:

*Table 2 State of the art and 2030 target performance of PEMEL [12]*

<b>Parameter</b>	<b>Unit</b>	<b>2020 SoA</b>	<b>2030 Target</b>
Capital cost	€/kW	900	500
O&M cost	€/(kg/d)/y	41	21
Electricity consumption	kWh/kg	55	48
@nominal capacity			
Degradation	%/1000h	0,19	0,12
Cold start ramp time	sec	30	10
Current density	A/cm <sup>2</sup>	2,2	3

The cost reduction is associated with a reduction of the utilization of critical raw materials as catalysts, from 2,5 mg/W registered in 2020 SoA to the target value of 0,25 mg/W in 2030.

## 2.4 Water treatment

PEM electrolyzers cannot be operated directly with seawater, because its direct use can cause corrosion damage and lead to chlorine production [3]. In particular, electrolyzers need to process water with a water purity of maximum 0.5 ppm total dissolved units (TDS) [13]. Therefore, prior to operating the electrolyzer, the necessary water treatment, namely desalination and purification, must be carried out to ensure the electrolyzer's required water quality and prevent the system from damage.

A water treatment system is normally composed of a pretreatment unit, a desalination unit and a post-treatment unit [14]. The post-treatment performed after desalination typically involves chemical processes, which consist in the use of a filter containing chemicals to collect any remaining ion and other dissolved solids in the desalinated water. Chemicals have to be refilled or changed in the post treatment unit, therefore this represents an additional challenge in the offshore liquid hydrogen production [13].

The different proven desalination technologies for sea water can be divided into electrical and thermal solutions. The Reverse Osmosis is the most common desalination technology and it is seen as the most promising technology for offshore deployment. Moreover, it was already successfully employed paired with PEMEL technology in marine applications, without notably affecting the electrolyzer performances [3]. A disadvantage of the Reverse Osmosis consists in the lower output water quality and consequently in the necessity of more sophisticated post-treatment with respect to thermal solutions [13].

In the proposed system, the Reverse Osmosis (RO) desalination technology was considered. Moreover, the desalination unit was considered to be powered directly by the floating offshore wind farm electricity output.

The RO desalination unit electricity demand is directly depending on the seawater salinity, and the overall specific energy consumption lies within the 2-4 kWh/m<sup>3</sup>H<sub>2</sub>O. The energy consumption is almost negligible with respect to that of an electrolyzer, therefore a total cost increase of hydrogen in the range 0,0088-0,018 €/kg has been estimated [3].

In the centralized electrolysis configuration the seawater treatment presents also environmental issues, mainly deriving from the brine disposal and to the associated risk for the marine life [3].

## 2.5 Liquefaction

Liquid hydrogen has a density of  $70,8 \text{ kg/m}^3$ , namely roughly 775 times compared to the density of gaseous hydrogen at atmospheric conditions [15]. Therefore, the main advantage to work with liquid hydrogen is to deal with a much more denser fluid. Moreover, the storage volumes are decreased and this is an important point in mobility applications, as it is the analyzed case of the maritime shipping sector, and in offshore bunkering facilities, where space is limited.

However, the volumetric energy density of liquid hydrogen is around (8,6 MJ/L), that is much lower with respect to that of diesel fuel (36,3 MJ/L). This reduced energy density is an important aspect for the required vessel storage space and bunkering (refueling) times. In particular the switch from traditional diesel fuels to liquid hydrogen in ships increases the required weight and storage tanks volume on board of a ship [15].

The liquefaction process is performed by cooling down the gaseous hydrogen, in the proposed plant produced by the electrolyzer, to reach the hydrogen boiling point temperature of  $-253^\circ\text{C}$ . Different cooling processes were proved to be suitable for hydrogen liquefaction, namely the Claude, the Linde-Hampson, the pre-cooled Claude cycle and the helium refrigerated system. The most efficient systems are the helium cooled, whereas the one employed in the industrial plants is instead the pre-cooled Claude [15].

Hydrogen undergoes liquefaction at  $-253^\circ\text{C}$ , and under standard ambient conditions it requires a theoretical minimum energy equal to 3,3 kWh/kg for this transformation [16], whereas if gaseous hydrogen is supplied at a pressure of 20 bar it requires 2,3 kWh/kg. Furthermore, a catalytic conversion process which transforms normal hydrogen into 100% para-hydrogen requires an energy input of approximately 0,65 kWh/kg. This conversion is employed to minimize the boil-off formation during subsequent storage [17].

The real energy consumption of a liquefaction system depends on the liquefaction technique, the amount of hydrogen processed and the efficiency of the plant. Nowadays energy consumptions in the range 12,5-15 kWh/kg, which corresponds to 37-45% of the LHV of hydrogen are registered in industrial plants [15]. However, as reported in [18], the European Research Project called IDEALHY has successfully developed an efficient and economically viable process for future large scale hydrogen production plants. In particular, the innovation introduced in the IDEALHY project has the potential to reduce the specific energy consumption required in the hydrogen liquefaction process from current values down to 6,4 kWh/kg. The proposed process consists in five phases: compression, chilling, pre-cooling down to 130 K, cryogenic cooling with Brayton cycles to 26,8 K and finally an expansion and liquefaction stage where liquid hydrogen at 22,8 K is obtained. However, to reach this energy consumption reduction a shift of the coolant was necessary utilizing, instead of liquid nitrogen which is widely available, a combination of liquid helium and neon called Nelium 25 (75% helium and 25% neon),

which instead are rare resources. The adoption of liquid helium was crucial due to its extremely low boiling point, which is  $-269^{\circ}\text{C}$  instead of  $196^{\circ}\text{C}$  of nitrogen. This change of coolant was of primarily importance to reach the desired energy efficiency [18]. A table reporting a comparison of the IDEALHY process and the currently used process is reported below:

Table 3 Currently used liquefaction process and IDEALHY preferred process comparison [18]

	Currently used process	IDEALHY Preferred Process
<b>Hydrogen pressure in process</b>	20 bar	80 bar
<b>Pre cooling</b>	Open $\text{LN}_2$	Mixed refrigerant closed loop
<b>Brayton cycle refrigerant</b>	Hydrogen or helium	Nelium
<b>Brayton cycle compressor</b>	Dry piston compressor or oil lubricated screw compressor	Turbo compressor
<b>Final expansion</b>	Throttle valve or ejector	Gas bearing turbines or piston expander

Nowadays, every large-scale liquefaction facility rely on a version of pre-cooled Claude cycle [16]; therefore, in the proposed plant a pre-cooled Claude cycle was selected for hydrogen liquefaction to be coherent with current technological state. A scheme of this cycle is presented in the following figure:

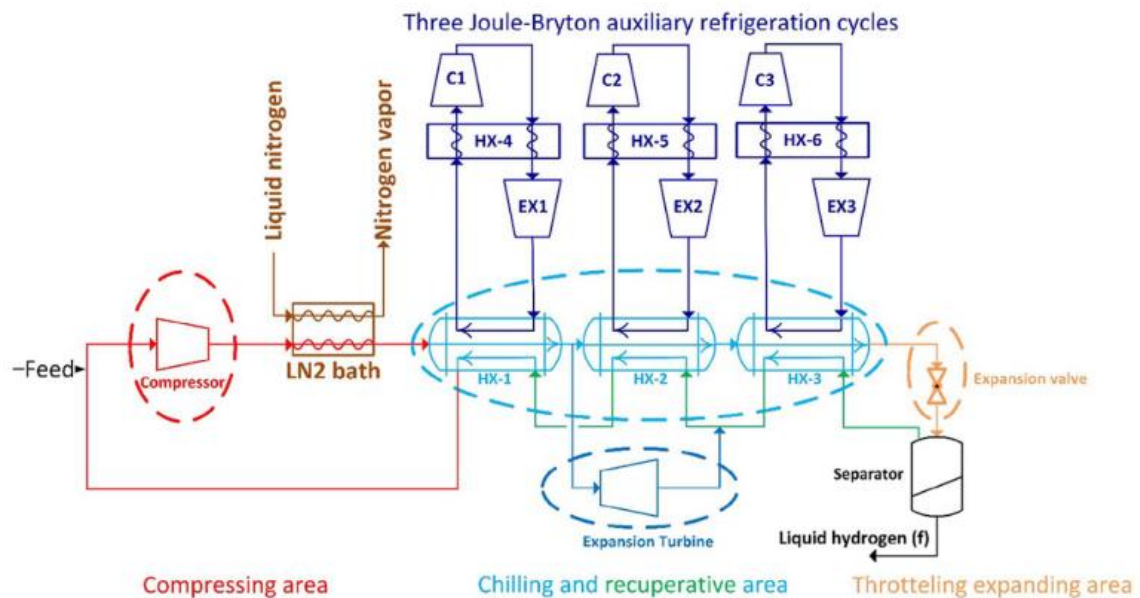


Figure 13 Scheme of the pre-cooled Claude cycle [19]

## 2.6 Storage

The liquid hydrogen produced by the liquefaction system has to be stored in specially insulated cryogenic tanks at temperatures below the hydrogen boiling point, which corresponds to  $-253^{\circ}\text{C}$ .

Cryogenic fuels as Liquefied Natural Gas (LNG) are nowadays widely used in the shipping sector and the gained experience with cryogenic components could be transferred to the Liquid Hydrogen applications. However, the challenges to face in the shipping sector associated to the use of LH are larger with respect to LNG. In fact, with respect to the LNG, the LH is roughly  $90^{\circ}\text{C}$  colder, while the specific heat capacity and the density are lower [15].

In the automotive sector, the shape of the cryogen storage tanks is typically cylindrical with capacities up to 10 kg of liquid hydrogen. To maximize the volume to surface ratio, large volumes of liquid hydrogen are normally stored in double walled spherical tanks with an insulation system. Different insulation systems are available, between them an alternative is represented by the multilayer insulation, which comprises several layers of aluminum foils separated by polymer spacers [17].

Significant technological advancements of LH storage derived from aerospace programs, such as NASA's Space Shuttle programs. The largest LH tank in the world was developed by NASA and is in operation since the 1960's, with a volume of  $3800\text{ m}^3$ [17] and a diameter of 20 m [15].

The technological progress in the cryogenic storage is mainly related to the used materials and tank insulation system. In the NASA abovementioned tank, the insulation is realized with vacuum jacket filled with perlite powder, rather than the multi-layer insulation [17]. Moreover, another insulation system which will be employed in the NASA recently commissioned tank of  $5683\text{ m}^3$  capacity, consists in the replacement of perlite powder with glass bubbles, which demonstrated to better perform with respect to perlite [17].

According to [17], the dimension of future LH storage tanks will increase with time, reaching capacities up to 3500 tons, namely 13 times bigger than the abovementioned existing NASA cryogenic storage, as it is showed schematically in Figure 13.

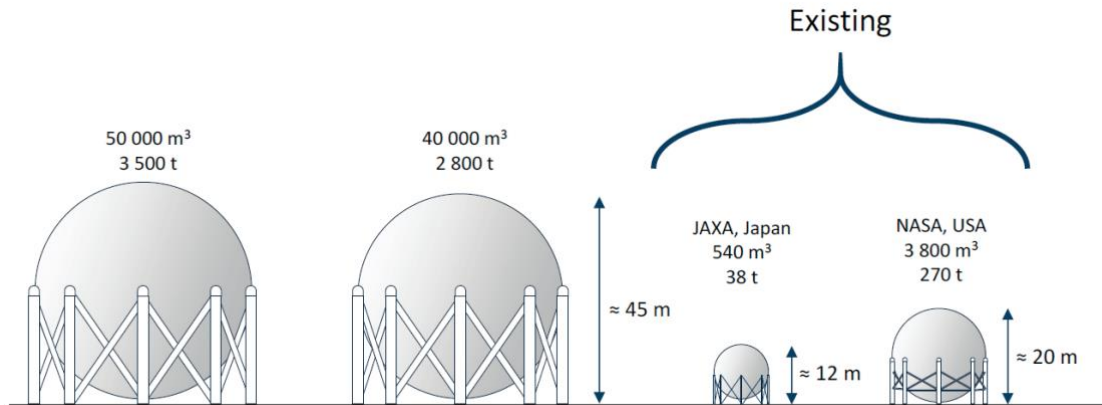


Figure 14 Present and future dimensions of LH storage tanks [17]

The different insulation systems are developed with the objective of reduce the liquid hydrogen losses due to evaporation, called boil-off. The boil-off is connected to the tank size and the insulation system, for instance the evaporated fraction corresponds to 0,4% per day in a 50 m<sup>3</sup> tank and 0,06% in a 20000 m<sup>3</sup> tank [23].

However, in the proposed system the liquid hydrogen boil-off represents a marginal loss. More specifically, due to the constant and high liquid hydrogen demand for ship refueling, the liquid hydrogen is not stored for prolonged time and this consequently results in a marginal loss associated to the boil-off phenomenon. Moreover, considering also the proposed dimensions of the storage tank (around 3000 m<sup>3</sup>) and the abovementioned data from literature, these losses are assumed to be negligible in this work.

As far as concerns the liquid hydrogen utilization in hydrogen powered ships, the boil-off is less problematic with respect to stationary applications. In stationary applications, the evaporated fraction has to be vented in atmosphere resulting in a waste of hydrogen. Contrarily, in the context of hydrogen-powered vessels that utilize liquefied hydrogen for propulsion, the ships could also be designed to operate using the evaporated liquid hydrogen, similarly to LNG carriers [15].

## 2.7 Refueling Station

The most significant challenge in liquid hydrogen refueling process is represented by the extremely low operating temperatures necessary to mitigate the evaporation. Special insulation materials are of fundamental importance in order to minimize the heat flux in into the tank [15]. Moreover, beyond the hydrogen evaporation, different phenomena can occur in the refueling process, including condensation and solidification of substances in contact with LH. Consequently, the LH refueling equipment must be exceptionally well-insulated. Additionally, the presence of air in pipes and ship tanks must be avoided and it has to be eliminated by purging with helium. Moreover, it is necessary the system cool down and warm up to prevent the formation of excessive thermal gradients. [17]

As reported in [24], in order to minimize the refueling time, the vessel storage tank should undergo a pre-cooling process before arrive for bunkering.

Three options were identified by [17] to perform the LH transfer from the storage tank of the plant to the ship storage tank: by pressure differential, using cryogenic pump and combining the two.

The LH transfer by pressure differential method consists in the generation of a pressure differential between the two tanks (storage tank and ship tank). The use of a pressure-build loop consists in the evaporation of a fraction of LH through the use of a vaporizer in the supply tank. The gaseous hydrogen return at the top of the tank and drive the LH flow. Using a pressure differential it is not required the use of power, but cause a heat increase in the tank and consequently of the overall boil-off [17].

The utilization of a cryogenic pump is the most indicated approach when substantial quantities of LH has to be transferred. Cryogenic pumps are built using materials able to work at ultra-low temperature. These pumps must achieve a pressure slightly above 5 bar, matching the maximum operating pressure of the ship tank, to deliver a flowrate ranging from 300 to 1200 kg/min. An additional advantage of employing these pumps consists in the fact that allow a reduced footprint in the refueling station since there is not requirement for refrigeration or high pressure storage [17]. In the refueling station used in ship bunkering, the so called loading arm system (LAS) is often used.

The LAS is a system composed of various components, including valves, dry break couplings, flexible LH hoses, fixed pipelines and safety devices [17].

An application of this type of system for liquid hydrogen ship refueling is represented by the LAS system utilized to transfer LH in the world first LH tanker called Suiso Frontier, developed and built in the HySTRA project to transport liquefied hydrogen from Australia (Hastings) to Japan (Kobe).

To conclude, the liquid hydrogen refueling stations must be equipped with a flow rate meter to monitor the fueling, safety relief devices, pressure sensors, dispenser hose and connectors [17].

# 3 Methodology

## 3.1 Plant location methodology

In the selection of the precise location of an offshore plant producing liquid hydrogen for ship refueling various aspects have to be considered. In particular, vessel route density, bathymetry, mean wind speed, regulatory framework and marine geohazard phenomena have been considered for the localization of the plant.

In this paragraph these aspects are discussed and the precise location of the plant is presented.

### 3.1.1 Vessels route density

First of all, the plant must be placed in an area characterized by a high density of long-distance vessel routes. In this regard, even if the vicinity of an offshore wind farm to an area characterized by a high vessel traffic normally is considered as a disadvantage, from the perspective of performing the refueling operation directly in the sea it represents an advantage.

In fact, this facilitates and increases the speed of the refueling operation by avoiding docking in a port, where ships are subjected to different port fees and tariffs to use port facilities and services such as mooring, pilotage, and towing.

To evaluate the vessel density it has been used the European Marine Observation and Data Network (EMODnet) [25]. EMODnet map viewer catalogue gives access to a rich variety of information. In particular, in the EMODnet Human Activities layers section, the Route Density Map presents the number of routes per square km per year, per season and per month both for all vessels category and each vessel category.

In Figure 14 is showed the annual route density map for all vessels category in the Mediterranean Sea.

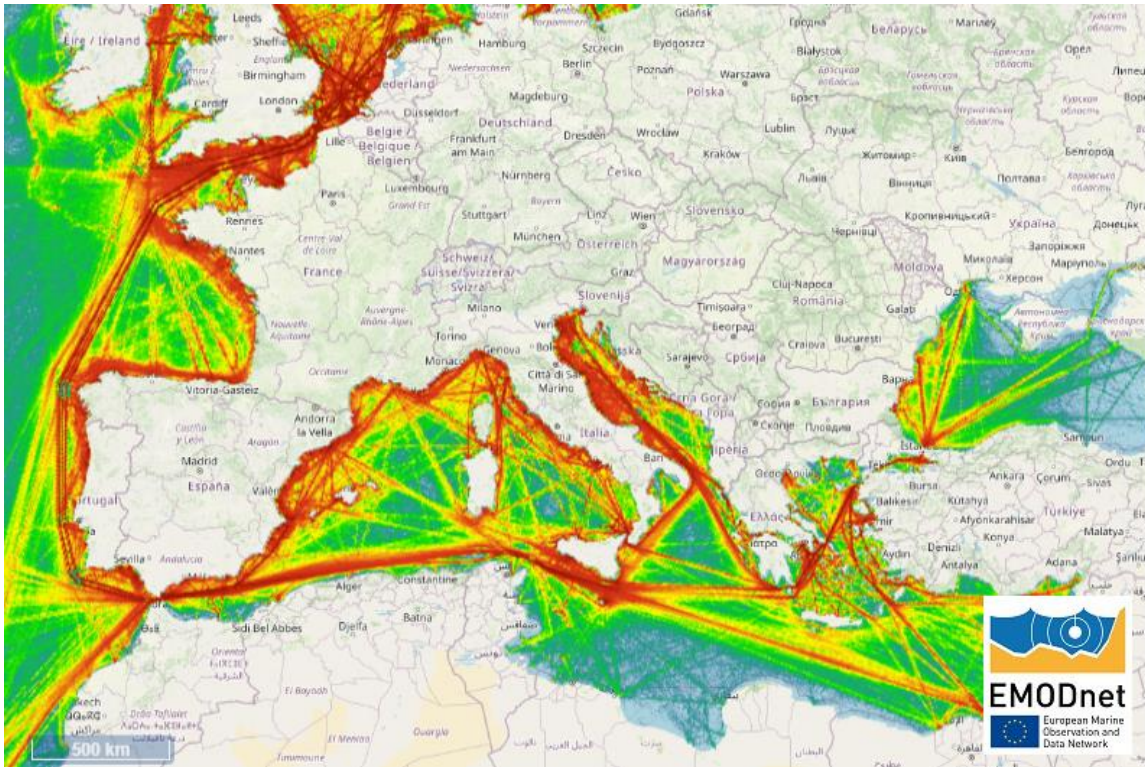


*Figure 15 Annual route density map for all vessels categories [25]*

In the reference scenario of this work, the analysis regarding the utilization of liquid hydrogen as fuel for ship propulsion was restricted to the cargo vessel category only, which typically transport goods for long distances from one port to another one.

Passenger vessels have been excluded from the analysis because of the risk for passengers associated with the offshore refueling. Other vessel categories present in the EMODnet portal have been excluded because of the generality of information. Indeed, this implies a high variability of ship dimensions and fuel tanks capacities, which are fundamental to know to assess the refueling time and to model the liquid hydrogen demand.

The route density map for cargo vessel is represented in the Figure 15.

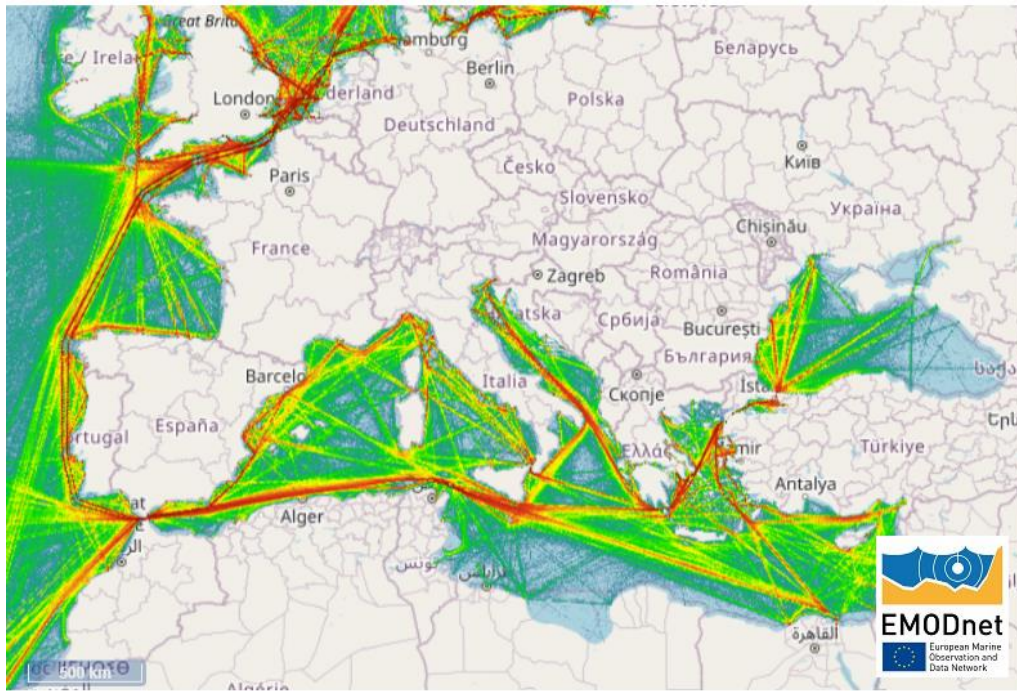


Figure 16 Annual route density map for cargo vessel category [25]

As can be noticed from the map, in the Mediterranean Sea an area of high interest for the localization of the plant is the Strait of Sicily, especially the area between Sicily, Pantelleria island and Malta. This area of the Mediterranean is interested by a high marine traffic deriving especially from Suez Channel to the Atlantic Sea, passing through the Strait of Gibraltar.

The route density map of cargo vessels for the abovementioned area is showed in the following figure:

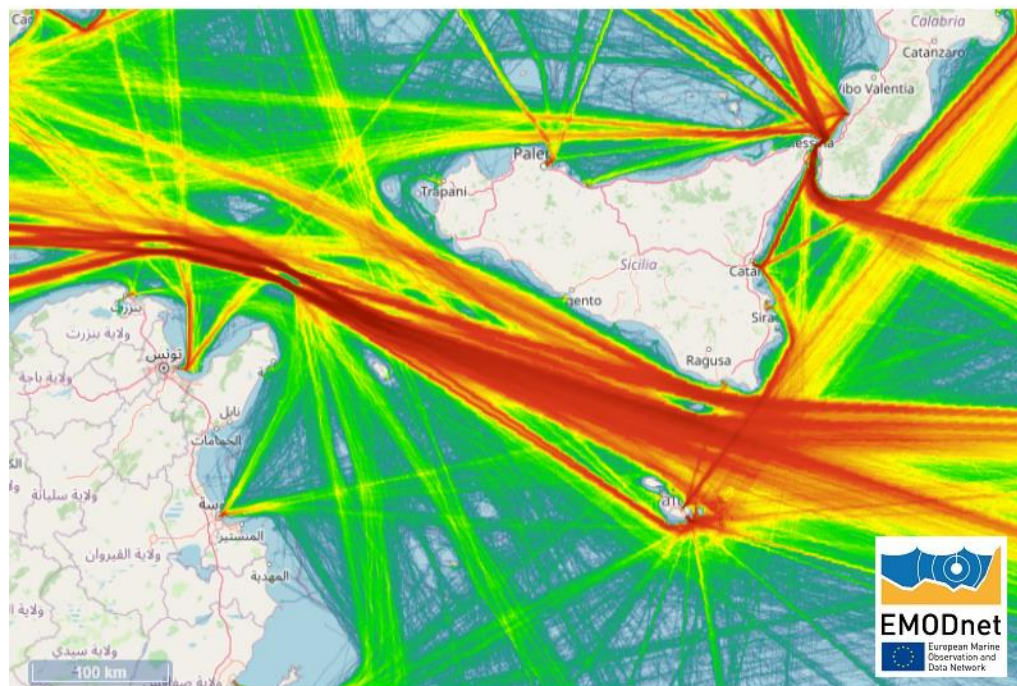


Figure 17 Annual route density map for cargo vessels category in the Strait of Sicily [25]

### **3.1.2 Bathymetry**

The second aspect that has to be considered for the selection of the plant location is the bathymetry of the area of interest, which influences especially the choice of the wind turbine technology, its installation and its cost.

In this work, the offshore floating wind turbine technology has been selected, excluding the bottom fixed one.

Wind turbines with bottom fixed foundations are not economically feasible for water depth higher than 50 m. Moreover, just in specific areas of the world (as the North Sea) the depth is enough low and contemporaneously the mean wind speed enough high for a profitable application of this technology. In fact, considering for instance the Mediterranean Sea, moving away few kilometers from the coastline a depth increase above this limit is normally observed.

Therefore, even if the bottom fixed is a more mature technology with respect to the floating one, and that in the area of interest there exist areas suitable for bottom fixed wind turbines installation, the choice of adopting floating wind turbines has been performed in order to ensure a higher degree of replicability of the model.

The minimum and maximum water depths required for the installation of floating platforms is function of the considered technology. For most floating platform designs, the necessary water depth is roughly 50 m. This is the case of TLP, multi/hybrid and semi-submersible platforms which are suitable for the application in maximum water depths of around 400 m. Whereas, spar floating platforms are capable of operating in deeper waters (up to 500 m) but, due of the large draft required, their minimum water depth is at least 100 m. [6].

Therefore, considering this technological constraint a minimum depth of 50 m has been considered.

From a morphological perspective, the Strait of Sicily is characterized the broad African and Sicilian continental shelves separated by scarp areas and by deep basins, interrupted by submarine mountains and volcanoes, banks and plateaus.

The bathymetric map of the Strait of Sicily is therefore presented in Figure 17.

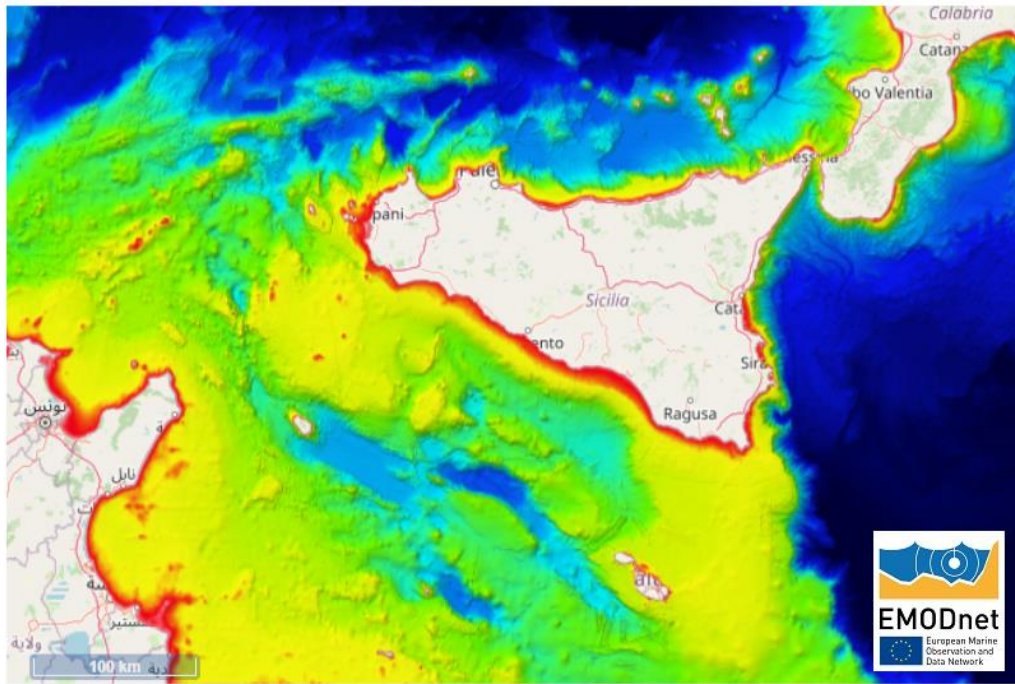


Figure 18 Bathymetric map of the Strait of Sicily [25]

In order to perform the selection of the precise location of the plant, the route density map and the bathymetric contour map have been overlapped, as showed in the following figure:

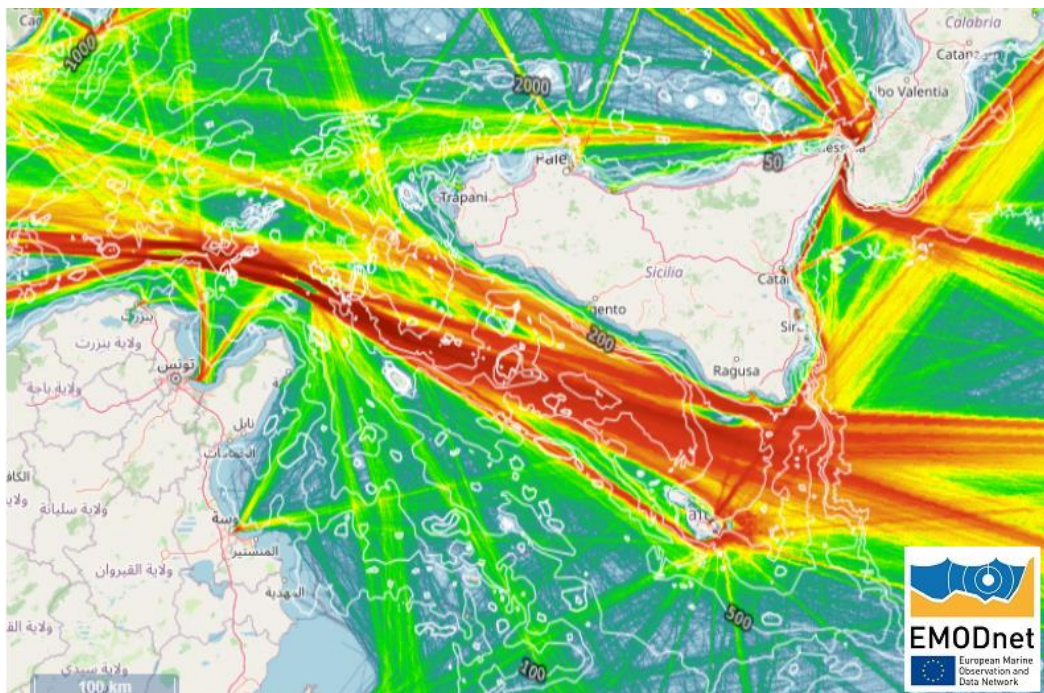


Figure 19 Route density map and the bathymetric contour map overlapping [25]

### 3.1.3 Wind resource

The third constraint considered in the site selection is the wind resource. In particular, the mean wind speed (m/s) at 150 m above the sea level of the specific area of interest showed in Figure 18 has been analyzed. These data have been retrieved from Global Wind Atlas 3.3 [26], a web-based application useful to identify the potential high wind resource areas suitable for wind power generation.

In Global Wind Atlas it is possible to select the height above the sea level (10, 100, 150, 200 m) and the corresponding mean wind speed map is automatically displayed. In this analysis a height of 150 m above the sea level has been selected, corresponding to the hub height of the selected turbine's hub height. For the selection of the site the selected height can be also different, but to have data in line with the following steps of the work the 150 m option has been selected.

The wind speed is a measure of the wind resource and normally a higher mean wind speed indicates better wind resource. The map of the mean wind speed at 150 m is presented showed in the following figure:

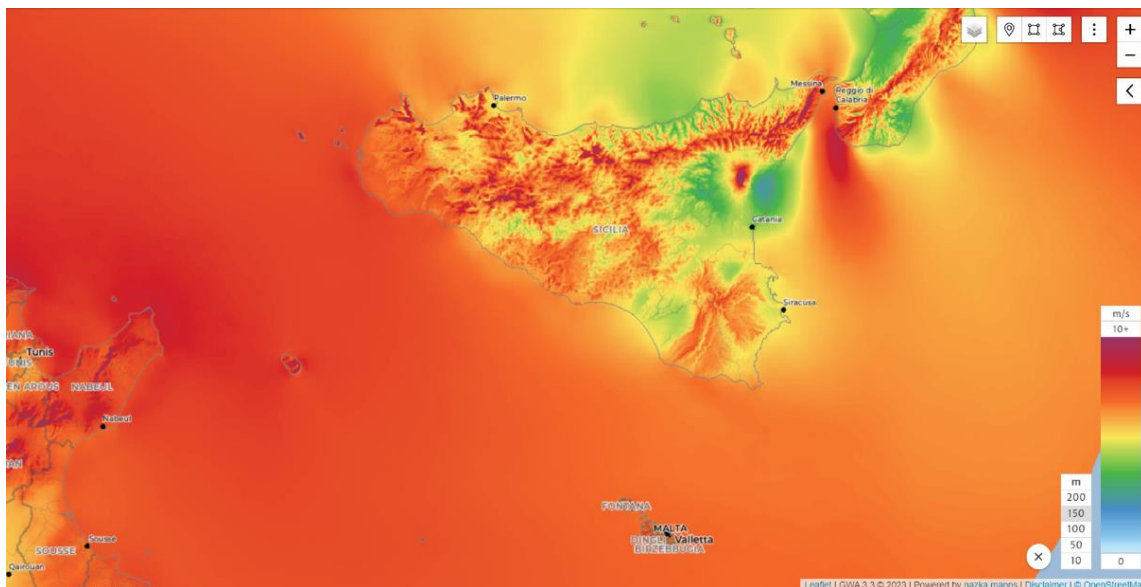


Figure 20 Mean wind speed at 150 m a.s.l [26]

As it can be observed from the map, the mean wind speed at 150 m in the area of interest is relatively homogenous, and not significant variations are present. More specifically, differently from the onshore environment, where the orography and elevation variations are responsible of pronounced variability of the mean wind speed in an area, in the offshore environment the roughness and orography are constant. This results in a more homogeneous wind resource.

In the Strait of Sicily, the wind resource comes predominantly from one direction, as can be appreciated in the wind frequency rose of Figure 20, relative for the site showed on the left of the same Figure 20. Both the map of figure (x) and figure (x) have been obtained from Global Wind Atlas.

The wind rose (wind direction probability distribution) shows the frequency distribution of wind directions at a certain site, therefore gives indication of where the wind comes from.

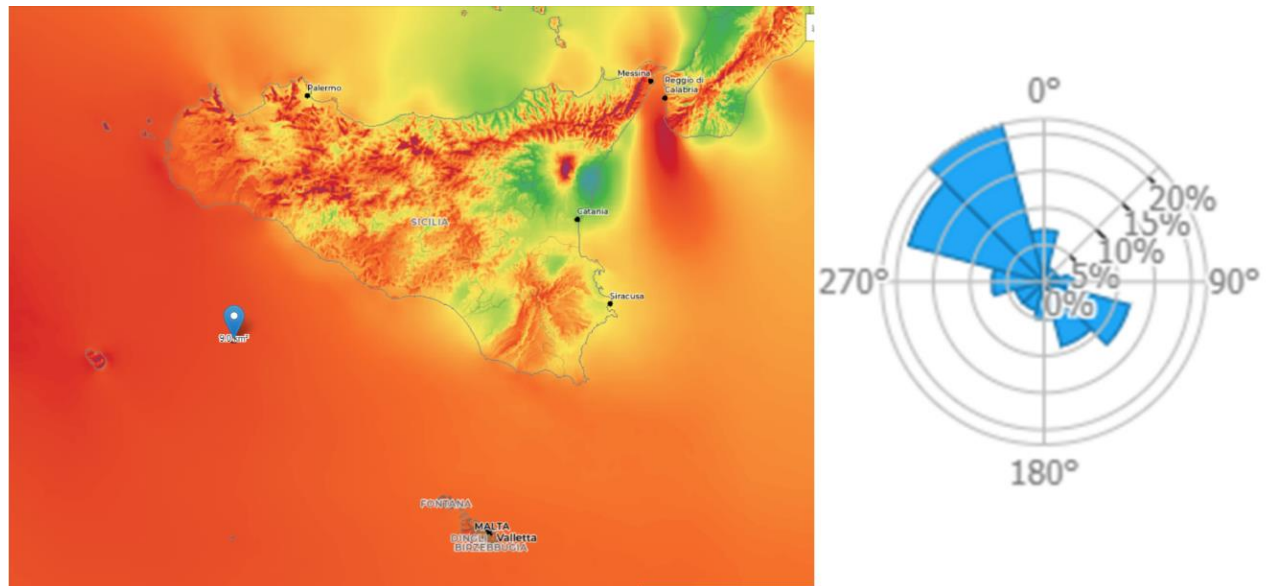


Figure 21 Wind frequency rose of the point indicated in the map [26]

Therefore, the mean wind speed in the Strait of Sicily, even if not subjected to strong variations, is gradually reducing in southeast direction, approaching the Malta Channel (sector of the Strait of Sicily between Sicily and Malta).

### 3.1.5 Geological considerations

The northern side of the Strait of Sicily exhibits notably irregular bathymetry as previously seen in the bathymetry map of Figure 17. This area includes shallow continental shelves like the so called Siculo-Maltese Shelf and the Adventure and Malta plateaus, as well as deep depressions and topographic highs in the form of several small-to middle-scale banks of sedimentary origin including the Nerita, Pinne, Nameless, Terrible and Madrepora banks [27]. The main undersea features cited above are showed in Figure 21.

This uneven bathymetry is the result of the complex tectonic of the area, which is responsible for underwater seismic and volcanic activity in the area. The complex tectonic of the area and the main underwater volcanic structures are showed in Figure 22, where the red dots represent the position of volcanic centers, while the brown and yellow dots sedimentary banks [27].

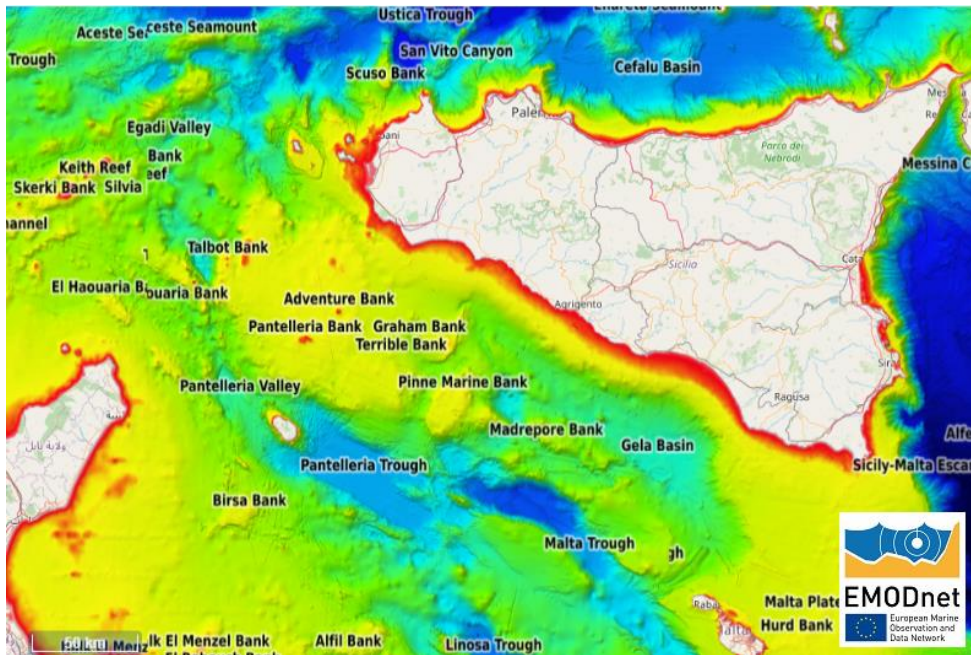


Figure 22 Main undersea features of the Strait of Sicily [25]

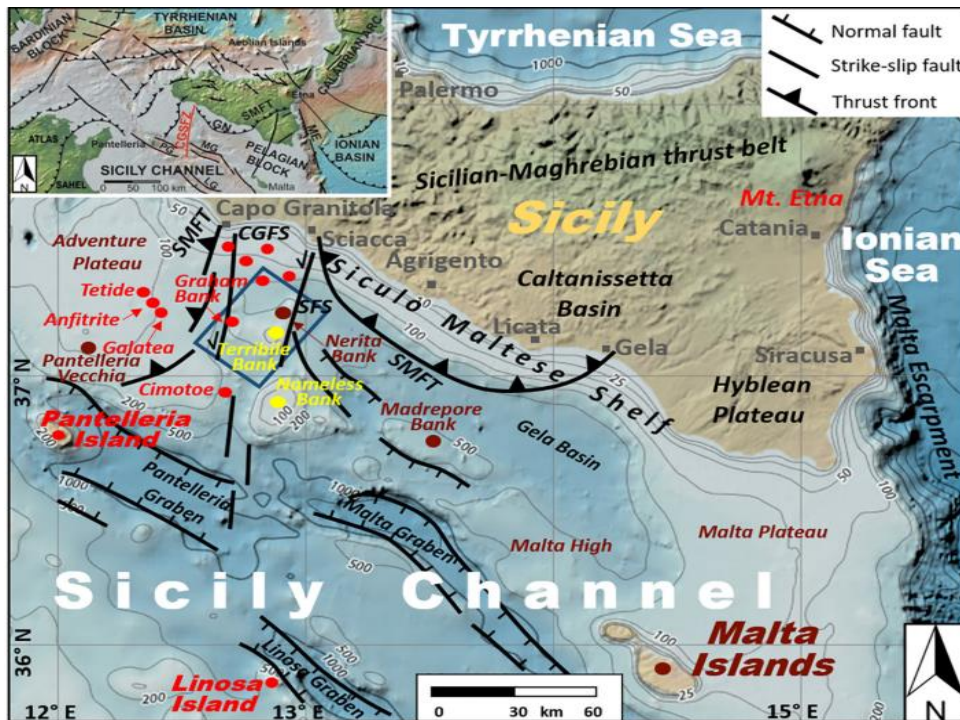


Figure 23 Tectonic of the area and the main underwater volcanic structures in red [27]

The presence of seamounts and underwater volcanoes has been taken in consideration in the selection of the plant location because their presence is associated in both cases to high seabed slope and in the latter case to a higher geohazard. More specifically, the volcanic and seismic activities could create shaking of the seabed and activate slope failures that could damage the anchoring and mooring systems of the plant. To conclude,

the presence of underwater volcanoes could also pose constraints on the choice of the type of anchoring system [28].

### 3.1.6 Habitat preservation

In the selection of the precise location of the plant have been also taken into account the areas which compose the Natura 2000 [29]. Natura 2000 is the main instrument of European Union policy for the preservation of biodiversity. It is an ecological network spread throughout the Union and was created in accordance with the Habitats Directive 92/43/EEC. Its primary objective is to guarantee the long-term preservation of natural habitats and the protection of both fauna and flora inside the European Union.

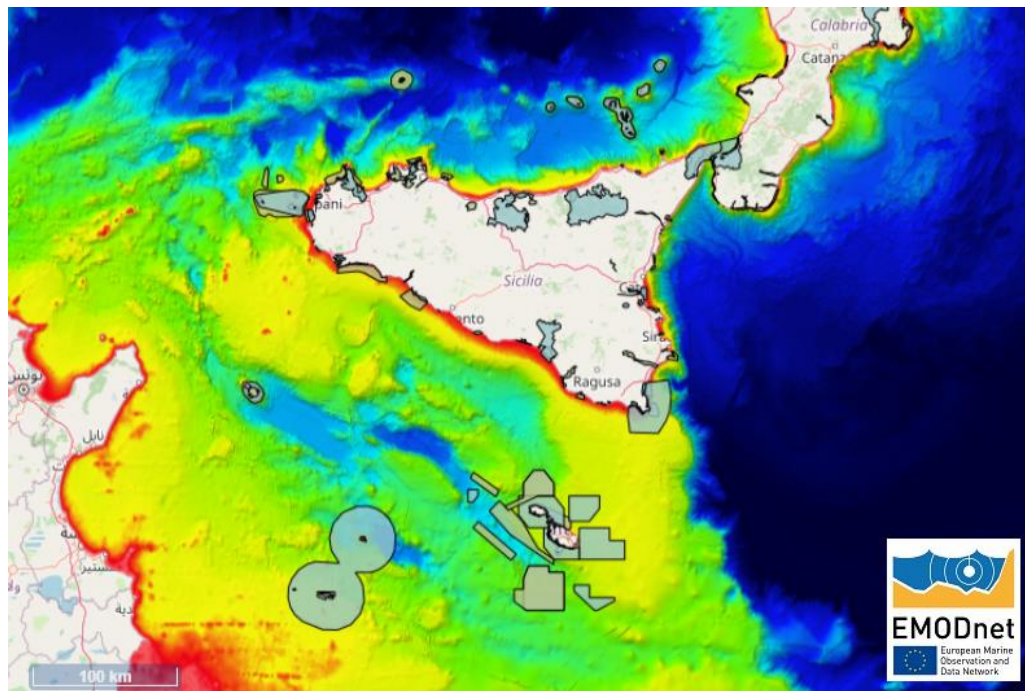


Figure 24 Natura 2000 Network in the areas in the Strait of Sicily

### 3.1.7 Additional considerations

The additional considerations that have been performed for the selection of precise plant location regard the distance from shore, the presence of power and telecommunication cables and the maritime boundaries.

The distance from the coastline is strictly related to the visual impact of the plant, which often has been a determining factor for the public acceptance of the plants. The floating offshore wind turbines utilization make possible the increase of the distance from coast, therefore minimizing the visual impact to avoid interference with the landscape, fisheries and any other type of coastal activities. A minimum distance from the coast of 35 km has been considered to make negligible these impacts.

To conclude, power and telecommunication cable presence has been also assessed in the area and the maritime boundaries have been considered Figure 24. In particular, as

regards the latter point the choice of the precise location of the plant has been performed considering the belonging to the Italian territory.

#### EMODNET CENTRAL PORTAL

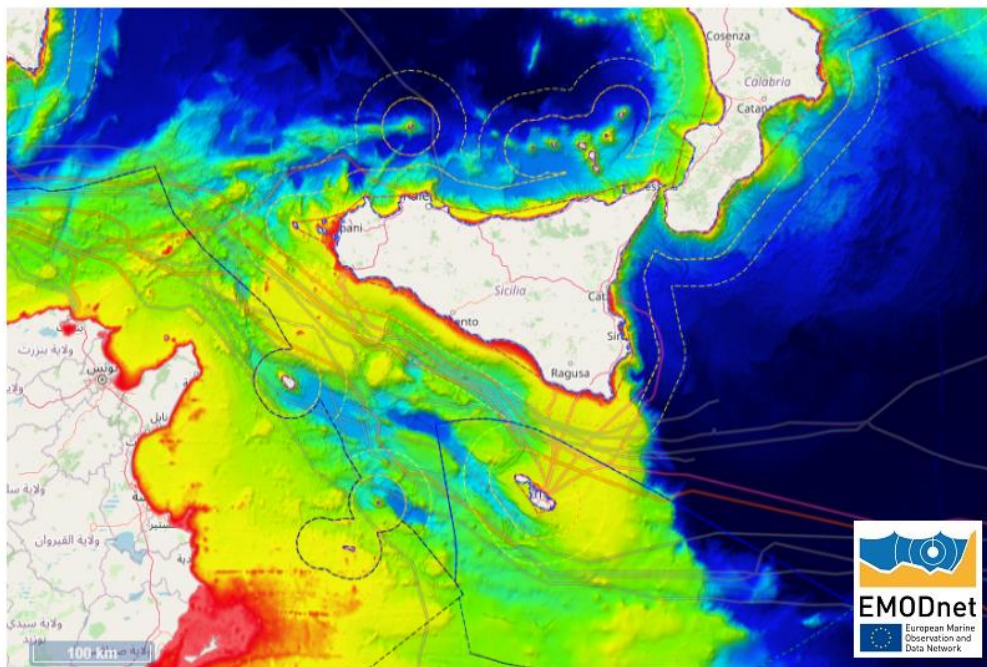


Figure 25 Power and telecommunication cable map and maritime boundaries map overlapping [25]

## 3.2 Wind power model

The floating offshore wind power plant model was developed to estimate the green electricity production. Results of this model are the input parameters of the liquid hydrogen production model.

The procedure followed to model the electricity production consists of three steps:

1. Estimation of the annual energy production (AEP) through the use of the WAsP (Wind Atlas Analysis and Application Program) software.
2. Estimation of the annual energy production of the wind farm through the use of Matlab software.

These two steps were followed because the WAsP software gives as output the annual energy production value, therefore no data regarding hourly energy production values for the whole reference year are provided.

Since the aim of the model is to build an annual energy production curve representing the hourly electricity production values for each hour of the year, it was necessary to model this curve through the use of Matlab software.

Additionally, in the second step of the wind power model it was necessary to manipulate the results obtained in the Matlab model, regarding the single wind turbine power production, in order to make these results congruent with the results obtained in the WAsP software. More specifically, the annual energy production curve with hourly time steps of a single wind turbine obtained in Matlab was scaled with a fitting coefficient to take into account wake and turbulence effects which are instead modeled in WAsP.

### 3.2.1 WAsP model

WAsP [30] is a powerful software for wind resource assessment, siting and energy yield calculations for wind farms developed by the Danish Technical University (DTU) Wind and Energy Systems.

It includes numerous physical models that describe wind climate and wind flow over various terrains and near sheltering obstacles. WAsP also includes a wake model to account for wind farm wake effects and a stability model that employs ERA5 stability inputs to take in consideration the local atmospheric stability conditions. WAsP utilizes the built-in linear IBZ model for horizontal and vertical extrapolation, which is appropriate for flat to moderately complicated terrain. Wind-climatological input might be obtained via measurements of wind at a nearby meteorological mast or from mesoscale modeling results. The elevation characterization may be obtained from space shuttle elevation data or other data sets. The land cover classification and surrounding sheltering

obstacles may be derived from topographic maps, satellite images (Google Earth) or databases [31].

The WAsP software is an application of the *Wind Atlas Methodology*, shown in Figure 25. The wind atlas methodology consists in the prediction of the wind climate at a certain point B, given the wind measurements in another point A and assuming that the wind climates in the two points considered are governed by the same large- (meso-) scale wind forcing. The generalized wind climate (GWC) represents the wind field distribution that would occur in the absence of orography and a homogenous surface roughness, meaning a smooth surface with uniform surface roughness.

Moreover, WAsP relies upon two fundamental assumptions: firstly, the GWC exhibits a substantial degree of similarity between the observed (meteorological station) and predicted sites (wind farm); secondly, it is assumed that historic wind data are representative of future wind conditions in the timeframe of interest for wind installations (i.e., the 20 years life time of the wind turbines) [31]. Therefore, the wind climate at any specific site can be estimated from the generalized wind climate.

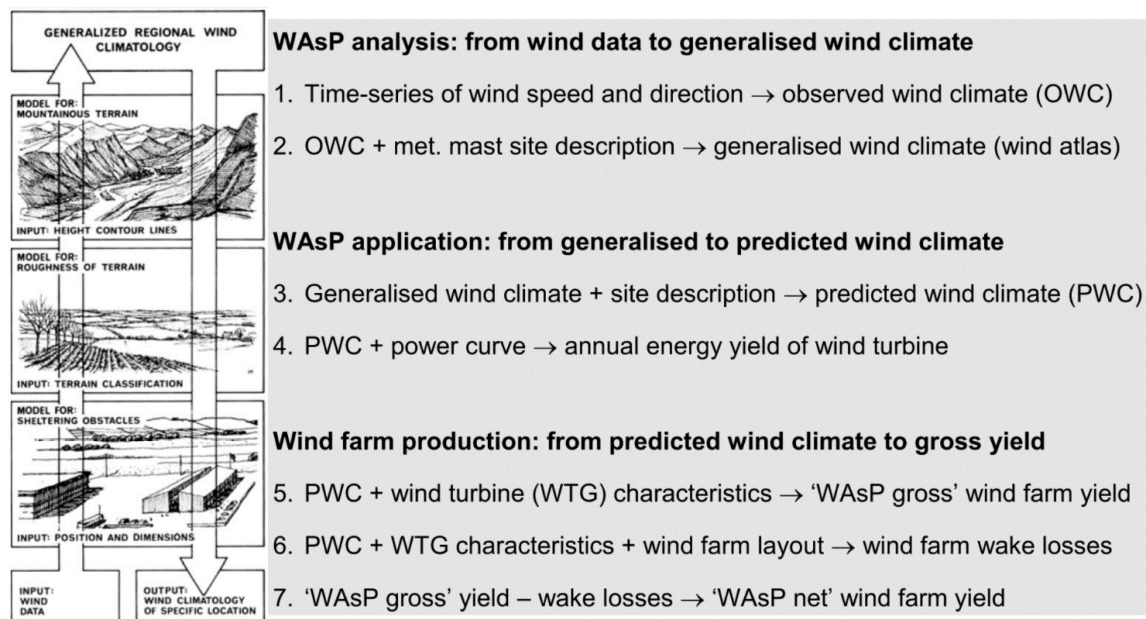


Figure 26 Wind Atlas Methodology [31]

In this work, the WAsP software was utilized to calculate of the net annual energy production (AEP) of the wind farm for the specific site selected through the plant location methodology.

First of all, a file containing the *Generalized Wind Climate* of the selected area has been downloaded from the Global Wind Atlas platform and imported to the WAsP workspace. The GWC file contains important information such as the wind rose and the Weibull  $k$  and  $a$  parameters. Moreover, the GWC is specified for different standard heights above the ground level (10, 25, 50, 100 and 200 m a.g.l.) and different roughness classes represented by values of roughness lengths,  $z_0$  of 0, 0.03, 0.10, 0.40 and 1.5 m. WAsP is able to interpolate between these default values, and if the turbine hub height is between

these values the heights can be modified to take into account of the project characteristics. [31].

This is the case of the analysis performed in this work, where turbine hub height was selected equal to 150 above sea level.

The *Climate Data tab*, showed in Figure 26, exhibits a table which contains, for different height values and roughness classes, the corresponding mean wind speed. Moreover, the climate data tab also contains a wind rose on the bottom left, segmented into 12 sectors, each spanning 30 degrees, that visually represents both the direction and the frequency of wind flow occurrence and on the bottom right the sector-wise distributions of mean wind speed. Moreover, for a fixed height and R-class it is possible to select a certain sector to represent the distribution of the mean wind speed for the specific sector, which will be displayed on the bottom right graph.

In particular, in Figure 26 it is represented the omni-directional wind speed distribution (relative for all sectors) and the wind rose for a height of 150 m and R-class 1. These parameters corresponds respectively to the hub height of the selected wind turbine and the roughness length ( $z_0=0$ ) of the sea, representative of the analyzed case study.

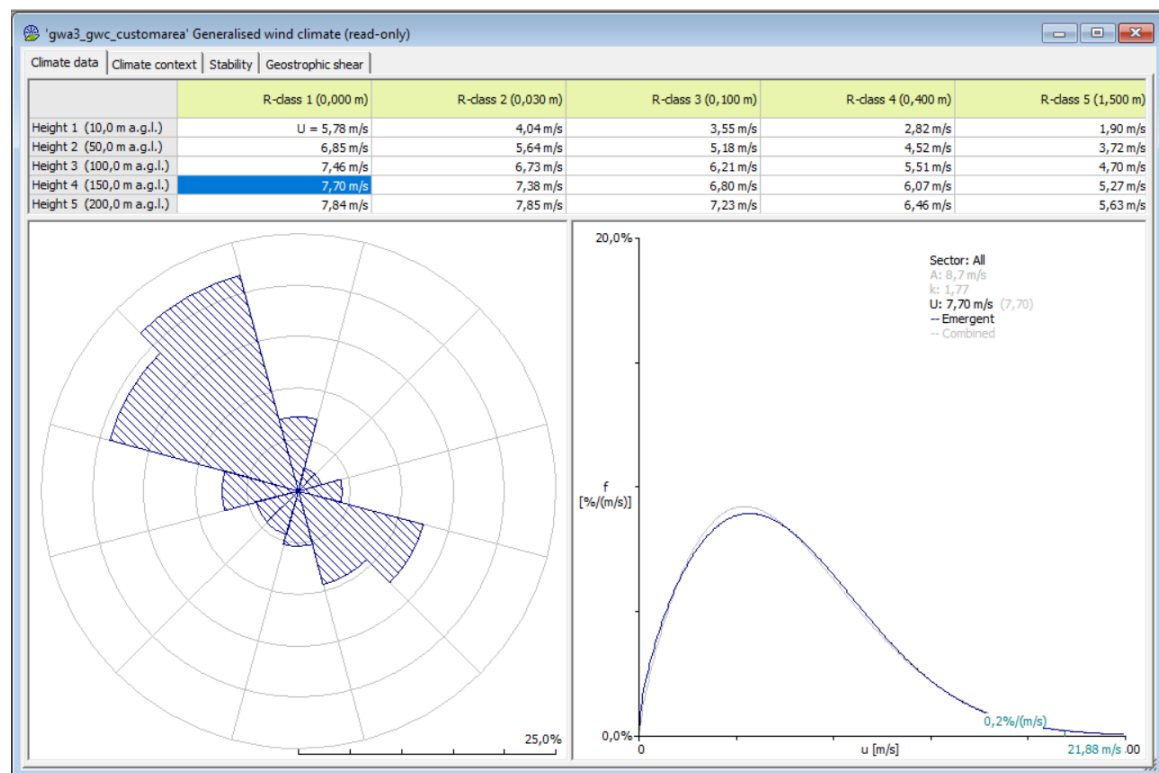


Figure 27 Generalised wind climate results example, Climate Data tab in WAsP software

The next step that has been performed was the importation of the topographical inputs to WAsP of the selected site.

WAsP utilizes topographical data presented in the form of a *Vector Map*, which may include height contour lines and lines indicating changes in surface roughness. Moreover, the map coordinates and the elevations have to be expressed in meters and employ a Cartesian map coordinate system. In particular, the *Vector Map* was built through the use of the *WAsP Map Editor*. The *Vector Map* contains two layers of data: orography and roughness. The orography map describes the height contours of the area, while the roughness map consists of various land cover classes, each associated to a distinct roughness length value  $z_0$ . [31].

The orography (or elevation) and roughness maps have been downloaded from the Global Wind Atlas and then imported into the *Map Editor*. The elevation map and roughness maps must have the same center coordinates and size. Both elevation and roughness maps extend several kilometers away from the site center. The map extension in this study has been selected equal to 100 km. The *Vector Map* was obtained merging together the information of the elevation and roughness maps. In the case of the selected site, being the plant location at an offshore site far from the coastline, no variations in the terrain surface as elevation or land cover were encountered by the software, therefore a single contour has been added by the software, with the contour property “*Landcover/roughness=Water surface*” and  $z_0=0$  for the whole area.

After the definition of the generalized wind climate and topographical inputs, the wind turbine generator has been selected. The wind turbines comprised in the turbine generators catalogue of WAsP are of too small dimensions for the aim of this work, being turbines of maximum 3 MW. Therefore, it was necessary to use the *WAsP Turbine Editor* to add a turbine generator of sufficiently high power rating.

The selected turbine generator is the IEA Wind 15-Megawatt offshore reference wind turbine. The power and thrust curve for the wind turbine were acquired from reference [32] and subsequently inputted manually into *WAsP Turbine Editor* to construct the generator model. A screenshot of the required parameters inserted in the Turbine Editor are presented in Figure 27. For each value of wind speed were inserted the corresponding values of thrust coefficient and power. To conclude, also rotor diameter (m), hub height (m), rated power (MW) and control system have to be specified to build the wind turbine model.

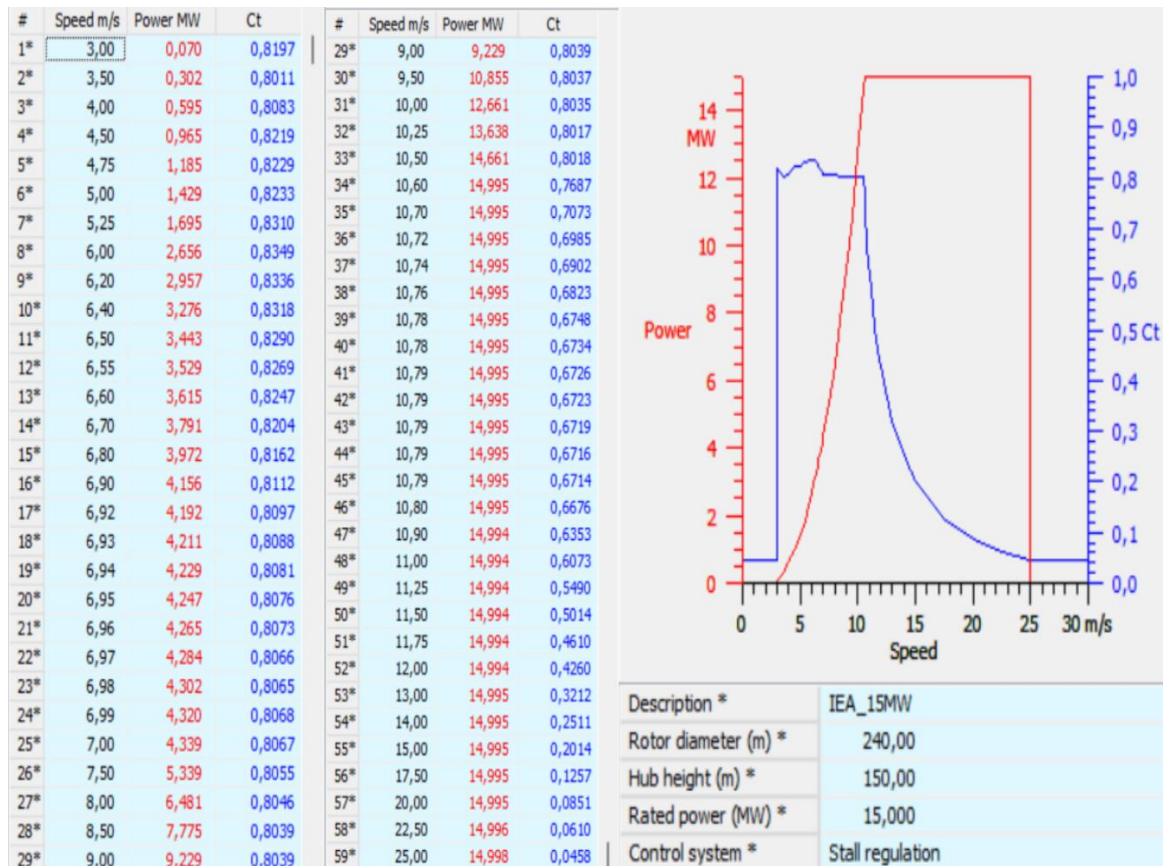


Figure 28 IEA Wind 15-Megawatt reference wind turbine power and thrust curve in WAsP Turbine Editor

Furthermore, as can be appreciated from the figure: the cut-in speed of the generator, which is the minimum wind speed at which the wind turbine start producing power is equal to 3 m/s; the cut-out speed, which is the maximum wind speed at which the wind turbine produces power, corresponds to 25 m/s; above the cut-out speed the power output of the generator is null; in the range between the rated wind speed, which is equal to 10,59 m/s, and the cut-off wind speed the power output is equal to the turbine rated power (15 MW). Finally, between the cut-in velocity and the rated velocity the power output is a function of the wind velocity, therefore it gradually increases with the wind speed.

After the selection of the wind turbine generator, the following step was to design the wind farm layout within the area selected through the site location methodology.

In this work, a number of 20 turbines was chosen, in order to reach a total nominal power installed equivalent to 300MW, a value which is in line with other proposed floating offshore projects.

As explained in reference [31], WAsP lacks in advanced layout design tools, therefore it was necessary to design free-hand the wind farm layout. The layout can be created rapidly within the *Vector Map* by duplicating the turbine site and then manually relocating the turbine site to a new position.

A useful function that was employed during the design phase of the wind farm layout, to facilitate the maintenance of specific distances between the turbines, was to select

distance circles equals to 12 times the turbine diameter in the direction of the prevalent wind speed of the site, and distance circles equal to 7 times the turbine diameter in the direction perpendicular to the prevalent wind speed direction. These circles around each turbine site, can be displayed in the *Spatial View*, facilitating the positioning of each turbine. It is important to select a sufficient distance between the turbines of the wind farm to minimize the wind farm wake losses, which are responsible for the reduction of the final power output of the wind farm.

Regarding the wake modelling, the *PARK2* model has been chosen and the offshore terrain context was manually set. Therefore the wake losses were modelled using *PARK2* and using the default coefficients for offshore environment. The hub height for all the sites was set equal to 150 m above the sea level.

To conclude, after the definition of the wind farm layout “*all feasible calculations for the wind farm*” were performed. The tab which automatically opens after the calculation contains important information such as the *statistics* for the overall wind farm, where the total net annual energy production, the capacity factor, the proportional wake loss and other results are displayed. Additionally, in the section “*site list*” results relative to each wind turbine of the wind farm are displayed.

### **3.2.2 Wind Profile Model**

In order to calculate the hourly liquefied hydrogen production profile along the year, the results obtained in WASP were not sufficient. The *Total Net AEP*, in fact is a value representative of the cumulative annual production of the wind farm. In order to compute the hourly LH production it was necessary instead to build a curve representing, for each hour of the year, the power output of the wind farm. To fulfil this requirement, a Matlab script was written and the subsequently explained procedure has been followed. This procedure aims at calculating the following data: the annual energy production value and hourly power outputs throughout the whole year of the selected IEA Wind 15 MW offshore reference wind turbine, considering as reference year the 2018; the wind farm annual energy production value, and the hourly power output throughout the reference year.

More specifically, to calculate the abovementioned data of the wind farm it was assumed that both the power curves of the wind turbines and the hourly power outputs of the wind turbines are equal for all the 20 turbines composing the wind farm.

The first step of the procedure followed in the Matlab model consists in the calculation of the annual energy production and hourly power outputs of the selected 15 MW turbine.

First of all the, from reference EXOS [33] the hourly mean wind speed data set was downloaded in the form of excel file. EXOS utilizes the ERA5 reanalysis data, which is generated by the European Center for Medium-Range Weather Forecasts (ECMWF).

ERA 5 provides state of the art global dataset on atmospheric, land surface and ocean wave data, which spans from 1979 up to almost the present, with a time resolution of one hour. In the EXOS map available in the portal, each specific point corresponds to the center of a grid area measuring 0,25 by 0,25 degrees. Each location data is a representation of this grid box area. The point of the EXOS map that has been selected in the analysis takes into account two considerations: firstly, the proximity to the area of interest; secondly, the prevalent wind direction in the area. The consideration relative to the wind direction was performed because the area of interest is in the middle of two points in the EXOS map.

Secondly, the hourly wind speed data set was then modified because of the difference in height between the turbine hub and the available data form EXOS. More specifically, the hourly wind speed data obtained from EXOS are representative for a height of 100 m above the sea level, while the turbine hub height is 150 m above the sea level. Each value of the wind speed measured at 100 m above the sea level was scaled applying the following formula, assuming a simple logarithmic wind profile:

$$\frac{U(z)}{U(z_r)} = \frac{\ln\left(\frac{z}{z_0}\right)}{\ln\left(\frac{z_r}{z_0}\right)} \quad (4)$$

Where  $U(z)$  is the wind speed at  $z = 150$  m,  $U(z_r)$  is the wind speed at  $z_r = 100$  m,  $z_0$  is the roughness length of the site, corresponding to  $z_0 = 0,0001$  m.

The methodology followed in the Matlab script to calculate the hourly power production is based on the knowledge of the hourly wind speed data for a year, consisting therefore in 8760 values, and on the knowledge of the power coefficient curve of the IEA Wind 15-MW offshore reference wind turbine. The power coefficient values were acquired from reference [32]. Through the use of “*interp1*” function in Matlab, a 1-D interpolation of the power coefficient data was performed.

The equation (5) used in the Matlab model represents the power output of a wind turbine at varying wind speed.

$$P(t) = \begin{cases} 0, & v < v_{ci} \\ P_f(v), & v_{ci} \leq v < v_r \\ P_r, & v_r \leq v < v_{co} \\ 0, & v_{co} \leq v \end{cases} \quad (5)$$

For wind speed lower than the cut-in velocity of the wind turbine and equal or higher than the cut-out velocity of the wind turbine the power output is equal to 0. For wind equal or higher than the cut-in velocity and lower than the rated velocity of the turbine the power output is function of the wind speed. For wind speed equal or higher than the rated velocity and lower than the cut-out velocity of the turbine the power output is equal to the rated power output.

The value of  $P_f(v)$  is described by the cubic law, as described in the following equation:

$$P_f(v) = \frac{1}{2} \rho_{air} A C_p v^3 \quad (6)$$

where  $C_p$  (%) corresponds to the power coefficient,  $\rho_{air}$  (kg/m<sup>3</sup>) the density of air,  $A$  (m<sup>2</sup>) the rotor swept area and  $v$  (m/s) the hourly wind speed upstream the turbine. The power coefficient gives a measure of the efficiency of the energy transfer between the wind stream and the blades of the turbine generator [14].

In the Matlab script, a loop throughout each hour year was designed. In the loop, starting from the first hour of the year until the 8760<sup>th</sup>, the hourly wind speed value for the current hour is selected; the power output for the current hour, based on the wind speed conditions is then calculated through the equation (5). In the wind speed range  $v_{ci} \leq v < v_r$ , the proper power coefficient  $C_p$  corresponding to the wind speed value for the current hour is automatically selected from the power coefficient curve and then is inserted into equation  $P_f(v)$ .

The 8760 hourly power output values are then written in an excel file, because represent the fundamental inputs for the calculation of the hourly liquid hydrogen production curve. Additionally, the annual energy production is calculated and displayed by the script in the *command window*, summing all the hourly power output values.

The second step of the procedure followed in Matlab consists in the manipulation of the data obtained in the first step.

In particular, a fitting procedure was adopted to take into account the wake losses of the wind farm, namely the losses arising from the interference between different turbines in the wind farm. These negative contributions are instead calculated by the WAsP software. More specifically, as expected, the annual energy production of the single turbine obtained in the Matlab script was higher with respect to the net annual energy production relative to the single turbine obtained in WAsP. As value representative for the net annual energy production for a single turbine in WAsP was selected the *mean net annual energy production* value displayed in *wind farm statistics*.

Therefore, a correction coefficient, which in the code is called scaling factor ( $SF$ ), lower than one was calculated. It corresponds to the ratio between mean net annual energy production calculated in WAsP ( $AEP_{mean,WAsP}$ ) and the annual energy production value calculated in Matlab ( $AEP_{Turb,MAT}$ ), as showed in the following equation:

$$SF = \frac{AEP_{mean,WAsP}}{AEP_{Turb,MAT}} \quad (7)$$

Each value of the hourly power output curve obtained though the Matlab script was multiplied by the scaling factor  $SF$  and a new excel file was written.

The third step of the Matlab model consists in the calculation of the wind farm annual energy production and hourly power output curve for the reference year.

The scaled hourly power output curve obtained in step second step was multiplied by the number of wind turbines of the plant, fixed equal to 20. The resulting curve is representative to the wind farm production in the selected area. The integral of the curve gives as output the annual energy production of the wind farm, which coincides with the total net annual energy production calculated in WAsP. The hourly wind farm power output curve is the final result of the wind model and it is used as input set of data in the liquid hydrogen production model, for the calculation of the hourly liquid hydrogen curve, as explained in the following paragraph 3.3.

### 3.3 Liquid hydrogen production model

The approach that was followed in this work to calculate the hourly liquid hydrogen production is common in literature. In particular, the main references that were used to design the calculation script implemented in Matlab are: [23, 34].

The hourly wind farm power output curve, obtained as was explained in the wind power model section, is the main set of data used as input in the liquid hydrogen production model. Therefore, the hourly liquid hydrogen production curve modeled by the Matlab script is representative for the hydrogen production of the whole wind farm.

The hydrogen generation plant is assumed to be an off-grid plant connected only to the wind farm; hence, the energy demand was considered to be entirely fulfilled by the wind farm itself. Therefore, the hourly electricity power output of the wind farm was considered to be entirely used to supply electricity to the electrolyzer and the other components of the plant, namely: the water treatment system, the liquefaction unit and the liquid hydrogen refueling station.

The energy consumption of each system component was expressed in kWh/kg<sub>H<sub>2</sub></sub>, indicating therefore the amount of electricity consumed by each component for the production 1 kg of hydrogen.

The proton exchange membrane electrolyzer's (*PEMEL*) electricity consumption was considered constant and equal to the  $E_{elec} = 52$  kWh/kg<sub>H<sub>2</sub></sub> in the range 10-100% of its rated capacity. This choice was followed because of the low efficiency of the electrolyzer in the range 0-10%, which make the liquid hydrogen production not profitable, considering also the high electricity consumption associated with the other components of the plant. More specifically, the selected  $E_{elec}$  value corresponds to the 2024 target value identified by [12]. This value refers to the following boundary conditions: input of AC power and tap water while output of hydrogen complying with ISO 14687-2 at a pressure of 30 bar and hydrogen purity equal to 5. Moreover, the electricity consumption of the electrolyzer includes the energy required by auxiliaries for the electrolysis stack cooling.

Therefore in the Matlab script, these considerations related to the efficiency were taken into account and to ensure sufficiently high efficient operation, the electrolyzer is switched off and put in standby when the hourly input power from the wind farm falls below a certain threshold [34].

The lower limit of the wind farm power output, named  $P_{Farm\_low}$  was selected equal to the 10% of the rated capacity of the electrolyzer, as showed in the following equation:

$$P_{Farm\_low} = 0.10 P_{H2\_Farm} \quad (8)$$

Where  $P_{H2\_Farm}$  represents the rated capacity of the electrolyzer. The determination of the  $P_{H2\_Farm}$  was performed based on the knowledge of the maximum hourly liquid hydrogen production, as expressed in equation (9).

$$P_{H2\_Farm} \leq \max W_{H2\_Farm,Th}(t) \times E_{elec} \quad (9)$$

The value of theoretical maximum hourly hydrogen production  $\max W_{H2\_Farm,Th}(t)$  (kgH<sub>2</sub>/h) was calculated with the equation (10) considering the maximum value between the 8760 hourly values of the reference year. The theoretical hourly hydrogen production value is time-varying and function of: wind farm power output, electricity consumption of the electrolyzer and electricity consumption of the additional components of the system, which were considered together in the term  $E_{pcl}$ .

$$W_{H2\_Farm,Th}(t) = \frac{P_{Farm}(t)}{E_{elec} + E_{pcl}} \quad (10)$$

The  $E_{pcl}$  term comprises the electricity consumption of water treatment system, liquefaction unit and liquid hydrogen refueling station.

The water treatment system commonly comprises a pre-treatment unit, a semi-permeable membrane to desalinate the seawater and a post-treatment unit [14]. The energy consumption of the water treatment system per kg of hydrogen produced ( $E_{wt}$ ) was calculated considering the energy consumed to produce one m<sup>3</sup> of demineralized water ( $E_{H2O}$ ) and how many cubic meters of demineralized water are needed to produce one kg of hydrogen using the selected electrolyzer ( $M_{H2O}$ ). Different desalination technologies are available in the market. Among the different technologies the reverse osmosis technology was selected in this study. Therefore, following the proposed procedure, the energy consumption of the water treatment system per unit mass of produced hydrogen was calculated as:

$$E_{wt} = E_{H2O} \times M_{H2O} \quad (11)$$

It was assumed  $E_{H2O} = 5 \text{ kWh/m}^3_{H2O}$  and  $M_{H2O} = 10 \text{ l}_{H2O}/\text{kg}_{H2}$  [14].

At the current technological state the process of hydrogen liquefaction is very energy consuming. This is a negative aspect for offshore hydrogen production because of the reduction of the energy available in input at the electrolyzer.

The specific energy consumption (kWh/ kgH<sub>2</sub>) of a liquefaction system varies with the system capacity and the considered technology. As reported in [19], the best in service industrial hydrogen liquefiers are characterized by specific energy consumption values ranging from 10-15 kWh/kgH<sub>2</sub>. However, the energy consumption is reducing with time and an energy consumption reduction towards the range 7.5-9 kWh/kgH<sub>2</sub> is expected. In [12] are presented state of the art values of 10-12 kWh/kgH<sub>2</sub> relative to 2020, target values of 8-10 kWh/kgH<sub>2</sub> for 2024 and 6-8 kWh/kgH<sub>2</sub> for 2030.

The energy consumption of the liquefaction system was selected equal to  $E_{liq} = 9 \text{ kWh/kg}_{H2}$ . This value is representative for the conversion of normal hydrogen at 20 bar and 25°C to liquid (para) hydrogen at 20 K and ambient pressure. Moreover it includes electricity contributions for compression drives, pre(cooling) cycles and other pumping duties. [12]

The energy consumption of the refueling station was selected equal to  $E_{rs}=0.5$  kWh/kg<sub>H2</sub>. This value represents the 2024 target value presented in reference [12].

The value of  $E_{pcl}$  (kWh/kg<sub>H2</sub>) was calculated as the summation of the three mentioned contributions, as showed in the following equation:

$$E_{pcl} = E_{wt} + E_{liq} + E_{rs} \quad (12)$$

Therefore,  $E_{pcl} = 9,55$  kWh/kg<sub>H2</sub>

In the following table the fixed parameters which were used in the Matlab model are summarized .

Table 4 Components' energy consumption values used in the model

Parameter	Value	Reference
Electrolyzer electricity consumption, $E_{elec}$	52 kWh/kg <sub>H2</sub>	[12]
Desalination system electricity consumption, $E_{H2O}$	5 kWh/m <sup>3</sup> <sub>H2O</sub>	[14]
Electrolyzer water consumption, $M_{HO}$	10 l/kg <sub>H2</sub>	[14]
Hydrogen liquefaction system electricity consumption, $E_{liq}$	9 kWh/kg <sub>H2</sub>	[12]
Refueling station electricity consumption, $E_{rf}$	0,5 kWh/kg <sub>H2</sub>	[12]
Aggregated components electricity consumption, $E_{pcl}$	9,55 kWh/kg <sub>H2</sub>	-

After the determination of  $maxW_{H2\_Turb,Th}(t)$  and  $P_{H2\_farm}$ , the value of  $P_{Farm\_low}$  was calculated and the theoretical liquid hydrogen values for each hour of the year were computed by a cycle, considering the condition that imposes the turning off of the electrolyzer. This step was performed in order to calculate the number of hours in a year in which the electrolyzer is turned off. The system of equation (13) utilized in the cycle is described below.

$$W_{H2Farm,Th}(t) = \begin{cases} \frac{P_{Farm}(t)}{E_{elec} + E_{pcl}} & \text{if } P_{Farm}(t) > P_{Farm\_low} \\ 0 & \text{if } P_{Farm}(t) \leq P_{Farm\_low} \end{cases} \quad (13)$$

Moreover, the hourly liquid hydrogen produced  $W_{H2Farm,pr}(t)$  [kg<sub>H2</sub>/h] by the plant for each hour of the year was calculated by the equation (x):

$$W_{H2Farm,Pr}(t) = \begin{cases} 0 & \text{if } P_{Farm}(t) \leq P_{Farm\_low} \\ \frac{P_{Farm}(t) \times 1 \text{hour}}{E_{elec} + E_{pcl}} & \text{if } P_{Farm}(t) < P_{H2Farm} \left(1 + \frac{E_{pcl}}{E_{elec}}\right) \\ \frac{P_{H2Farm} \times 1 \text{hour}}{E_{elec}} & \text{if } P_{Farm}(t) \geq P_{H2Farm} \left(1 + \frac{E_{pcl}}{E_{elec}}\right) \end{cases} \quad (14)$$

In the second condition of the last equation, the power from the wind farm is lower than the rated capacity of the electrolyzer, whereas in the third condition the power from the wind farm is limited by the rated capacity of the electrolyzer.

Additionally, the hourly liquid hydrogen curve calculated in the Matlab code is plotted. Each value of the curve represent the amount of liquid hydrogen produced in the current hour by the whole plant (kg<sub>H2</sub> per hour).

After the determination of the hourly liquid hydrogen production curve, the daily liquid hydrogen production curve was calculated. The calculation consisted in the summation of 24 hourly liquid hydrogen production values constituting a day, for each day of the year. The daily liquid hydrogen production curve was plotted in a graph.

To conclude, the maximum daily liquid hydrogen production value  $maxW_{H2,Day}$  was used in order to dimension the liquid hydrogen storage tank. The storage capacity  $V_{Stg}$  (m<sup>3</sup>) was determined with equation (15), as follows:

$$V_{stg} = \frac{2 \times maxW_{H2,Day}}{\rho_{LH2}} \quad (15)$$

where  $\rho_{LH2}$  (kg/m<sup>3</sup>) represents the liquid hydrogen density, equal to 70,8 kg/m<sup>3</sup> [14].

### 3.4 Technoeconomic analysis

The aim of the techno-economic analysis is to evaluate the effectiveness of the proposed hydrogen production plant in reducing the use of diesel fuels in the maritime sector and its economic feasibility. In particular, in this analysis two different scenarios were considered. The economic viability of the two considered scenarios was performed by computing the net present cost (NPC) and the related levelized cost of hydrogen (LCOH).

The main relationships implemented in the Matlab model to evaluate the levelized cost of hydrogen (LCOH) are presented below.

The levelized cost of hydrogen (in €/kg<sub>LH2</sub>) was computed as follows:

$$LCOH = \frac{C_{NPC,tot}}{\sum_{j=1}^{L_{pr}} \frac{H_{tot,j}}{(1+d)^j}} \quad (16)$$

where, the  $C_{NPC,tot}$  (€) is the total net present cost (NPC),  $H_{tot,j}$  (Kg<sub>H</sub>) is the total amount of hydrogen produced by the plant along the  $j$ -th year,  $d$  is the real discount rate and  $L_{pr}$  is the project lifetime. The real discount rate was calculated as follows:

$$d = \frac{d' - ir}{1 + ir} \quad (17)$$

where  $d'$  is the nominal discount rate while  $ir$  is the inflation rate.

The value of the  $H_{tot,j}$  was calculated through the hydrogen production model of paragraph 3.3, in the first scenario, whereas it was recalculated in the second scenario. It was then inserted as input parameter in the techno-economic model.

The value of the total net present cost was calculated as the sum of the present value of all the expenditures incurred from the building phase to the decommissioning phase of the system (the capital cost, the installation cost, the operation and maintenance cost, the replacement cost and the decommissioning costs) minus the present value of the salvage contributions over the system lifetime, as shown in the following equation:

$$C_{NPC,tot} = C_{cap,tot} + C_{inst,tot} + C_{NPC,O\&M,tot} + C_{NPC,repr,tot} + C_{NPC,dec,tot} - C_{NPC,sal,tot} \quad (18)$$

The different terms considered in the above NPC formula were calculated by the following equations:

$$C_{cap,tot} = \sum_{i=1}^{N_{c,tot}} C_{cap,i,0} \quad (19)$$

$$C_{inst,tot} = \sum_{i=1}^{N_{c,tot}} C_{inst,i,0} \quad (20)$$

$$C_{NPC,O\&M,tot} = \sum_{j=1}^{L_{pr}} \frac{\sum_{i=1}^{N_{c,tot}} C_{O\&M,i,j}}{(1+d)^j} \quad (21)$$

$$C_{NPC, repl, tot} = \sum_{j=1}^{L_{pr}} \frac{\sum_{i=1}^{N_{c, repl, tot}} C_{repl, i, j}}{(1+d)^j} \quad (22)$$

$$C_{NPC, salv, tot} = \sum_{j=1}^{N_{c, repl, tot}} \frac{C_{salv, i, L_{pr}}}{(1+d)^{L_{pr}}} \quad (23)$$

$$C_{NPC, dec, tot} = \sum_{j=1}^{N_{c, dec, tot}} \frac{C_{dec, i, L_{pr}}}{(1+d)^{L_{pr}}} \quad (24)$$

The  $C_{cap, i, 0}$ ,  $C_{inst, i, 0}$ ,  $C_{O\&M, i, j}$ ,  $C_{repl, i, j}$ ,  $C_{salv, i, L_{pr}}$ ,  $C_{dec, i, L_{pr}}$  (expressed in €) correspond to the initial investment, installation, operation and maintenance, replacement, salvage and decommissioning costs respectively, referred to the  $i$ -th component of the plant for the  $j$ -th year. The investment costs are considered to incur at the beginning of the analysis period, coinciding with  $j=0$  while the replacement cost is accounted at the end of its operational lifetime. Both the salvage costs and decommissioning costs were considered to occur at the end of the project lifetime, namely when  $j=L_{pr}$ . The salvage value is the economic value of the component at the end of the project lifetime. It was considered that the salvage value is directly proportional to the remaining lifetime:

$$C_{sal} = C_{rep, i} \frac{L_{rem, i}}{L_i} \quad (25)$$

The remaining lifetime of the component at the end of the project lifetime ( $L_{rem, i}$ ) was calculated considering the component lifetime ( $L_i$ ) and the hours of operation of the component from its last replacement to the end of the project period.

The general assumptions made in the technoeconomic analysis for both scenarios are given in the following table:

Table 5 Techno-economic model general assumptions

<b>General assumptions</b>	
Project lifetime ( $L_{pr}$ )	25 years
Nominal discount rate ( $d'$ )	7%
Inflation rate ( $ir$ )	2%

### 3.4.1 Scenario 1

The first scenario is the reference case described in the previous paragraphs. In this scenario the components of the plant are the wind farm, the water treatment system, the electrolyzer, the hydrogen liquefaction system, the refuelling station and the platform over which all the equipment necessary to produce the liquid hydrogen is positioned. The size of each component was determined following the methodology explained in the previous paragraphs. The liquid hydrogen produced is used to perform the refuelling of cargo vessels transiting in the area.

The only LH ship currently in operation is the Suiso Frontier tanker [35]. Up to date, LH cargo vessels are not currently in operation in the world. However, in the last years many feasibility studies on liquid hydrogen powered vessels were conducted [17]. Therefore, in this scenario was considered the container feeder concept design developed by Rohde and Sames [36]. This cargo vessel has a container capacity of 1000 TEU (twenty-foot equivalent unit), a trial speed of 15 knots, and a total length of 137 m. In the ship design, it was designed a hybrid system consisting on fuel cells and batteries in order to generate the necessary power for both onboard energy supply and propulsion. The liquid hydrogen is the fuel source and is stored in multiple pressurized International Maritime Organization (IMO) Type C tanks. The total capacity of the on-board storage tank corresponds to 920 m<sup>3</sup>, which was estimated to be able to sustain the ship for a 10-day journey [17]. The ship storage capacity was considered in the analysis to dimensions the plant storage and the refuelling station. Other concepts were recently developed, considering ships of higher dimensions, as the study conducted by [37], where a cargo vessel with a capacity of 2600 TEU and LH storage capacity of 2754 m<sup>3</sup> were designed. However, in this study the cargo vessel designed in [36] was considered because the vessel storage capacity is more congruent with the considered plant storage capacity, which is related to the dimension of the wind farm, and the needed refuelling time at the current state of the art of the cryogenic pumps.

At the current technological state, the mass flow rate of a single cryogenic pump is not congruent to perform the ship refuelling in a reasonable amount of time. Therefore, a number of 15 cryogenic pumps installed in parallel was considered, otherwise the required time to perform the refuelling of 930 m<sup>3</sup> of liquid hydrogen (representative for the tank capacity of the abovementioned reference ship) would be too prolonged. In this case, considering the single pump maximum flowrate of 1720 kg/h and 15 pumps slightly more than 2 and a half hours are required to perform the refuelling.

In Table 6 are expressed the economic input parameters of each component of the system for the reference case, used in the Matlab technoeconomic model.

Table 6 Economic input parameters Scenario 1

<b>Wind Farm</b>		
Wind turbine Capex	1,3 M€/MW	[20]
Turbine floating platform Capex	16,48 M€/turb	[38]
Mooring system Capex	1,92 M€/turb	[38]
Anchors Capex	0,65 M€/turb	[38]
Jewellery and topside connections Capex	0,44 M€/turb	[38]
Inter-array cables Capex	400 €/m	[20]
Floating offshore turbine assembly Installation	1,19 M€/turb	[38]
Anchoring and Mooring Installation	1,19 M€/turb	[38]
Inter-array cables Installation	33,72 M€	[38]
Wind farm Operation and Maintenance	16,89 M€	[38]
Floating wind turbine Decommissioning	0,12 M€/turb	[38]
Anchoring and mooring Decommissioning	0,69 M€/turb	[38]
Inter-array cables Decommissioning	25,3 M€	[38]
<b>Water treatment system</b>		
Capex	59,8 €/(m <sup>3</sup> /h)	[23]
Installation	10% Capex	
Operation and Maintenance	2% Capex	[23]
<b>Electrolyzer</b>		
Capex	700 €/kW	[12]
Installation	10% Capex	[39]
Operation and Maintenance	2% Capex	[12]
Replacement	50% Capex	[40]
<b>Liquefaction System</b>		
Capex	41,65 €/(kg/h)	[23]
Installation	10% Capex	
Operation and Maintenance	4% Capex	[23]
<b>Storage tank</b>		
Capex	65 €/kg	[12]
Installation	10% Capex	
Operation and Maintenance	4% Capex	

<b>Refuelling station</b>		
Capex	72000 €/ pump	[41]
Installation	10% Capex	
Operation and Maintenance	4% Capex	
<b>Platform</b>		
Foundation Capex	13,8 M€	[38]
Top side structure Capex	36,8 M€	[38]
Auxiliaries Capex	3,9 M€	[38]
Platform Installation	12,65 M€	[38]
Platform Decommissioning	13,8 M€	[38]

The replacement and salvage value were considered just for the electrolyzer, which is the component showing the lowest lifetime among the others. The decommissioning costs are instead considered just for the wind farm and the platform because for these components the share of this contribution is significant, and therefore not negligible, with respect to the total wind farm and platform total investment costs.

### 3.4.2 Scenario 2

In the second scenario, the reference plant was modified to take into account the placement of a subsea pipeline for gaseous hydrogen transportation. In this case the output of the plant is not liquid hydrogen, but gaseous hydrogen only. Therefore, the hydrogen liquefaction system, the liquid hydrogen storage tank were eliminated and the offshore refuelling station were eliminated. In this scenario, the platform hosts the water treatment system, the electrolyzer and a compressor, necessary to push the gaseous hydrogen towards the shore.

The yearly gas hydrogen production curve was recalculated, modifying the hydrogen production model to take into account the lower energy needs of the system without the liquefaction system. Therefore, water treatment system and electrolyzer rated powers were recalculated to take into account the variation of maximum hourly hydrogen production. The platform, previously dimensioned to host the liquefaction system, the storage and the refuelling dispensers was reduced in size.

The considered pipeline is directed towards the Porto Empedocle's port, which is one of the main ports of the southern coast of Sicily. The considered subsea pipeline has its starting section coinciding with the platform location and is 66 km long. The gaseous hydrogen transported in the pipeline is then stored in gaseous form in a hydrogen storage tank located in the abovementioned port.

Hydrogen pipelines represents a well-established technology, already existing onshore globally especially in USA and Belgium. Hydrogen necessitates approximately 3,85 times more energy than natural gas for the same energy flow. Furthermore, pressure drops occurs along the pipeline's length, which are estimated to range from 3 to 25 bar. Consequently, it is imperative to pressurize the hydrogen adequately to compensate the pressure reduction over the pipeline distance. However, a problem associated with hydrogen is the embrittlement, whose risk increases as pressure levels increase. The utilization of hydrogen pipelines compared to the high voltage submarine cables presents economic advantages, especially in the context of large-scale farms and long distances. However, submarine hydrogen pipelines have not reached the commercial maturity, and a comparison with submarine natural gas pipeline is necessary to assess their potential performances. The hydrogen pipeline design has to take into account the wind farm capacity, the distance from shore and the required output pressure. For instance it was studied that to transport a 1GW of offshore wind energy which has been converted into gaseous hydrogen over a distance of 100 km, a pipeline of 12 inches is required [3]. Therefore, in this analysis, considering the abovementioned estimation, it was considered to be sufficiently conservative to adopt the 8-inch diameter hydrogen transmission pipeline of reference [12].

Considering the maximum hourly hydrogen production value the water treatment system rated capacity was recalculated, whereas considering the maximum daily hydrogen production value, the storage size was designed. To be coherent with the reference case, the size of the storage was selected considering two consecutive days of maximum daily hydrogen production.

The output pressure of the considered electrolyzer is 30 bar, therefore a hydrogen compressor is considered to export onshore the produced hydrogen. In the hydrogen production model of scenario 2, was considered that the compressor's energy demand is satisfied by the wind farm.

Of the two main gas compression technologies, namely centrifugal and reciprocating, the second one are frequently employed in hydrogen applications when pressures exceeding 30 bars are required. Typically, a volume flow rate lower than 1700m<sup>3</sup>/h is elaborated by this type of compressor. In this techno-economic analysis, the energy consumption of the compressor was assumed to be equal to  $E_{\text{comp}}=2,5 \text{ kWh/kg}_{\text{H}_2}$ , which corresponds to the energy needed to compress the hydrogen from 30 to 200 bar [12]. This KPI is specific for pipeline application and large-scale compression systems.

The hydrogen storage tank considered in this analysis stores onshore the gaseous hydrogen coming from the pipeline. The space required to store gaseous hydrogen is higher with respect to that of liquid hydrogen. However, differently than the offshore scenario, where space constraint is relevant, being the storage tank placed in a port infrastructure it was assumed to have the required space availability.

The refuelling station has an output pressure of 350 bar [12] and also in this case, multiple pumps are required to guarantee an acceptable refuelling time. The refuelling

station was dimensioned considering the maximum hourly hydrogen production of the plant, in order to be able to empty the hydrogen storage in one day.

In Table 7 are expressed the economic input parameters of the components of the second scenario, used in the Matlab technoeconomic model. The economic input parameters of the wind farm, water treatment system and electrolyzer are not reported because are equal to that of scenario one.

*Table 7 Economic input parameters Scenario 2*

<b>Compressor</b>		
Capex	1000 €/kW	[12]
Installation	10% Capex	
Operation and Maintenance	0,03€/kg/y	[12]
Replacement	100% Capex/14y	[12]
<b>Pipeline</b>		
Capex	1 M€/km	[12]
Operation and Maintenance	5% Capex	[23]
Decommissioning	187k€/km	[42]
<b>Storage tank</b>		
Capex	700 €/kg	[12]
Installation	10% Capex	
Operation and Maintenance	4% Capex	
<b>Refuelling station</b>		
Capex	62,5 €/kg/h	[12]
Installation	10% Capex	
Operation and Maintenance	4% Capex	
<b>Platform</b>		
Foundation Capex	9,2 M€	[38]
Top side structure Capex	24,53 M€	[38]
Auxiliaries Capex	2,6 M€	[38]
Platform Installation	8,43 M€	[38]
Platform Decommissioning	9,2 M€	[38]

In the reference case, the selection of the precise locations of the plant was performed considering only the cargo vessel category, because it is the better suited to perform the refuelling directly on the sea. However, if refuelling is performed onshore, different categories of vessels of smaller dimensions could be suitable for the utilization. However, it is worth to mention, that the time required to perform the refuelling of gaseous hydrogen is much longer with respect to that of liquid hydrogen and also that the utilization of gaseous hydrogen in vessels is challenging, due to the reduced volumetric energy density of gaseous hydrogen, which imply the utilization of on-board storage tanks of significant dimensions, even at high pressures.

Therefore, considering these aspects, the utilization of the gaseous produced hydrogen is more suited for ships of lower dimensions and that do not pose stringent limitations regarding the refuelling time. Therefore, due to the lower ship autonomy, the interested segment of the maritime sector interested by this possible application is the domestic navigation and short distance routes, rather than long distance routes. Moreover, considering that even a 50/50 mixture of heavy fuel oil and hydrogen could reduce CO<sub>2</sub> emissions by up to 43% per ton-kilometer [2], the produced hydrogen could be also utilized in dual fuel internal combustion engines. This could result an interesting option, especially in the short term, due to the smaller ship hydrogen on board storage and to the associated lower refuelling time.

A part from this maritime application, even if not treated in this analysis, it could be possible the employment of part of the gaseous hydrogen stored onshore for other mobility applications or to serve the hard to abate industrial plants of the area.

# 4 Results

## 4.1 Plant location

The methodology outlined in section 3.1 has been employed to identify the most favorable location for the proposed plant. In the Strait of Sicily more than one area may be considered suitable for the installation of floating wind farms. Nevertheless, for the proposed concept of a hydrogen generation hub powered by offshore wind farm for ship refueling, one specific area aligns perfectly with all the constraints presented.

The mean wind speed gradually decreases towards southeast direction, approaching the Malta Channel (sector of the Strait of Sicily between Sicily and Malta). Therefore, as far as concern the wind resource, the area called Adventura Plateau, between Pantelleria and Egadi Islands represents a possible area of interest, with mean wind speed values at 150 m above the sea level in the range 7,8-8 m/s [26]. Nevertheless, this area was ultimately not chosen due to the identification of two critical factors analyzing the different constraints. Firstly, the presence of numerous underwater volcanoes results in uneven seabed depth and in increased geohazard risks associated to seismic and volcanic activities. Secondly, the route vessel density, in the sector of the Plateau which is part of the Italian continental shelf, is not notably high compared to other regions of the Strait.

The vast area of the Malta Plateau, situated between Sicily and Malta is characterized by consistently lower mean wind speed values, not exceeding 7 m/s at 150m above the sea level. Consequently, despite its bathymetry is particularly favorable for floating offshore wind technology (being comprised for the majority between 90 and 150 m), despite the route vessel density is particularly high and the absence of underwater mounts and volcanoes, the area has been excluded from the analysis because of the lower mean wind speed.

Figure 28 illustrates the most suitable area of the Strait of Sicily, which has been determined by taking into account the various constraints outlined in paragraph 3.1.

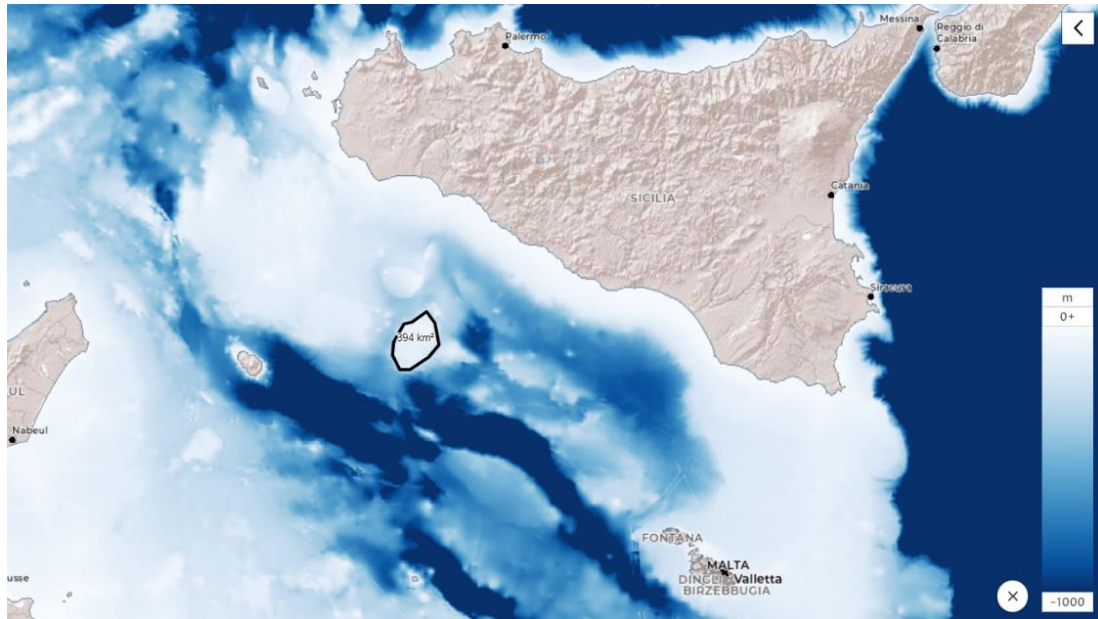


Figure 29 Selected plant area in bathymetry map [26]

The surface of the selected region is of 394,14 km<sup>2</sup> and the coordinate of the center are (Lat 36,884188°, Long 12,872269°). This area is called Pinne Marine Bank. The minimum distance with respect to Pantelleria island is 62 km and with respect to the closest point of the Sicily coastline is 52km.

The mean wind speed of the area measured at 150 m above the sea level ranges between 7,62 and 7,75 m/s, showing therefore slightly lower values (around -0,2 m/s) with respect to the Adventura Plateau area, and higher values (around +0,7 m/s) with respect to the Malta Plateau. The selected plant area in the mean wind speed map is showed below:

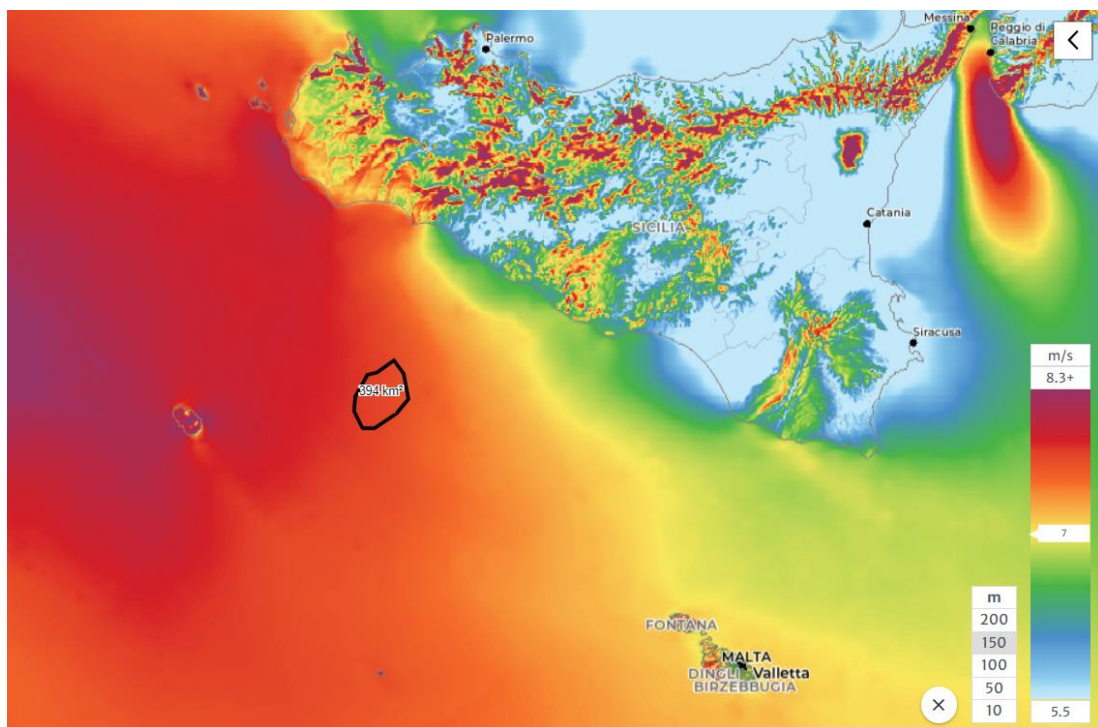
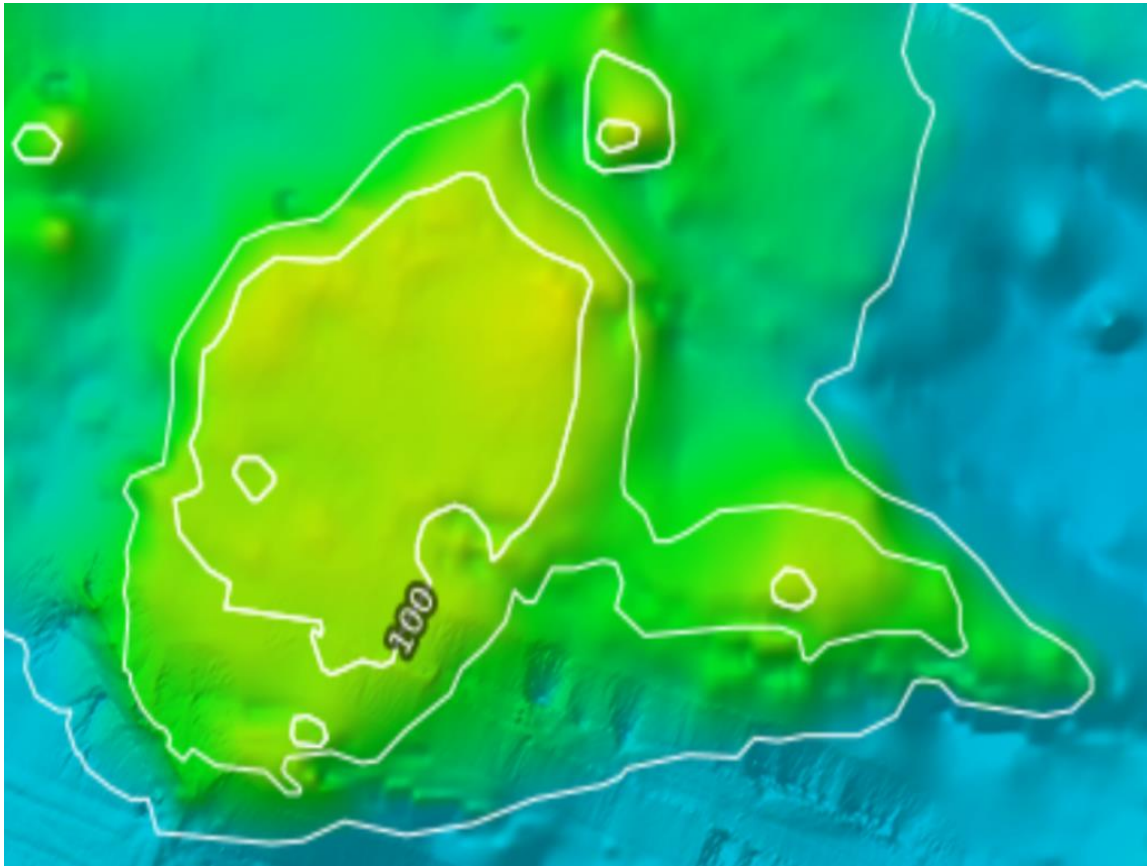


Figure 30 Selected plant area in mean wind speed map [26]

The bathymetric contour lines and the mean depth of the Pinne Marine bank are reported in the following figure:



*Figure 31 Bathymetric contour lines and seabed mean depth of the selected area [25]*

The depth of the selected area is not exceeding 200 m. The majority of the area is characterized by a mean depth between 75-100 m, except in a small sector immediately inside the upper right part of the 100 m contour line where the mean depth is just below 60 m. Between the 100 and 200 meters bathymetric contour lines it can be appreciated a gradual increase of the mean depth in the lower part, while it is more pronounced in the upper and lateral parts, resulting therefore in a higher slope. Considering that the more pronounced is slope of the seabed and the more pronounced is the geohazard risk, these considerations have been taken into account in the placement of the turbines. In particular, the plant does not cover the entire area, but has been concentrated in the central-lower part of the Pinne Marine Bank, as will be better explained in the following paragraph.

This area is interested by one of the highest route vessel densities in the Mediterranean Sea, due to the conjunction of cargo ships routes mainly directed from the Suez Channel, the Black Sea and the Adriatic Sea towards the Strait of Gibraltar. The route vessel density of the mentioned area is lower just to some specific spots of the Mediterranean Sea where, due to geographical constraints, the available sea space is restricted and consequently the route density increases. The cargo vessel route density ranges in the

order of 780 routes per square kilometer per year in the lower part of the area, and 400 routes per square kilometer per year in the upper part.

Furthermore, it's worth noting that this area is not included in the Natura 2000 network, meaning that there are no constraints related to the implementation of human activities. Consequently, the drilling activities required for anchoring system installation are permitted.

Moreover, the presence of power cables and telecommunication cables, which could potentially create interference in the placement of the wind turbines, does not pose a real constraint and was not considered as a determining factor for the determination of the wind farm site location. This because, any such interference could be mitigated in accordance with IEC-103-6 standards, if necessary. However, the absence of power and telecommunication cables is undoubtedly a favorable factor.

The identified site is situated within the Southern Sicily Continental Shelf (area IMC/6), as indicated in the following figure:

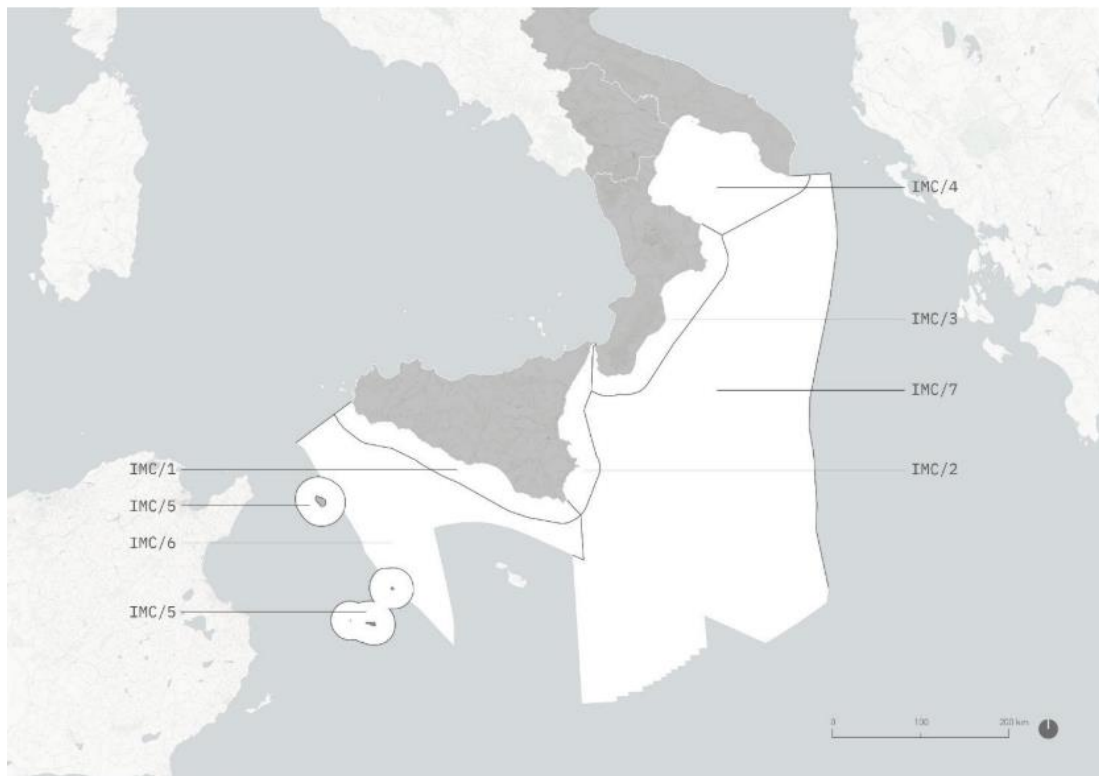


Figure 32 Maritime areas: see Southern Sicily Continental Shelf (area IMC/6) [43]

According to the MIMS (Ministero delle Infrastrutture e delle Mobilità Sostenibili) [43] one of the primary objectives for the energy sector in the area of the Southern Sicily Continental Shelf is the promotion of the energy generation from offshore renewable energy sources, with specific focus on wind energy.

## 4.2 Wind Farm Production

To calculate the wind farm production the methodology explained in paragraph 3.2 was employed. In this paragraph the results of the WAsP and Wind Profile Model simulations are presented.

### 4.2.1 WAsP results

The result of the WAsP software simulation for the proposed wind farm in the selected area are given in the following figure:

Variable	Total	Mean	Min	Max
Total gross AEP [GWh]	1105,531	55,277	55,277	55,277
Total net AEP [GWh]	1067,222	53,361	52,583	54,436
Proportional wake loss [%]	3,47	-	1,52	4,87
Capacity factor [%]	40,6	-	40,0	41,4
Mean speed [m/s]	-	7,70	7,70	7,70
Mean speed (wake-reduced) [m/s]	-	7,56	7,51	7,64
Air density [kg/m <sup>3</sup> ]	-	1,187	1,187	1,187
Power density [W/m <sup>2</sup> ]	-	590	590	590

Figure 33 WAsP simulation results for the proposed wind farm

The gross AEP is equal for each turbine since in this calculation it is utilized a flow model to transform the observed wind climate at the mast site to the predicted wind climate at the turbine site [31], taking into account just the reference yield and the terrain effects. Therefore, due to the fact that in the selected offshore area the terrain variations are not present, the value is constant for each turbine.

The net AEP is instead calculated using a wake model, which estimate the wake losses for each turbine site and subtract these losses from the gross AEP [31]. Therefore, the resulting net AEP value is different for each turbine.

The mean net AEP is the most important data obtained from the simulation. This value represents the net annual energy production of a single wind turbine of the farm and is calculated dividing the total net AEP by the number of turbines (20) of the wind farm. This value plays a crucial role in the subsequent step of the wind model, in which it is employed to calculate the scaling factor SF. As can be seen in Figure 32 the mean net power output  $AEP_{mean,WAsP} = 53,361$  GWh.

More detailed information regarding each wind turbine are provided in Figure 33. In particular, a selection of data retrieved from the WAsP *site list* is presented.

	Site description	Ht [m]	$U(w)$ [m/s]	$\rho$ [kg/m <sup>3</sup> ]	Gross [GWh]	Net. [GWh]	Loss [%]	CF [%]
✱	Turbine site 001	150,0	7,64	1,187	55,277	54,436	1,52	41,4
✱	Turbine site 002	150,0	7,61	1,187	55,277	54,108	2,11	41,1
✱	Turbine site 003	150,0	7,60	1,187	55,277	53,897	2,50	41,0
✱	Turbine site 004	150,0	7,60	1,187	55,277	53,873	2,54	41,0
✱	Turbine site 005	150,0	7,60	1,187	55,277	53,877	2,53	41,0
✱	Turbine site 006	150,0	7,59	1,187	55,277	53,797	2,68	40,9
✱	Turbine site 007	150,0	7,63	1,187	55,277	54,299	1,77	41,3
✱	Turbine site 008	150,0	7,62	1,187	55,277	54,178	1,99	41,2
✱	Turbine site 009	150,0	7,55	1,187	55,277	53,230	3,70	40,5
✱	Turbine site 010	150,0	7,53	1,187	55,277	52,909	4,28	40,2
✱	Turbine site 011	150,0	7,51	1,187	55,277	52,688	4,68	40,1
✱	Turbine site 012	150,0	7,52	1,187	55,277	52,714	4,64	40,1
✱	Turbine site 013	150,0	7,52	1,187	55,277	52,769	4,54	40,1
✱	Turbine site 014	150,0	7,52	1,187	55,277	52,799	4,48	40,2
✱	Turbine site 015	150,0	7,54	1,187	55,277	52,937	4,23	40,3
✱	Turbine site 016	150,0	7,52	1,187	55,277	52,717	4,63	40,1
✱	Turbine site 017	150,0	7,51	1,187	55,277	52,583	4,87	40,0
✱	Turbine site 018	150,0	7,52	1,187	55,277	52,633	4,78	40,0
✱	Turbine site 019	150,0	7,54	1,187	55,277	53,003	4,11	40,3
✱	Turbine site 020	150,0	7,60	1,187	55,277	53,775	2,72	40,9

Figure 34 Wind turbines WAsP simulation results

The wake reduced mean wind speed  $U(w)$  at the hub height of 150 m above the sea level is fairly uniform in the selected area, ranging between a minimum of 7,51 to a maximum of 7,64 m/s. This reduced variability is due both to the wind resource, which is homogeneous in the area, and to the layout optimization process which was followed. The aim of the layout optimization was to reduce the wake effect between the wind turbines, which would result in a reduction of the net AEP of the wind farm. Wind turbines were placed respecting a distance equal to 7 turbine diameters along the direction perpendicular to the prevalent wind speed direction and 12 turbine diameter distance along the direction of the prevalent wind speed. The minimum recommended distances are lower, corresponding to 5 and 10 diameters, respectively. However, in this case higher distances were selected mainly for two reasons: firstly, the abundant availability of space in the selected area made possible a little increase of the distances between the turbines; secondly, the area of the wind farm is characterized by one of the highest mean wind speed in the Mediterranean Sea, but if compared to other regions of the world, as for example the North Sea, the wind resource is not so elevated. Therefore, a slight increase of the distance with respect to the minimum recommended distances make possible a reduction of the wake losses and consequently an increase of the annual energy production.

The wind turbines were disposed in three rows. The first and the second row are composed of 7 turbines each while the third of 6 turbines. The disposition of the wind turbines, together with the representation of the net AEP and wake losses for each wind sector is obtained from the WAsP *spatial view* is illustrated in Figure 34.

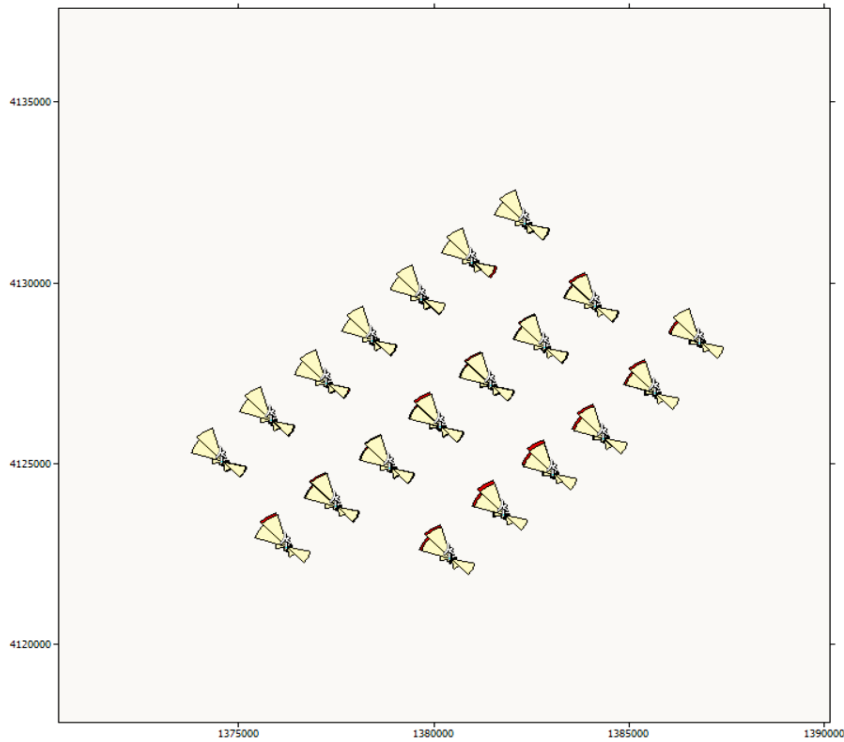


Figure 35 WASP spatial view results

As it can be appreciated both from the Figure 34 and the results of Figure 33, the wind turbines placed in the first row are the most productive, because of the reduced wake losses. These corresponds to turbine sites 1-7 and have lower wake loss proportion values (*loss %*) and higher capacity factors (*CF*).

In WASP, synchronizing the spatial view with the virtual globe it is possible to represent the wind farm in Google Earth Pro. Together with the turbine sites, in Google Earth Pro the bathymetry of the area is also visible, facilitating the identification the selected area.

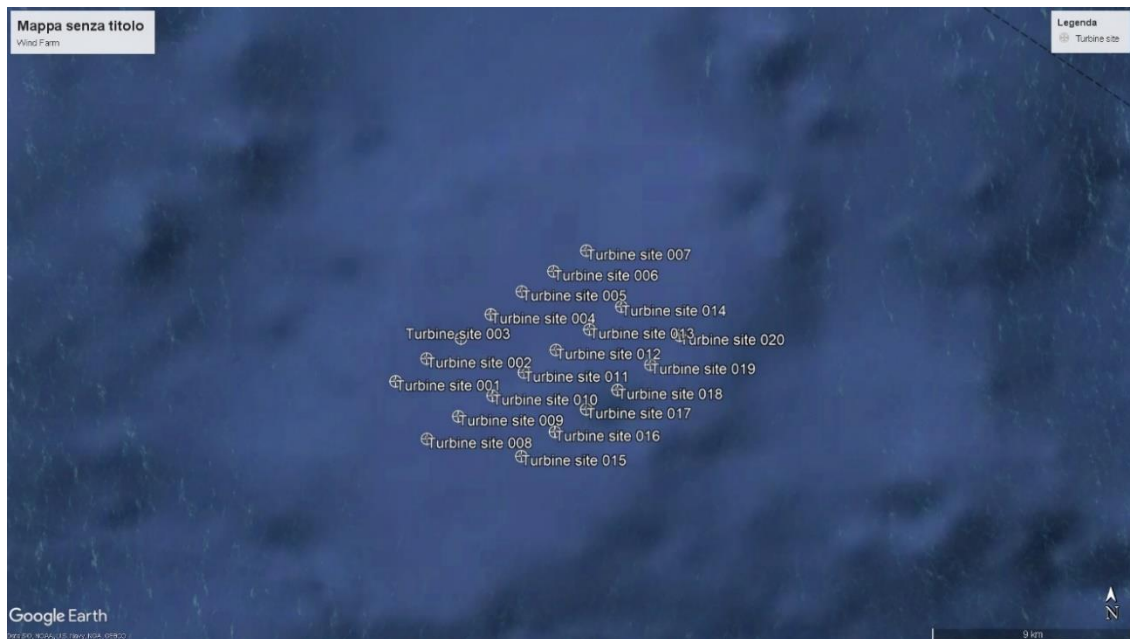


Figure 36 Wind farm in Google Earth Pro

The wind turbine sites' coordinates and corresponding bathymetry values are reported in the following table:

*Table 8 Turbine sites' coordinates and bathymetry*

<b>Turbine site</b>	<b>Longitude E</b>	<b>Latitude N</b>	<b>Bathymetry</b>
1	12°47'54,61''	36°51'54,63''	91
2	12°48'49,92''	36°52'27,89''	87
3	12°49'51,55''	36°52'56,37''	93
4	12°50'45,74''	36°53'30,69''	87
5	12°51'39,21''	36°54'03,00''	85
6	12°52'34,06''	36°54'30,78''	80
7	12°53'33,13''	36°55'00,80''	78
8	12°48'52,42''	36°50'33,97''	88
9	12°49'35,04''	36°51'00,16''	85
10	12°50'48,08''	36°51'35,34''	78
11	12°51'42,49''	36°52'07,87''	85
12	12°52'39,69''	36°52'40,28''	80
13	12°53'37,76''	36°53'09,32''	84
14	12°54'35,15''	36°53'41,07''	78
15	12°51'37,13''	36°50'09,74''	82
16	12°52'37,10''	36°50'44,87''	78
17	12°53'32,88''	36°51'16,75''	90
18	12°54'27,66''	36°51'44,32''	93
18	12°55'26,25''	36°52'19,56''	80
20	12°56'17,02''	36°53'00,70''	81

All the wind turbines of the farm were placed inside the 100 m contour line of Figure 30. The maximum depth corresponds to 93m while the minimum one to 78m. Therefore, it does not exist a high depth variability. This is a positive aspect both for the choice of the floating wind turbine components, namely the floating substructure, mooring and anchoring systems, and of technology required for the installation of the mooring systems. The substation coordinates are (12°56'00'',44 E ; 36°55'32'',00 N). This point was selected because it is the only point of the area with a sea depth not exceeding 60 m. Its bathymetry corresponds to -55 m.

## 4.2.2 Wind Profile Model results

The first results obtained with the Wind Profile Model are the hourly, daily and monthly power output curves of the IEA Wind 15-Megawatt offshore reference wind turbine. These three curves are showed in Figures 37, 38 and 39 respectively.

December, January, February and March are the most productive months of the year. The maximum monthly power output value is reached in March, where a monthly power output of 6,87 GWh is measured. On the contrary, the less productive month is August, where a monthly power output of 1,75 GWh is calculated.

The annual energy production of the wind turbine is equal to 58,57 GWh.

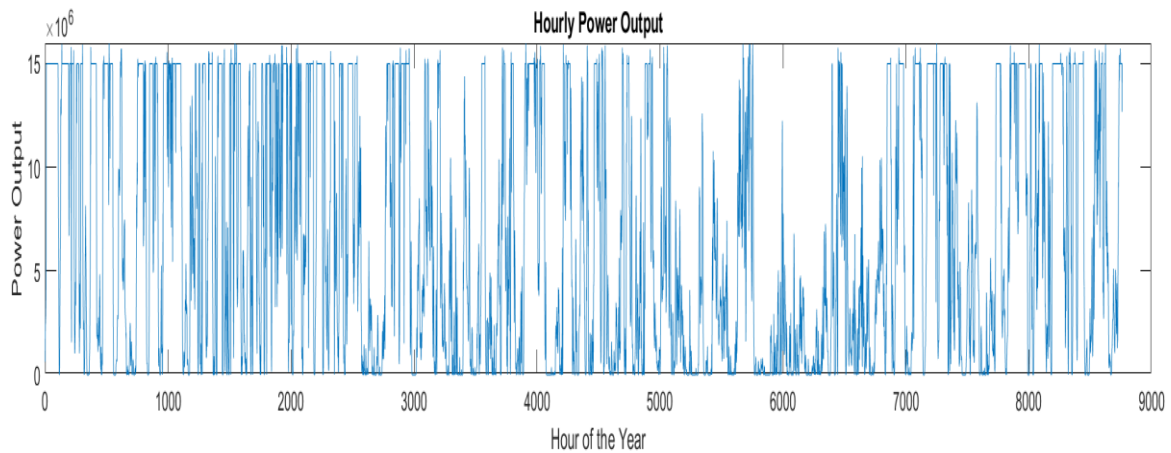


Figure 37 Hourly power output

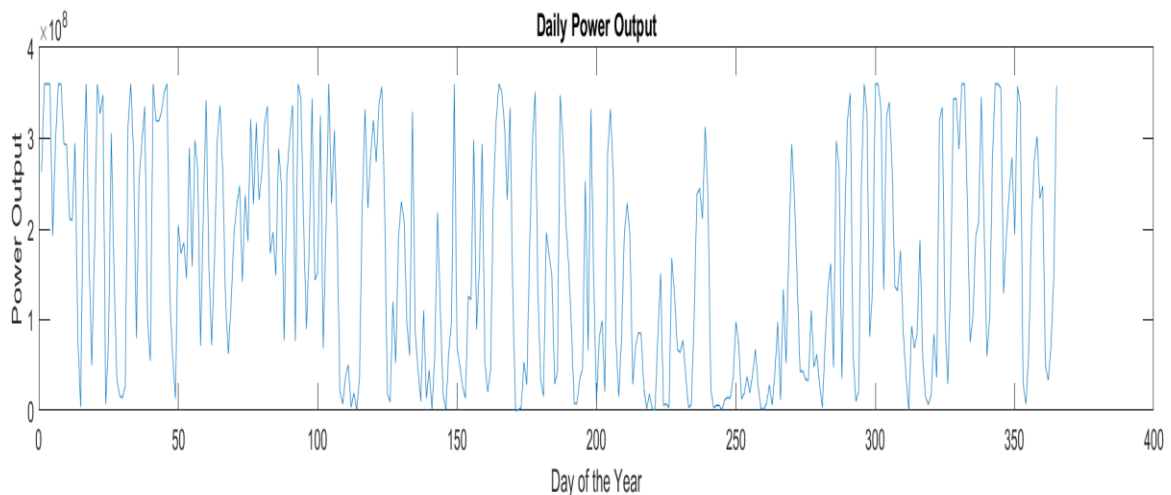


Figure 38 Daily power output

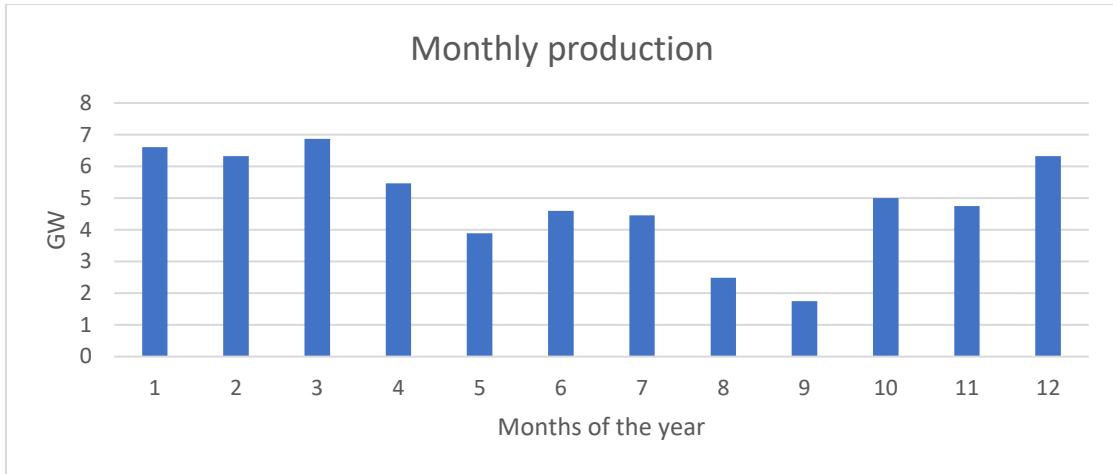


Figure 39 Monthly power output

To take into account the wake effects in the wind farm, which are modeled in the WASP software but are not taken into account in the Matlab model, it was necessary to multiply the results by a fitting parameter, namely the scaling factor  $SF$ . As explained in the description of the methodology, the scaling factor was calculated as the ratio of the mean net annual energy production obtained in WASP ( $AEP_{mean,WASP} = 53,36$  GWh) and the annual energy production of the wind turbine obtained in Matlab ( $AEP_{Turb,MAT} = 58,57$  GWh). A value of scaling factor equal to  $SF=0,911$  was obtained and then used to multiply each hourly wind speed data of the IEA. The resulting curve is showed in the following figure:

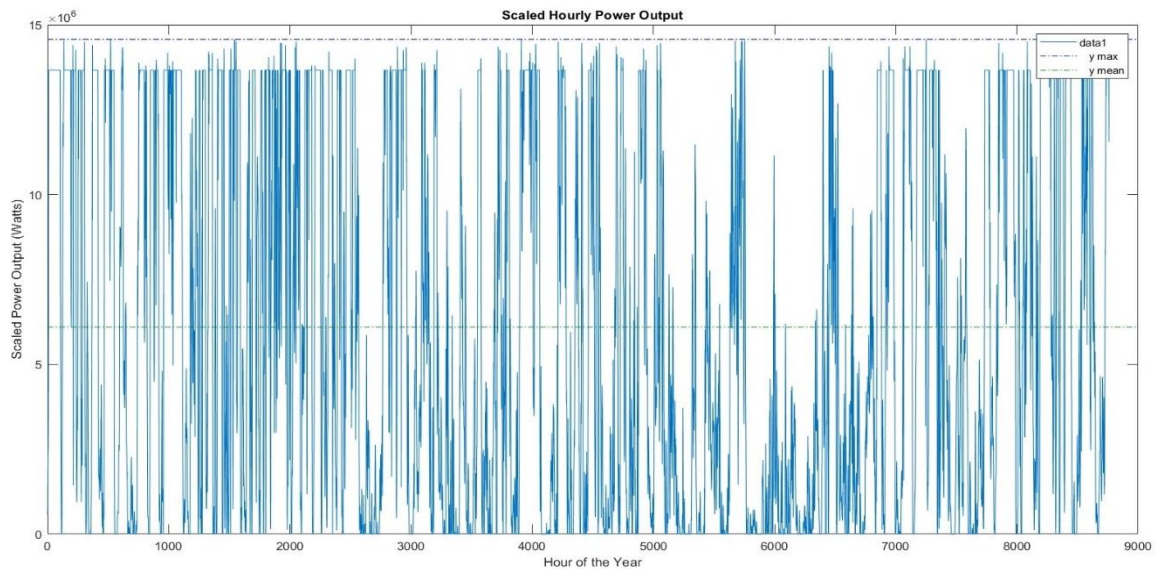
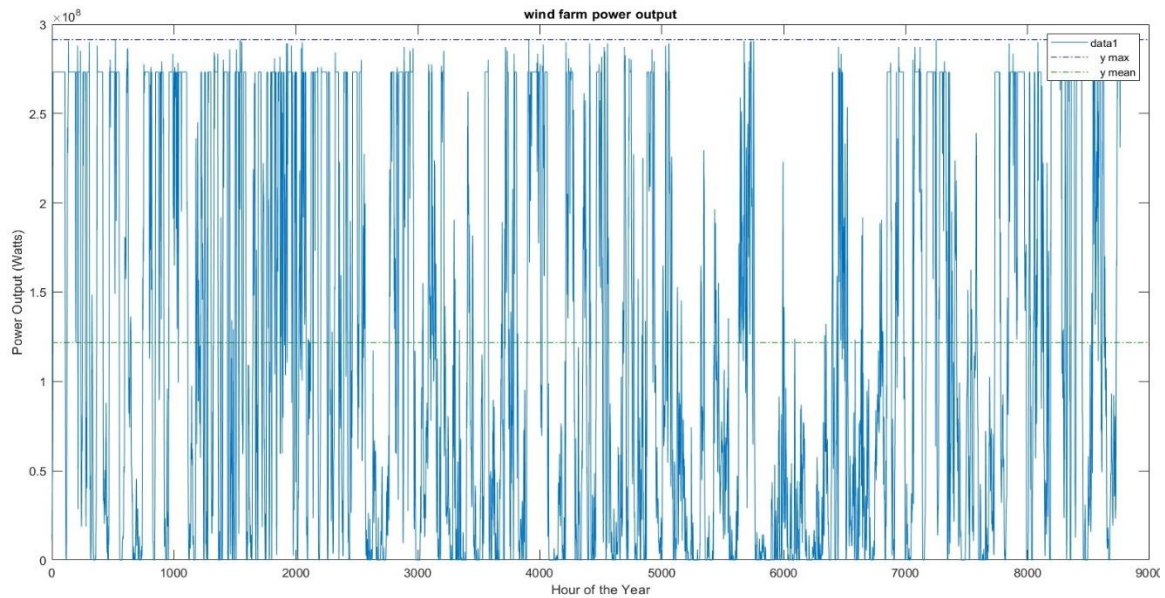


Figure 40 Scaled hourly power output

The maximum power output value of the turbine in the scaled curve corresponds to 14,57 MW, therefore the turbine above its rated speed is not producing anymore 15 MW. The mean power output of the curve corresponds to almost 6.01 MW.

Assuming that the hourly power output curve of each turbine in the wind farm is equal, the last result obtained in the wind Matlab model is the wind farm hourly power output

curve. The wind farm power output was calculated multiplying the scaled hourly power output curve of the reference wind turbine by the number of wind turbines in the plant, namely 20 turbines. The curve resulting from this calculation is represented in the following figure:



*Figure 41 Wind farm power output*

The maximum hourly power output of the wind farm corresponds to 291,4 MW, while the mean yearly value to 121,8 MW.

This curve is the fundamental set of data used in the Matlab model for the determination of the hourly liquid hydrogen production curve.

## 4.3 Liquid hydrogen production

To estimate the hourly liquid hydrogen production and the daily liquid hydrogen production of the plant the methodology presented in paragraph 3.3 was employed.

The hourly liquid hydrogen production curve obtained in the Matlab model is presented in the following figure:

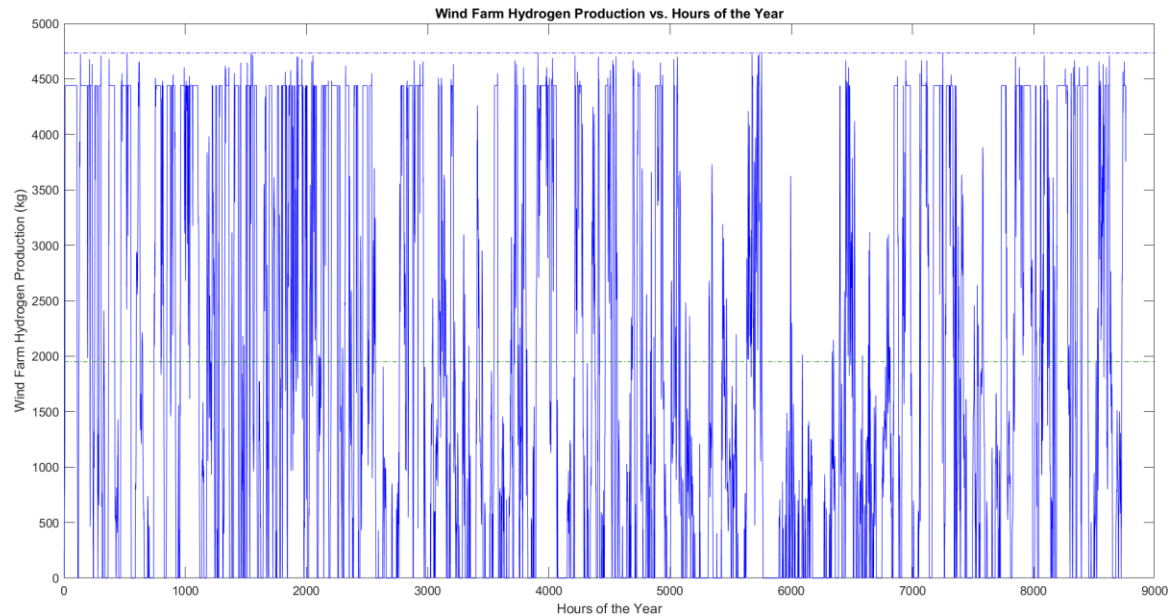


Figure 42 Hourly liquid hydrogen production

The maximum hourly liquid hydrogen production corresponds to 4733 kg<sub>H2</sub>/h, the mean value to 1951 kg<sub>H2</sub>/h, the median value to 1416 kg<sub>H2</sub>/h.

During the year, the wind farm power output is equal to zero for 1277 hours. This number is related to the wind resource, in particular to the mean wind speed, which for 1277 hours is lower with respect to the cut-in speed of the wind turbines. Obviously, these hours are not profitable for the production of liquid hydrogen and consequently all the components of the plant were assumed to be switched off and put in standby.

The rated capacity of the electrolyzer corresponds to  $P_{H_2\_farm} = 246,13$  MW. To ensure efficient operation of the system, the electrolyzer is switched off when the hourly input power from the wind farm falls below 10% of the rated capacity of the electrolyzer. Therefore, the lower limit of wind farm power production, below which the electrolyzer is turned off, corresponds to  $P_{farm\_low} = 24,61$  MW. More specifically, taking into account this consideration, during 2627 hours in the year the electrolyzer is turned off.

Considering that during 1277 hours the wind farm power output is zero, for the remaining 1350 hours the mean wind speed is sufficiently high (meaning above the turbine cut-in speed) to make the turbine generators producing energy, but the overall contribution of the 20 turbines composing the farm is not sufficient to overcome the 24,61 MW threshold value.

The remaining 6133 hours of the year the offshore liquid hydrogen system is running producing liquid hydrogen. The liquid hydrogen produced was considered to be stored in a cryogenic storage tank, connected to the refueling station.

Furthermore, the daily liquid hydrogen production curve is showed in the following figure:

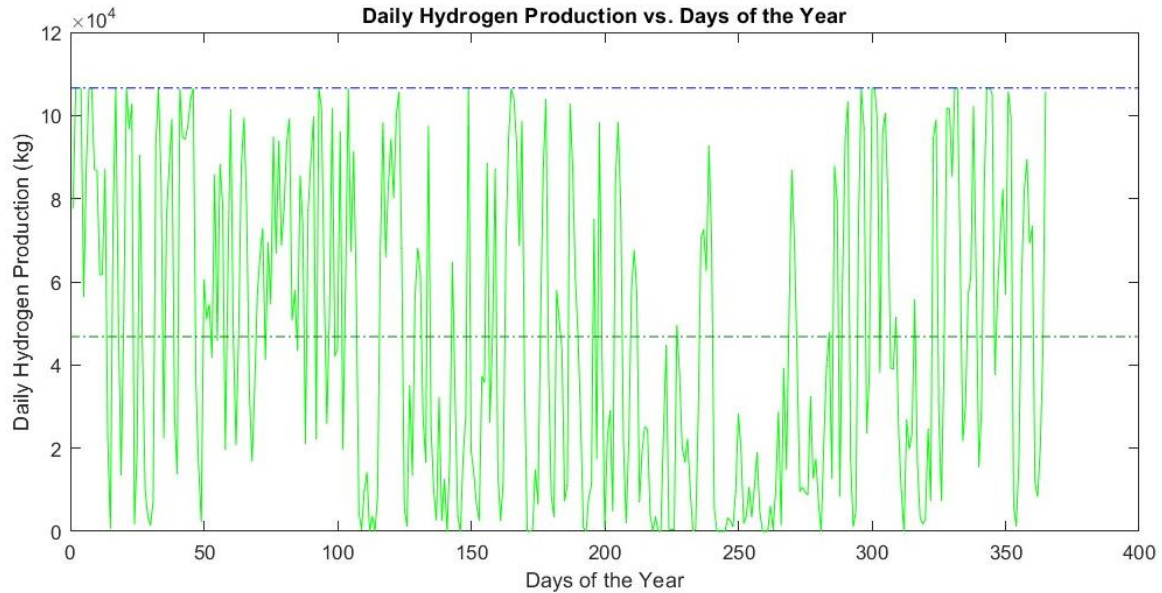


Figure 43 Daily liquid hydrogen production

To conclude, the mean daily liquid hydrogen production corresponds to  $meanW_{H_2,Day} = 46,8$  ton while the maximum daily hydrogen production is equal to  $maxW_{H_2,Day} = 106,6$  ton.

Taking into account the  $maxW_{H_2,Day}$ , the liquid hydrogen storage tank was dimensioned. In particular, the storage size was selected in order to allow the storage of an amount of liquid hydrogen corresponding to two consecutive days of maximum daily hydrogen production. Considering that the  $maxW_{H_2,Day} = 1506 m^3$ , the storage size corresponds to:

$$V_{stg} = \frac{2 \times maxW_{H_2,Day}}{\rho_{LH_2}} = 3012 m^3$$

## 4.4 Technoeconomic analysis

To estimate the levelized cost of hydrogen (LCOH) in the two analyzed scenarios a technoeconomic model was developed in Matlab.

### 4.4.1 Scenario 1

In the Matlab model of the first scenario, the economic parameters were those considered in the paragraph 3.4 and the results of the liquid hydrogen production model of paragraph 4.3 were used.

The size of each component used in the first scenario is presented in the following table:

*Table 9 Components's size in Scenario 1*

<b>Component</b>	
Wind farm	300 MW
Inter-array cable length	41,4 km
Water treatment system	47,33 m <sup>3</sup> /h
Electrolyzer	246,13 MW
Liquefaction system	4733 kg/h
LH <sub>2</sub> storage tank	213 t
Refuelling station	15 pumps of 1720kg <sub>LH<sub>2</sub></sub> /h

The main results of the first scenario are given in the following table:

*Table 10 Results Scenario 1*

Capex	1,0384 B€
Installation	112,66 M€
Opex	298,13 M€
Replacement - Salvage value	81 M€
Decommissioning	16,7 M€
NPV	1,5468 B€
Total LH <sub>2</sub> production	427180 t
LCOH	6,36 €/kg

The Capex represents the total investment cost of the uninstalled components of the plant. The Installation represent the sum of all installation costs. The Opex represents the total operational expenditures incurred in the whole lifetime of the project. The Decommissioning, instead, is the cost incurred to dismantle the wind farm and the platform, calculated at the end of the lifetime project. The salvage value represents the value of electrolyzer at the end of the plant lifetime. The total LH<sub>2</sub> production is equal to the amount of liquid hydrogen produced during the whole project life, calculated as the sum of the yearly liquid hydrogen production for each year, which is assumed to be constant. The net present value is calculated from the abovementioned contributions.

The levelized cost of hydrogen, in this scenario, represents the cost of the produced liquid hydrogen, which is intended to be sold directly in the platform to liquid hydrogen-powered cargo vessels. The decomposition of the expenditures is showed in the following figure:

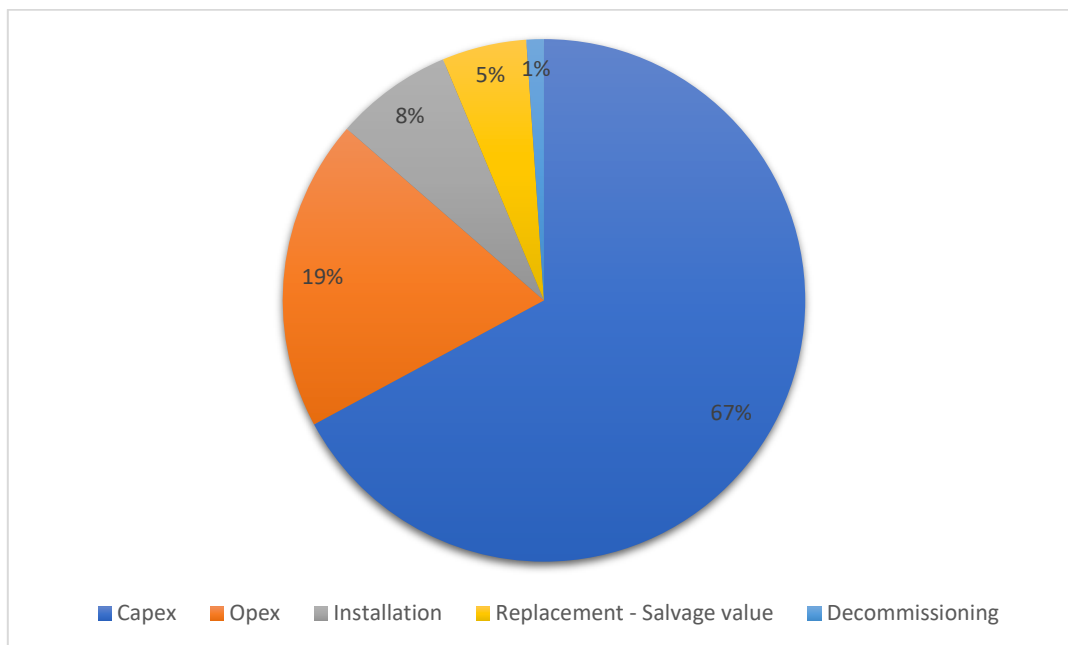


Figure 44 Project expenditures break down in scenario 1

The Capex is the expenditure that influences more the LCOH, therefore the Capex of the plant can be decomposed showing the contribution of each plant component, as shown in the Figure 45.

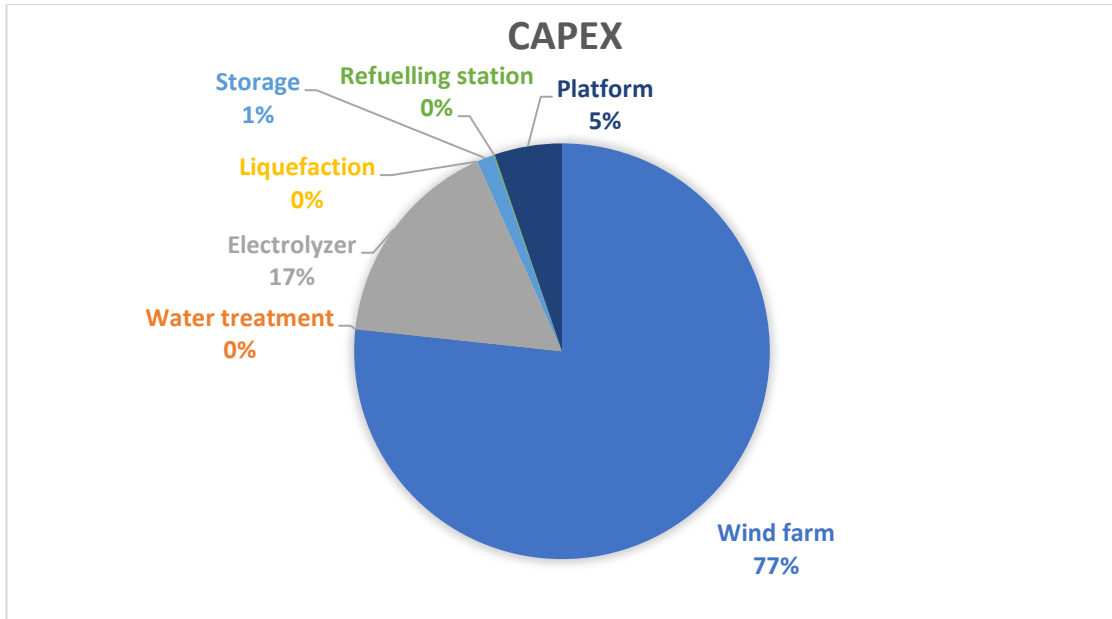


Figure 45 Plant Capex break down in scenario 1

#### 4.4.2 Scenario 2

In the second scenario, the hydrogen production model was modified, eliminating the energy consumption of the hydrogen liquefaction system and of the refuelling offshore station. The energy consumption of the refuelling station onshore was not considered in this model. The energy consumption of the compressor, placed in the platform, was taken into account in the calculation of the hourly and daily hydrogen production. The daily hydrogen production curve for the reference year is represented in Figure 46. The maximum hourly hydrogen production corresponds to 5370 kg<sub>H2</sub>/h. The increase of the maximum hourly hydrogen production is justified by the lower energy consumption of the whole system in the second scenario, since it is excluded the highly energy demanding process of hydrogen liquefaction. The maximum daily hydrogen production value corresponds to 121 t.

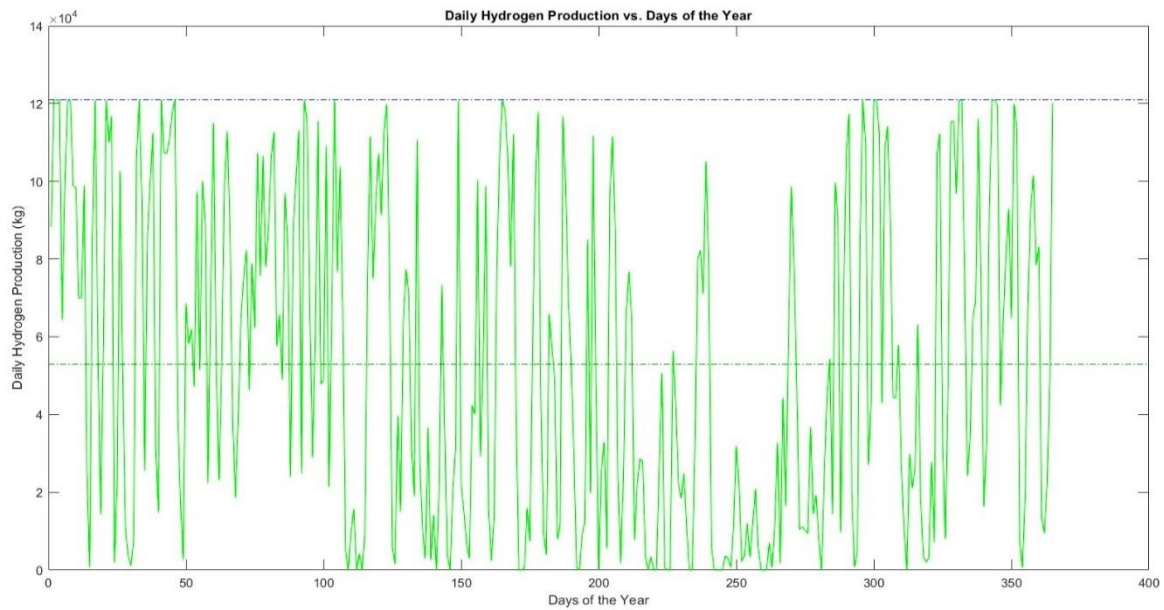


Figure 46 Daily gaseous hydrogen production

The onshore hydrogen storage tank was dimensioned to store the maximum daily hydrogen production of 121 t. The main results of the hydrogen production model developed for the second scenario are reported in the following table:

Table 11 Component's size in Scenario 2

Component	
Water treatment system	53,7 m <sup>3</sup> /h
Electrolyzer	279,25 MW
Compressor	13,425 MW
Pipeline	66 km
Storage	121 t

The results of the techno-economic model are reported in the following table:

Table 12 Results Scenario 2

Capex	1.193 B€
Installation	119,09 M€
Opex	399,73 M€
Replacement – Salvage value	98,71 M€
Decommissioning	19,03 M€
NPV	1,829 B€
Total H <sub>2</sub> production	483270 t
LCOH	6,65 €/kg

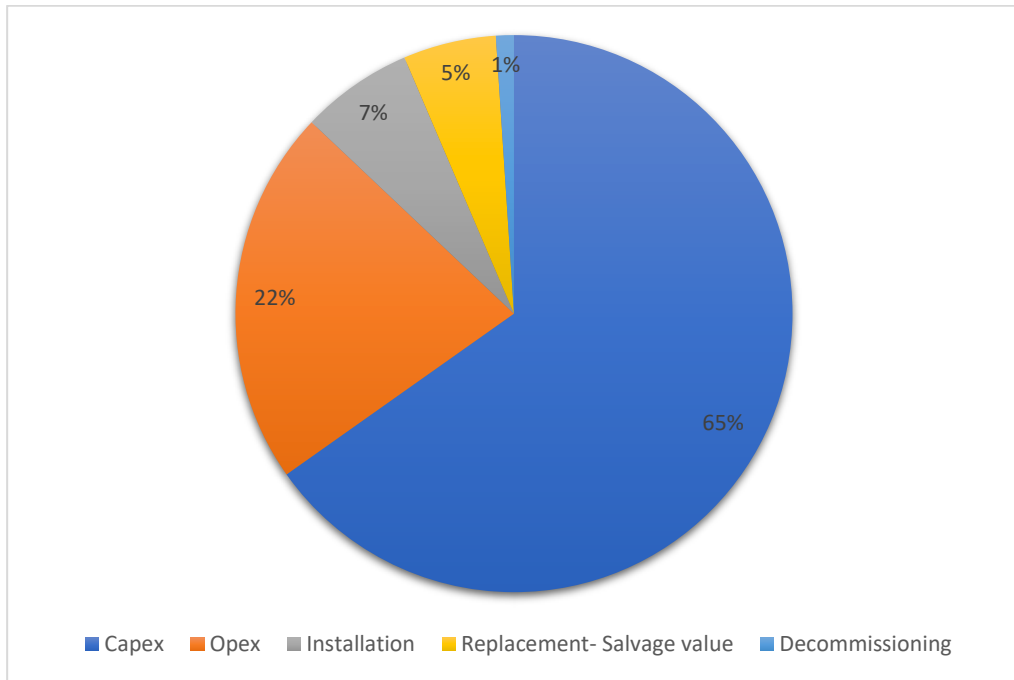


Figure 47 Project expenditures break down in scenario 2

The Capex is the expenditure that influences more the LCOH, therefore the Capex of the plant can be decomposed showing the contribution of each plant component, as shown in the following figure:

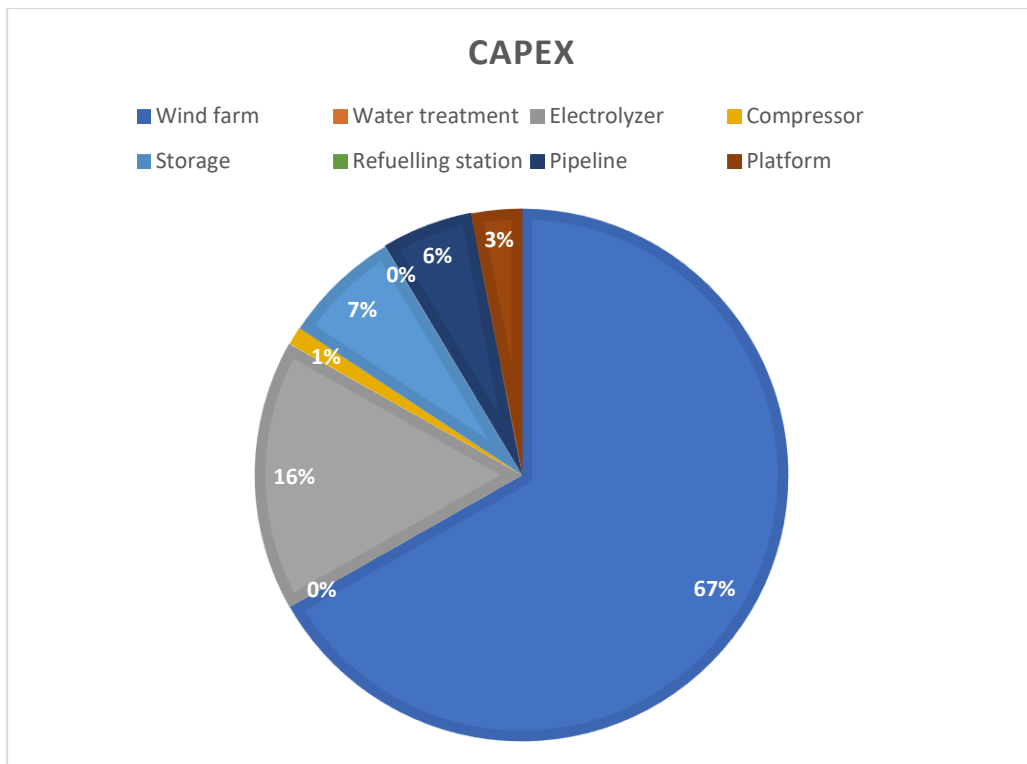


Figure 48 Plant Capex break down in scenario 2

# 5 Discussion and conclusion

In this work, the techno-economic assessment of an offshore Mediterranean hydrogen generation hub powered by an offshore floating wind farm for the decarbonization of the maritime shipping sector was performed. Two scenarios were evaluated, considering two different plant configurations and two target ship categories. In both scenarios the size of the wind farm was considered equal to 300 MW, to be coherent with the dimensions of the proposed offshore floating wind farm projects in the Mediterranean Sea.

To obtain a significant acceleration of the reduction of GHG associated to the maritime shipping sector, it is of fundamental importance to identify the locations that could push rapidly the energy transition. The Mediterranean Sea is one of these locations, because of its strategic position between Pacific and Atlantic oceans, accounting for the 15% of the global shipping activity. This high value is mainly due to the route passing through the Suez Canal and the Strait of Gibraltar, which is one of the key international maritime routes. More specifically, this route lies in the Strait of Sicily, which was selected as the area of interest for the installation of the proposed plant.

With the aim to identify a system location the more realistic as possible, the precise plant location in the Strait of Sicily was determined considering different aspects, namely: vessel route density, bathymetry, mean wind speed, regulatory framework and marine geohazard risk. In the two analyzed scenarios, the offshore hydrogen production system was considered to be placed in the same location. Among the different vessel categories, cargo vessels were selected to identify the plant location. Other categories of vessels were excluded from the analysis to reduce the variability of ship dimensions and ship tanks capacities and to focus on the vessel category to which is associated one of the highest GHG contribution. It is important to mention that, the maximum seabed depth was set equal to 200 m. This assumption was done to limit the cost of the floating offshore wind farm. Indeed, even if the technical readiness level (TRL) of floating wind turbines at seabed depth higher than 200 m was already demonstrated, their cost remains high and could lower just with commercialization. The surface of the selected region is of 394 km<sup>2</sup>, the minimum distance with respect to the Pantelleria island is 62 km while with respect to the closest point of the Sicily coastline is 52 km. The underwater structure on which are placed the 20 wind turbines is called Pinne Marine Bank, which is a bank of sedimentary origin. In this type of seabed, are not present particular limitations on the selection of the anchoring type of the floating wind turbine. The wind turbine selected in this study is the IEA 15-MW Offshore Reference Wind Turbine [9], while the substructure is the UMaine VoltturnUS-S Reference Platform, specifically designed for the reference IEA 15 MW reference turbine. Catenary moorings connects the floating turbine to the anchoring system, considered in this case of drag-embedded. This mooring configuration is

characterized in a larger footprint associated to the lower section of the chain that rests on the seabed which moves in stormy conditions. However, their utilization in the selected area is not problematic, since the area does not enter in the Natura 2000 network [29], which is the main instrument of the European Union policy for the preservation of natural habitats and protection of flora and fauna. Moreover, according to the MIMS [43] one of the primary objectives for the energy sector in the area of the Southern Sicily Continental Shelf, in which the considered area is comprised, is the promotion of the energy generation from offshore renewable energy sources, with specific focus on wind energy. The wind resource at 150 m above the sea level in the area ranges between 7,62 m/s and 7,75 m/s resulting in one of the windiest areas of the Mediterranean Sea. In the Strait of Sicily, areas at west of the selected area are even slightly more windy, but their selection was excluded due to the presence of a significant number of underwater volcanoes and seamounts, which are associated in both cases to high seabed slope and in the latter case to a volcanic and seismic activities, which could create slope failures that could damage the wind farm.

In the first scenario, the plant is composed by a dedicated wind farm, a water treatment system, an electrolyzer, a hydrogen liquefaction system, a liquid hydrogen storage tank, a refuelling station and an offshore bottom-fixed platform, above which are placed the facilities to produce, store and distribute hydrogen. Among the different ship categories, the analysis regarding the utilization of the liquid hydrogen as fuel for ship propulsion, was restricted to the cargo vessel category only, which enters within the 20% of the global fleets that are responsible for 85% of the net GHG emissions of the shipping sector. The offshore refuelling of cargo ships could facilitate and increase the speed of liquid hydrogen refueling operation by avoiding docking in a port. Moreover, ships at ports are subjected to different port fees and tariffs to use port facilities and services such as mooring, pilotage, and towing. Therefore, in the context of utilization of liquid hydrogen as alternative fuel, the offshore refuelling could represent an advantage. However, it is worth mentioning that technological advancement of refuelling stations is needed to perform a faster refuelling, and also of the liquid hydrogen storage and management systems on ships. Due to its low volumetric energy density, extremely low temperature ( $-293^{\circ}\text{C}$ ) at which it has to be stored and managed, challenges exist in the utilization of liquid hydrogen in ships. These problems justify the inexistence of liquid hydrogen powered ships up to now. However, different concepts are tested, under construction or in design phase [17], showing an increasing interest for the application of liquid hydrogen as fuel both in PEMEFC technology and dual mixture internal combustion engines. As far as concern the energy demand of the plant components, in the first scenario, it is completely satisfied by the dedicated wind farm, resulting in a totally self-sufficient system. Among the different components, the PEMEL electrolyzer is the most energy consuming, but a relevant portion of the wind farm electricity production is consumed also by the liquefaction system. In order to perform a realistic analysis, 2024 or 2025 target values for the energy consumption and operational lifetime of the components were considered. Therefore, considering the forecasted technological progress by [12], a

reduction of the energy consumption of these two components will lead to a higher liquid hydrogen production.

In the second scenario the output of the plant is not liquid hydrogen, but gaseous hydrogen only, which is transported from the offshore substation through a subsea pipeline 66 km long towards the port of Porto Empedocle, where it is stored. Therefore, the hydrogen liquefaction system, the liquid hydrogen storage tank and the offshore refuelling station were eliminated. The energy required to perform the ship refuelling was considered to be satisfied by the Sicilian electricity grid, therefore differently from the first scenario, the system is not completely self sufficient and needs the support of the grid. This is a negative point of the system, because the overall GHG emission are higher with respect to the first scenario, even if not associated to the fuel combustion itself in ships. The energy consumption of the offshore system is reduced, because of the elimination of the energy consumption associated to the liquefaction system and to the refuelling station, previously decurted from the wind farm electricity production. Therefore, the daily hydrogen production of the second scenario is higher with respect to the reference case, increasing from 106 t to 121 t. While in the first scenario the liquid hydrogen storage tank was dimensioned considering two days of maximum hydrogen production, in the second scenario, the gaseous hydrogen storage tank was dimensioned considering one day to take into account a realistic storage dimension. The gaseous hydrogen presents problems related to the onboard ship storage, because of its low volumetric energy density even at 350 bar. Moreover, the refuelling time of gaseous hydrogen for ship of big dimension is a concern, therefore the target vessel category for the produced hydrogen cannot be the same of the first scenario, where a 930 m<sup>3</sup> storage tank was considered. In particular, the utilization of the gaseous produced hydrogen is more suited for ships of lower dimensions and that do not pose stringent limitations regarding the refuelling time. Moreover, due to the lower ship autonomy, the domestic navigation and short distance routes, rather than long distance routes are preferred.

In both scenarios, to perform an analysis representative of the near term LCOH for such systems, were considered 2024 or 2025 target values for the economic inputs. The LCOH of both scenarios is in line with the results of the other literature studies, considered as reference. The levelized cost of liquid hydrogen corresponds to 6,36 €/kg, a value slightly lower than that of gaseous hydrogen, which is 6,65 €/kg. Even if the hydrogen produced by the system in the first scenario (427180 t) is lower than the second (483270 t), the levelized cost of liquid hydrogen is lower than that of gaseous hydrogen. In both scenarios the Capex is the most relevant cost component influencing the LCOH, followed by the Opex and the Installation cost. In both scenarios, the wind farm Capex represents the highest contribution, affecting therefore significantly the LCOH. A reduction of the wind farm Capex is therefore required to significantly impact on hydrogen cost. Similarly, in both scenarios, the electrolyzer is the second component which have the highest Capex. Therefore, economy of scales for large plant capacities and a reduction of the investment costs for both technologies are of fundamental importance to reduce the LCOH, which in this study results higher with respect to that produced from natural gas

and coal with carbon capture and storage (0,7-2,6 USD/kg) [14]. A relevant difference in the two scenarios regards the storage system. In particular, in the second scenario the gaseous hydrogen storage tank Capex accounts for the 7% of the total, while in the first scenario just for the 1%. This is important to mention, also because in the first scenario the storage was dimensioned to store an amount of hydrogen equivalent to two times the maximum daily hydrogen production of the plant, while in the second case to store the amount of one day. However, in the two scenarios, the storage tank and the other components of the plant have a negligible impact on the cost of hydrogen, if compared with the abovementioned wind farm and electrolyzers. Therefore, it is easy to understand, that the LCOH in scenario two is higher due to the higher size of the electrolyzer with respect to scenario 1.

Considering the abovementioned considerations, it can be stated that offshore liquid hydrogen liquefaction is technically and economically feasible. Moreover, since the volumetric energy density of liquid hydrogen is higher than that of gaseous hydrogen, it is preferred in maritime shipping sector. The plant producing liquid hydrogen can also be replicated similarly for different locations rescaling the technologies. Therefore, building such new infrastructure, in which different plants are located along or in close proximity of the main shipping routes, for the production and refueling of liquid green hydrogen directly sold offshore, could significantly contribute to decarbonize the maritime shipping sector.

# References

- [1] IRENA (2021), A pathway to decarbonise the shipping sector by 2050, International Renewable Energy Agency, Abu Dhabi
- [2] Hydrogen Europe (2021), HOW HYDROGEN CAN HELP DECARBONISE THE MARITIME SECTOR, POLICY PAPER JUNE 2021
- [3] Ibrahim, Omar S., et al. "Dedicated large-scale floating offshore wind to hydrogen: Assessing design variables in proposed typologies." *Renewable and Sustainable Energy Reviews* 160 (2022): 112310. <https://doi.org/10.1016/j.rser.2022.112310>
- [4] Calado, Gonçalo, and Rui Castro. "Hydrogen production from offshore wind parks: Current situation and future perspectives." *Applied Sciences* 11.12 (2021): 5561. <https://doi.org/10.3390/app11125561>
- [5] Martinez, A., and Gregorio Iglesias. "Multi-parameter analysis and mapping of the levelised cost of energy from floating offshore wind in the Mediterranean Sea." *Energy Conversion and Management* 243 (2021): 114416. <https://doi.org/10.1016/j.enconman.2021.114416>
- [6] Carbon Trust, Floating Offshore Wind: Market and Technology Review, June 2015
- [7] Italian Ministry of the Environment and Land and Sea Protection. Environmental Evaluations and Authorizations: Project for the Construction of a Floating Offshore Wind Farm in the Sicilian Channel, Consisting of 25 Turbines Each with a Nominal Power of 10 MW, for a Total Power of 250MW. Available online: <https://va.minambiente.it/it-IT/Oggetti/Documentazione/7273/10503#collapse>
- [8] Cerfontaine, Benjamin, et al. "Anchor geotechnics for floating offshore wind: Current technologies and future innovations." *Ocean Engineering* 279 (2023): 114327. <https://doi.org/10.1016/j.oceaneng.2023.114327>
- [9] Gaertner, Evan, Jennifer Rinker, Latha Sethuraman, Frederik Zahle, Benjamin Anderson, Garrett Barter, Nikhar Abbas, Fanzhong Meng, Pietro Bortolotti, Witold Skrzypinski, George Scott, Roland Feil, Henrik Bredmose, Katherine Dykes, Matt Shields, Christopher Allen, and Anthony Viselli. 2020. Definition of the IEA 15-Megawatt Offshore Reference Wind. Golden, CO: National Renewable Energy Laboratory. NREL/TP-5000-75698. <https://www.nrel.gov/docs/fy20osti/75698.pdf>
- [10] Allen, Christopher, Anthony Viselli, Habib Dagher, Andrew Goupee, Evan Gaertner, Nikhar Abbas, Matthew Hall, and Garrett Barter. Definition of the UMaine VoltturnUS-S Reference Platform Developed for the IEA Wind 15-Megawatt Offshore Reference Wind Turbine. Golden, CO: National Renewable Energy Laboratory. NREL/TP-5000-76773. <https://www.nrel.gov/docs/fy20osti/76773.pdf>.

- [11] Appunti del corso di Polygeneration and Advanced Energy Systems - Politecnico di Torino – a.a. 2022-2023
- [12] Clean Hydrogen Joint Undertaking, Strategic Research and Innovation Agenda 2021 – 2027, Annex to GB decision no. CleanHydrogen-GB-2022-02
- [13] Meier, Konrad. "Hydrogen production with sea water electrolysis using Norwegian offshore wind energy potentials: Techno-economic assessment for an offshore-based hydrogen production approach with state-of-the-art technology." *International Journal of Energy and Environmental Engineering* 5 (2014): 1-12. <https://doi.org/10.1007/s40095-014-0104-6>
- [14] Bonacina, Camilla Nicol, Nima Bordbar Gaskare, and Gianluca Valenti. "Assessment of offshore liquid hydrogen production from wind power for ship refueling." *International Journal of Hydrogen Energy* 47.2 (2022): 1279-1291. <https://doi.org/10.1016/j.ijhydene.2021.10.043>
- [15] Van Hoecke, Laurens, et al. "Challenges in the use of hydrogen for maritime applications." *Energy & Environmental Science* 14.2 (2021): 815-843. DOI: 10.1039/d0ee01545h
- [16] Norwegian Centres of Expertise Maritime CleanTech, Norwegian future value chains for liquid hydrogen, [Maritime CleanTech – Cluster for Clean Maritime Solutions](#)
- [17] Ustolin, F.; Campari, A.; Taccani, R. An Extensive Review of Liquid Hydrogen in Transportation with Focus on the Maritime Sector. *J. Mar. Sci. Eng.* 2022, 10, 1222. <https://doi.org/10.3390/jmse10091222>
- [18] Stolzenburg, K., et al. "Efficient liquefaction of hydrogen: results of the IDEALHY project." *Proceedings of the XXth Energie—Symposium, Stralsund, Germany.* 2013. <https://www.researchgate.net/publication/335033448>
- [19] Aasadnia, Majid, and Mehdi Mehrpooya. "Large-scale liquid hydrogen production methods and approaches: A review." *Applied energy* 212 (2018): 57-83. <https://doi.org/10.1016/j.apenergy.2017.12.033>
- [20] Ghigo, Alberto, et al. "Platform optimization and cost analysis in a floating offshore wind farm." *Journal of Marine Science and Engineering* 8.11 (2020): 835. <https://doi.org/10.3390/jmse8110835>
- [21] Wu, Xiaoni, et al. "Foundations of offshore wind turbines: A review." *Renewable and Sustainable Energy Reviews* 104 (2019): 379-393. <https://doi.org/10.1016/j.rser.2019.01.012>
- [22] Norwegian University of Life Sciences, Bjerkseter et Agotnes, “ Levelised cost of energy for offshore floating wind turbine concepts (2013)
- [23] Giampieri, Alessandro, Janie Ling-Chin, and Anthony Paul Roskilly. "Techno-economic assessment of offshore wind-to-hydrogen scenarios: A UK case

study." *International Journal of Hydrogen Energy* (2023).  
<https://doi.org/10.1016/j.ijhydene.2023.01.346>

[24] Sandia National Laboratories, Joseph W. Pratt and Leonard E. Klebanoff ,  
“Feasibility of the SF-BREEZE: a Zero-Emission, Hydrogen Fuel Cell, High-Speed  
Passenger Ferry” (2016)

[25] [European Marine Observation and Data Network \(EMODnet\) \(europa.eu\)](https://www.europa.eu)

[26] [Global Wind Atlas](https://www.globalwindatlas.com/)

[27] Cavallaro D and Coltelli M (2019)The Graham Volcanic Field Offshore  
Southwestern Sicily (Italy) Revealed by High-Resolution Seafloor Mapping and ROV  
Images. *Front. Earth Sci.* 7:311. doi:10.3389/feart.2019.00311

[28] Randolph, Mark, and Susan Gourvenec. *Offshore geotechnical engineering*. CRC  
press, 2017.

[29] [Natura 2000 Viewer \(europa.eu\)](https://www.natura2000viewer.europa.eu/)

[30] [Wind energy industry-standard software - WAsP](https://www.wasp.dk/)

[31] Mortensen, N. G. Wind resource assessment using the WAsP software. DTU Wind  
Energy. DTU Wind Energy E No. 174 (2018).

[32] [GitHub: Let's build from here · GitHub](https://github.com/DTUWindEnergy/WAsP)

[33] [LAUTEC | ESOX - Map: Download and Analyze Metocean Data](https://www.esox.com/)

[34] Leahy, Paul, et al. "Development of a viability assessment model for hydrogen  
production from dedicated offshore wind farms." *international journal of hydrogen  
energy* 46.48 (2021): 24620-24631. <https://doi.org/10.1016/j.ijhydene.2020.04.232>

[35] <https://www.hydrogenenergysupplychain.com/supply-chain/the-suis>

[36] Rohde, F.; Sames, P. Conceptual Design of a Zero-Emission Open-Top Container  
Feeder. In Proceedings of the 8th International Conference on High-Performance Marine  
Vehicles (HIPER), Duisburg, Germany, September 2012; pp. 207–215.

[37] Ye, M.; Sharp, P.; Brandon, N.; Kucernak, A. System-Level Comparison of  
Ammonia, Compressed and Liquid Hydrogen as Fuels for Polymer Electrolyte Fuel Cell  
Powered Shipping. *Int. J. Hydrogen Energy* 2022

[38] BVG Associates, on behalf of the Offshore Renewable Energy Catapult The Crown  
Estate and Crown Estate Scotland, “Guide to a Floating Offshore Wind Farm”, May 2023

[39] Fraunhofer Institute for Solar Energy Systems ISE, “COST FORECAST FOR LOW-  
TEMPERATURE ELECTROLYSIS – TECHNOLOGY DRIVEN BOTTOM-UP  
PROGNOSIS FOR PEM AND ALKALINE WATER ELECTROLYSIS SYSTEMS”,  
October 2021

[40] IRENA (2020), Green Hydrogen Cost Reduction: Scaling up Electrolysers to Meet the 1.5°C Climate Goal, International Renewable Energy Agency, Abu Dhabi

[41] U.S. Department of Energy (DOE) [DOE Technical Targets for Hydrogen Delivery | Department of Energy](#)

[42] Kaiser, Mark J. "FERC pipeline decommissioning cost in the US Gulf of Mexico, 1995–2015." *Marine Policy* 82 (2017): 167-180.  
<https://doi.org/10.1016/j.marpol.2017.05.006>

[43] Ministero delle infrastrutture e della mobilità sostenibili - Dipartimento per i trasporti e la navigazione. Piani dello Spazio Marittimo italiani Area Marittima “Ionio-Mediterraneo centrale”, Agosto 2022.

Figure 1 distribution of the energy consumption for the international shipping [1].....	7
Figure 2 Main international shipping traffic routes [1] .....	8
Figure 3 Suiso Frontier liquid hydrogen tanker [35] .....	10
Figure 4 Plant layout [14] .....	12
Figure 5 Floating and bottom fixed foundation structures [22].....	14
Figure 6 Main floating wind substructures [20] .....	15
Figure 7 Main mooring system classes [7] .....	16
Figure 8 Main anchor configurations [20] .....	18
Figure 9 Power and thrust curves of the reference turbine [9] .....	20
Figure 10 UMaine VoltturnUS-S Reference Platform [10].....	21
Figure 11 Proton exchange membrane cell schematic representation [11].....	23
Figure 12 Cell and system efficiency curves of the PEM electrolyzer [11] .....	23
Figure 13 Scheme of the pre-cooled Claude cycle [19].....	27
Figure 14 Present and future dimensions of LH storage tanks [17] .....	29
Figure 15 Annual route density map for all vessels categories [25] .....	32
Figure 16 Annual route density map for cargo vessel category [25] .....	33
Figure 17 Annual route density map for cargo vessels category in the Strait of Sicily [25] .....	33
Figure 18 Bathymetric map of the Strait of Sicily [25] .....	35
Figure 19 Route density map and the bathymetric contour map overlapping [25] .....	35
Figure 20 Mean wind speed at 150 m a.s.l [26].....	36
Figure 21 Wind frequency rose of the point indicated in the map [26] .....	37
Figure 22 Main undersea features of the Strait of Sicily [25].....	38
Figure 23 Tectonic of the area and the main underwater volcanic structures in red [27]..	38
Figure 24 Natura 2000 Network in the areas in the Strait of Sicily.....	39
Figure 25 Power and telecommunication cable map and maritime boundaries map overlapping [25].....	40
Figure 26 Wind Atlas Methodology [31] .....	42
Figure 27 Generalised wind climate results example, Climate Data tab in WAsP software .....	43
Figure 28 IEA Wind 15-Megawatt reference wind turbine power and thrust curve in WAsP Turbine Editor .....	45
Figure 29 Selected plant area in bathymetry map [26].....	63
Figure 30 Selected plant area in mean wind speed map [26] .....	63
Figure 31 Bathymetric contour lines and seabed mean depth of the selected area [25] ....	64
Figure 32 Maritime areas: see Southern Sicily Continental Shelf (area IMC/6) [43] .....	65
Figure 33 WAsP simulation results for the proposed wind farm .....	66
Figure 34 Wind turbines WAsP simulation results .....	67
Figure 35 WAsP spatial view results.....	68
Figure 36 Wind farm in Google Earth Pro.....	68
Figure 37 Hourly power output.....	70
Figure 38 Daily power output.....	70
Figure 39 Monthly power output .....	71
Figure 40 Scaled hourly power output.....	71

Figure 41 Wind farm power output.....	72
Figure 42 Hourly liquid hydrogen production .....	73
Figure 43 Daily liquid hydrogen production .....	74
Figure 44 Project expenditures break down in scenario 1 .....	76
Figure 45 Plant Capex break down in scenario 1 .....	77
Figure 46 Daily gaseous hydrogen production .....	78
Figure 47 Project expenditures break down in scenario 2 .....	79
Figure 48 Plant Capex break down in scenario 2 .....	79